Titre: Title:	The Impact of Hydrogen and Oxidizing Impurities in Chemical Vapor Deposition of Graphene on Copper
Auteur: Author:	Saman Choubak
Date:	2015
Type:	Mémoire ou thèse / Dissertation or Thesis
Référence: Citation:	Choubak, S. (2015). The Impact of Hydrogen and Oxidizing Impurities in Chemical Vapor Deposition of Graphene on Copper [Ph.D. thesis, École Polytechnique de Montréal]. PolyPublie. https://publications.polymtl.ca/1732/

UNIVERSITÉ DE MONTRÉAL

THE IMPACT OF HYDROGEN AND OXIDIZING IMPURITIES IN CHEMICAL VAPOR DEPOSITION OF GRAPHENE ON COPPER

SAMAN CHOUBAK

DÉPARTEMENT DE GÉNIE PHYSIQUE

ÉCOLE POLYTECHNIQUE DE MONTRÉAL

THÈSE PRÉSENTÉE EN VUE DE L'OBTENTION

DU DIPLÔME DE PHILOSOPHIAE DOCTOR

(GÉNIE MÉTALLURGIQUE)

AVRIL 2015

UNIVERSITÉ DE MONTRÉAL

ÉCOLE POLYTECHNIQUE DE MONTRÉAL

Cette thèse intitulée:

THE IMPACT OF HYDROGEN AND OXIDIZING IMPURITIES IN CHEMICAL VAPOR DEPOSITION OF GRAPHENE ON COPPER

présentee par: CHOUBAK Saman

en vue de l'obtention du diplôme de : Philosophiae Doctor

a été dûment acceptée par le jury d'examen constitué de :

M. ROCHEFORT Alain, Doctorat, président

M. DESJARDINS Patrick, Ph. D., membre et directeur de recherche

M. MARTEL Richard, Ph. D., membre et codirecteur de recherche

M. MASUT Remo. A., Ph. D., membre

M. FINNIE Paul, Ph. D., membre externe

ACKNOWLEDGEMENTS

The completion of this thesis has been an amazing journey filled with many experiences from graphene growth to intellectual growth!

I had the opportunity to work under the direction of truly astonishing individuals: Patrick Desjardins and Richard Martel. Thank you for accepting me into your group and providing me your guidance and support.

Dear Patrick, there have been numerous occasions where I remember feeling disheartened and skeptical about the path that I am taking, but inevitably, a meeting with you has refreshed my enthusiasm and raised my spirits immeasurably. Your dedicated support and guidance have been invaluable over the past five years and I feel incredibly privileged to have you as my supervisor. Needless to say, I enjoyed every minute of our discussions and I will long remember those days.

Dear Richard, your wisdom, knowledge and exceptional passion for science has inspired me and enriched my growth as a student and researcher. Your enthusiasm in every stage of this project energized me and helped me to stay committed to attain excellence. I am extremely honored to work under your supervision.

I would like to express my gratitude to Pierre Levesque for his advice and crucial contribution to this research and thesis. I remember the day he asked me to work on graphene. I am glad that I accepted and played a part in a great scientific contribution to the field of material science. I owe him most of my hands-on skills related to vacuum systems. Thank you for kindly granting your time and for patiently answering so many of my questions.

I greatly appreciate the time and commitment of my dissertation committee members, Professor Alain Rochefort, Professor Remo Masut, and Dr. Paul Finnie to help me move this forward. Their questions and comments have certainly made great improvements to my thesis.

I would like to thank my research mates and collaborators, Maxime Biron, Etienne Gaufres, Philippe Gagnon, Minh Nguyen, Francois Lapointe, May Choueib, Beatrice Vanhorenbeke, Nathalie Tang, and Nicolas Cottenye for offering their expertise and advice all along this project.

I would like to gratefully acknowledge the help of Joel Bouchard, Khalid Laaziri for CVD system set-up and technical support and Josianne Lefebvre, Nicole MacDonald, Samir Elouatik, and Marie-Helene Bernier for providing their expertise in characterizing my samples.

These past several years have not been an easy ride, both academically and personally. Besides my incredible friends in Montreal and all around the world, I am extraordinarily fortunate to have a support group of former professors and colleagues who believed in me, encouraged me, and took a strong interest in my continued development and growth. Words fail me to express my gratitude to Robert Fleming, Toby Sainsbury, Emily Allen, Melisa Buie, and Franz Gisin.

Last but not least, I am grateful to my parents for their unconditional love and continued support. I would not have made it this far without them. Special thanks to my beloved Nader, without whose endless moral support, this task could have never been completed.

RÉSUMÉ

Le graphène, un matériau bidimensionnel constitué d'une monocouche d'atomes de carbone, a attiré l'attention des scientifiques et des technologues pour ses propriétés mécaniques, électriques et optoélectroniques remarquables. L'utilisation du graphène dans des applications pratiques nécessite toutefois le développement de méthodes de synthèse fiables et rentables pouvant produire de larges films de graphène avec une faible densité de défauts et une morphologie bien contrôlée. Une des méthodes les plus significatives est la croissance catalytique de graphène par dépôt chimique en phase vapeur (CVD) sur substrats métalliques. La croissance à haute température (850-1100°C) à partir d'un mélange d'hydrocarbures et d'hydrogène permet de produire de larges feuillets de graphène polycristallin et d'excellente qualité. Cette voie de synthèse est prometteuse car elle ouvre la voie à une production de graphène à grande échelle et une commercialisation massive de produits à base de graphène.

Cette thèse porte sur la synthèse du graphène sur des feuillets de cuivre polycristallin par la voie CVD à basse pression (LP-CVD) avec du méthane comme source de carbone et de l'hydrogène pour assurer un environnement réducteur. Plus précisément, elle porte sur la détermination du rôle de l'hydrogène et des impuretés oxydantes pendant la formation de graphène. Le but ultime de la thèse est d'élaborer les bases fondamentales pouvant mener à un procédé de croissance commercialement viable et reproductible de graphène de haute qualité pour d'éventuels procédés de fabrication industriels.

La première partie de la thèse traite du rôle de l'hydrogène moléculaire dans la croissance CVD de graphène. À partir d'expériences de recuits, certaines études ont affirmé que l'hydrogène moléculaire vient graver le graphène sur cuivre. Nous avons vérifié que cette gravure du graphène vienne plutôt de la présence de traces d'oxygène dans l'atmosphère du four ou dans la bombonne d'hydrogène. Pour cela, nous avons adopté une approche basée sur des expériences de recuits systématiques de graphène sur des feuilles de cuivre en présence d'hydrogène de différentes puretés. Le résultat le plus étonnant est la suppression de la gravure en présence d'hydrogène de ultra-haute pureté (UHP) à 825°C et 500 mTorr purifié avec un filtre commercial

pouvant éliminer l'oxygène. En contrepartie, l'exposition dans les même conditions de films de graphène à l'hydrogène UHP non-purifié ont généré une gravure du graphène. Cette réaction parasite a donc été associée non pas à l'hydrogène mais plutôt aux impuretés oxydantes présentes dans l'hydrogène UHP. Nous avons également déterminé que la gravure de graphène par les impuretés est catalysée par la surface de cuivre.

À la lumière de ces résultats, nous avons étudié plus systématiquement le rôle potentiel de l'hydrogène dans le procédé LP-CVD du graphène pendant la croissance et lors du refroidissement du réacteur. L'apport d'un mélange CH_4/H_2 pendant le refroidissement a été nécessaire afin d'éviter la gravure, ce qui est cohérent avec une compétition réactive des espèces pendant la croissance. Après la formation de graphène et en absence de méthane, le film de graphène est protégé de l'effet oxydant de l'oxygène résiduel pendant le refroidissement par une simple exposition à l'hydrogène UHP purifié.

Lorsque le niveau d'impuretés oxydantes est faible, des films continues et uniformes de graphène ont été obtenus en utilisant du méthane purifié (O_2 <1ppbV). En absence d'hydrogène, celui-ci joue un double rôle; d'abord un réducteur de l'oxyde de cuivre en surface pour former du cuivre métallique et ensuite d'une source de carbone pour la croissance. Ce résultat montre que la présence d'hydrogène n'est pas essentielle à la croissance de graphène lorsque l'atmosphère du réacteur est bien contrôlée. Différences morphologiques de graphène dans des conditions de purification contrôlée, c.-à-d. lorsque le niveau d'impuretés d'oxydantes est faible par rapport aux conditions standards, ont également été observées. Une couverture plus étendue et sous forme d'îlots de bi- et de multi-couches de graphène a été observée en présence uniquement de méthane purifié. La morphologie de ces îlots montre la présence d'une croissance non-commensurée (ou « twisted ») des couches subséquentes. Ces résultats suggèrent un comportement différent lors de croissance de graphène dans des conditions de purification contrôlées.

Après avoir déterminé le rôle de l'hydrogène et des impuretés oxydantes dans la synthèse de graphène par LP-CVD sur cuivre, la thèse aborde ensuite la problématique de la vitesse de croissance d'une monocouche continue. Les résultats en conditions contrôlées montrent une accélération importante de la cinétique de croissance du graphène sur cuivre. Avec cette

méthode, nous avons réduit le temps de croissance d'une couche complète à moins d'une minute, ce qui est entre 5 et 45 fois plus rapide par rapport aux recettes actuelles de la littérature. Cette accélération est attribuée à l'effet synergique de la diminution des résidus d'impuretés oxydantes grâce aux purificateurs de gaz et du rôle protecteur de l'hydrogène UHP purifié pendant la croissance et l'étape de refroidissement. Il est à noter que l'installation de purificateurs de gaz sur les lignes d'alimentation est entièrement compatible avec les procédés de fabrication industriels, car elle permet de réduire le coût de production de graphène en réduisant le temps de croissance et donc l'énergie nécessaire au procédé. Des mesures de spectroscopie Raman et de microscopie électronique à balayage ont permis de conclure que la qualité cristalline et l'uniformité des films de graphène demeurent inchangées, même pour ces conditions de croissance accélérées.

Enfin, en rassemblant tous les résultats obtenus dans cette thèse, nous remarquons que la croissance de multicouche de graphène est obtenue principalement dans des conditions de purification élevée et surtout par la présence d'un flux de méthane pendant le refroidissement. Sur la base de ces observations, une partie importante de bi- et de multi-couches semble se former pendant la phase de refroidissement plutôt que pendant la croissance. Bien qu'encore préliminaires, ces résultats surprenant pointent vers une hypothèse nouvelle que l'étape de refroidissement dans la formation de bi- et multicouche de graphène est à l'origine de la croissance multicouches.

L'ensemble des résultats de la thèse démontre que les impuretés oxydantes jouent un rôle important dans la croissance LP-CVD du graphène et explique les incohérences entre les recettes de croissance rapportées dans la littérature. Il montre également qu'il est nécessaire pendant la croissance de graphène de contrôler l'équilibre des pressions partielles venant des impuretés oxydantes avec de l'hydrogène. Finalement, cette thèse suggère une méthode générale qui permet d'améliorer l'uniformité et l'épaisseur de film de graphène sur des substrats de cuivre polycristallins.

.

ABSTRACT

Graphene, the single-atom layer of carbon, has attracted scientists and technologists due to its outstanding physical and opto/electronic properties. The use of graphene in practical applications requires a reliable and cost-effective method to produce large area graphene films with low defects and controlled thicknesses. Direct growth of graphene using chemical vapor deposition (CVD) on copper, in which carbonaceous gaseous species react with the metal substrate in the presence of hydrogen at high temperatures (850-1100° C), led to high coverage of high quality graphene, opening up a promising future for methods of this type and a large step towards commercial realization of graphene products.

The present thesis deals with the synthesis of graphene via low pressure CVD (LP-CVD) on copper catalyst using methane as the carbon precursor. The focus is mainly on the determination of the role of hydrogen and oxidizing impurities during graphene formation with an ultimate purpose: to elucidate a viable and reproducible method for the production of high quality graphene films compatible with industrial manufacturing processes.

The role of molecular hydrogen in graphene CVD is explored in the first part of the thesis. Few studies claimed that molecular hydrogen etches graphene films on copper by conducting annealing experiments. On the other hand, we speculated that this graphene etching reaction is due to the presence of trace amount of oxygen in the furnace atmosphere. Thus, we took another approach and designed systematic annealing experiments to investigate the role of hydrogen in the etching reaction of graphene on copper foils. No evidence of graphene etching on copper was observed when purified ultra high purity (UHP) hydrogen was used at 825 °C and 500 mTorr. Nevertheless, graphene films exposed to the unpurified UHP hydrogen were etched due to the presence of oxidizing impurities. Our results show that hydrogen is not responsible for graphene etching reaction and oxygen impurities are the main cause of this etching reaction. We have also determined that graphene etching reaction is catalyzed by the copper surface.

Next, we systematically investigated the role that hydrogen plays during the growth and coolingdown stage of LP-CVD of graphene on copper. We show that a flow of CH_4/H_2 is necessary during cooling for preventing graphene etching likely by the means of a competitive

action with carbon growth. After graphene formation, the film can be preserved from detrimental effect of oxygen in the absence of methane by its exposure to purified ultra high purity (UHP) hydrogen flow during cooling.

In conditions where the level of oxidizing impurities is low, we have obtained continuous and uniform graphene films using solely purified methane (O_2<1ppbV) serving a double role as a copper oxide reducer and carbon supply for the growth in the absence of hydrogen gas. This result shows that the presence of hydrogen is not necessary for graphene growth in a controlled atmosphere. Differences in graphene film morphology in purified conditions, where the level of oxidizing impurities is low (O_2<1ppb) compare to standard conditions (O_2<1ppm), have also been observed. A larger bilayer and multilayer coverage was noticed when only purified methane was used. These bi- and multi-layer graphene islands appeared to be twisted with respect to the first graphene layer. These overall results suggest a different graphene growth behavior in purified and controlled conditions.

Having investigated and understood the role of hydrogen and oxidizing impurities in LP-CVD of graphene on copper, we show a rapid and efficient growth of continuous monolayer graphene on copper within 1 min. This was achieved by minimizing the presence of oxidizing impurities with using gas purifiers installed on the gas lines and maintaining a flow of purified UHP hydrogen during the cooling down stage. With this method, we have reduced the graphene growth process time between 5 to 45 times compared to the current recipes in literature. Note that the installation of gas purifiers is entirely compatible with industrial manufacturing processes and is extremely profitable since it can lower graphene production cost by reducing process time and saving energy. Moreover, the crystalline quality and uniformity of the graphene films, determined by Raman spectroscopy and Scanning Electron Microscopy, stayed similar even at this short growth time.

Lastly, by gathering all the results during the evolution of this thesis, we notice that graphene multilayer growth is mainly occurring in highly purified conditions and most importantly when a flow of methane gas is present during the cool down stage. Based on these observations, a significant number of bi/multi layer formation can potentially arise when graphene is completed in the cooling stage. These results, although preliminary, point toward the influence of the cooling stage on graphene bi/multi layer formation.

The collection of our results presented in this thesis show that oxidizing impurities play a significant role in graphene LP-CVD and explain inconsistencies between growth recipes reported in the literature. They also provide a rational about the need to control the balance between oxygen and hydrogen pressures, for graphene growth pointing toward a general method for improving graphene layer thickness and uniformity on polycrystalline copper substrates.

TABLE OF CONTENTS

LIST OF FIGURES

NOMENCLATURE

Abbreviations

CNT	Carbon Nanotube
CVD	Chemical Vapor Deposition
AP-CVD	Atmospheric Pressure Chemical Vapor Deposition
LP-CVD	Low Pressure Chemical Vapor Deposition
UHV-CVD	Ultra High Vacuum Chemical Vapor Deposition
HF-CVD	Hot Filament Chemical Vapor Deposition
PE-CVD	Plasma Enhanced Chemical Vapor Deposition
UHP	Ultra High Purity
sccm	Standard Cubic Centimeter per Minute
SiC	Silicon Carbide
SLG	Single Layer Graphene
BLG	Bilayer Graphene
MLG	Multi Layer Graphene
TEM	Transmission Electron Microscopy
DF-TEM	Dark Field Transmission Electron Microscopy
WC	Wedding Cake
IWC	Inverted Wedding Cake
SEM	Scanning Electron Microscopy
FE-SEM	Field Emission Scanning Electron Microscopy
PMMA	Poly Methyl Methacrylate
AES	Auger Electron Spectroscopy
SAM	Scanning Auger Microscopy

LEEM	Low Energy Electron Microscopy
FE-LEEM	Field Emission Low Energy Electron Microscopy
LEED	Low Energy Electron Diffraction
N.A	Numerical Aperture
BTF	Bragg Tunable Filter
CCD	Charge Couple Device
HOPG	Highly Ordered Pyrolytic Graphite
ppm	Parts Per Million
ppb	Parts Per Billion
ppbV	Parts Per Billion by Volume

Symbols

r_i	Rate of reaction
P_X	Partial pressure of the element X
*	Unoccupied sites at the copper surface
θ_*	The fraction of free sites on the surface
θ_X	The fraction of the sites on the surface occupied by element X
k_i	Reaction constant
$k_i^{'}$	Counter reaction constant
K_i	Equilibrium constant of reaction
n	Order of the reaction
CH_4^*	Methane adsorbed onto the Cu surface
O_2^*	Oxygen adsorbed onto the Cu surface

LIST OF ANNEXES

CHAPTER 1 INTRODUCTION

1.1 The rise of graphene

Current technological developments in electronics result in miniaturization of devices which lead to denser, faster, and more power efficient circuits [1, 2]. During the past four decades, semiconductor industry has been able to improve the performance of electronic systems by making smaller devices. These advancements cannot continue everlastingly and will certainly encounter fundamental physical and technological limitations. The realization of the approaching limits has aroused a worldwide interest to develop alternative device technologies with new materials [1-4]. In the last two decades we have witnessed a remarkable shift of the dimensionality pattern in material science and technology. The rise of one dimensional carbon nanotubes (CNTs) opened new possibilities in nanotechnology that were not conceived in the past. An electrical conductivity as high as copper and thermal conductivity as great as diamond make them a perfect candidate for nanoelectronics [5, 6]. Their mechanical strength being 100 times more than steel while one sixth of the weight make them ideal for light structural materials. However, the constraints in processing, scaling up, and assembly methods remain a hurdle for many applications [5]. Next, graphene, a single atomic layer of sp^2-bonded carbon atoms packed to a two-dimensional honeycomb lattice, has attracted interest since its discovery in 2004 [7]. Its 2D structure and ease of lab scale processing favored fundamental research and opened an avenue to explore two-dimensional materials [7]. Graphene is endowed with many unique properties such as high carrier mobility at room temperature (~200000 $cm^2V^{-1}s^{-1}$) [8, 9], phenomenal optical transparency (~97.7%) [10], high tensile strength (Young's modulus of ~1TPa) [11], and excellent thermal conductivity (3000-5000 $Wm^{-1}K^{-1}$) [4, 12, 13].

Most studies investigating the fundamental properties of graphene have been performed using mechanically exfoliated graphene, known as scotch tape technique, from highly oriented pyrolytic graphite (HOPG) [1, 14]. Clean single sheets of graphene are produced using this method, which are suitable as a test-bed for fundamental research and exploration. Nonetheless, with exfoliation techniques micrometer- and sub-micrometer-sized graphene films are obtained

at random locations on the substrate making this method incompatible with industrial manufacturing processes due to the lack of reproducibility and scalability [1, 4, 15].

As mentioned above, graphene's exceptional electrical, optical, and mechanical properties make it a promising material for many technological applications such as flexible transparent electrodes [16, 17], high-frequency (GHz) transistors [18, 19], ultracapacitors [20], battery electrodes [21, 22], and composite materials [12, 23]. Since all of these applications require large area graphene produced via scalable techniques, finding alternative methods other than mechanical exfoliation becomes a topic of crucial importance. One possible approach is a top-down technique based on the chemical exfoliation of graphite or chemically reduced graphene oxide by sonication and intercalation in order to produce large quantities of graphene sheets [24]. However, the resulting layer is an ensemble of graphitic material containing residual oxygen that is far from having the high quality of the graphene monolayer produced using the scotch tape technique [12, 25]. The other alternative is the bottom-up epitaxial growth method, which results in high quality continuous but polycrystalline single layer graphene films [4, 12].

Early work on graphene synthesis focused on heating a silicon carbide (SiC) single crystal in high vacuum in order to remove the Si atoms from the crystalline surface and form a high quality graphene layer [26]. Although one of the fastest GHz circuits have been produced by this method [27], its commercial use seems unlikely. Silicon carbide substrate is very expensive and the heating process requires extremely high temperatures (i.e:1500° C), making it incompatible with manufacturing processes. The fact that the graphene layer grown on SiC cannot be transferred to other substrates is another drawback for this method [28, 29]. Later on chemical vapor deposition (CVD) of graphene on metal substrates became the most viable technique for producing large area graphene due to its scalability and compatibility with manufacturing processes [28, 30].

Up to now, graphene has been synthesized on polycrystalline Fe [31], Au [32], Ni [33], Cu [34] and on single crystals such as Ru (0001) [35], Ir (111) [36], Pt (111) [37] , Pd (111) [38], and Cu (111) [39]. The graphene growth mechanism on most of these metals (Ni, Ru, Ir, and etc.) is mainly precipitation-based since they can dissolve a large amount of carbon in bulk although some additional contributions from decomposition of the precursors on the metal surface attribute to the growth [28, 40]. During cool-down the carbon from the bulk precipitates at the

surface and forms graphitic layers. Controlling the number of layers at this stage is proven to be challenging [28, 40]. Moreover, some of the metals mentioned earlier are quite expensive since they are single crystals and high purity [40].

Copper reasonable price and low carbon solubility make it the best substrate for CVD graphene [28]. Currently, copper-based CVD is by far the most feasible production route for large-scale manufacturing of graphene films. Graphene sheets produced by this method present comparable quality to individual mechanically exfoliated graphite and they can be scaled up to hundreds of meters square by emerging roll-to-roll processes [41-43].

The most popular route for graphene growth was reported in 2009 by Li et al.[30]. They used methane as the carbon precursor and hydrogen as the reducing agent and carrier gas. Copper is exposed to a relatively low pressure of hydrogen and methane at high temperatures below its melting point and the graphene films are formed after 5-45 min depending on the recipe used [30]. Later on the method appeared as the most probable pathway for graphene commercialization followed by a large number of publications investigating wide gamut of graphene synthesis conditions.

The launch of this project coincided with the first report of the role of hydrogen in graphene CVD on copper. The conclusion drawn by those experimental observations led to defining molecular hydrogen as an etchant in the growth and post growth process shifting the attention of the graphene growth community towards controlling the amount or flowrate of hydrogen and its balance with methane during the graphene CVD. In the course of preparation of this thesis, initial studies on the understanding of the fundamental mechanisms that governs the kinetics of CVD growth of graphene considering hydrogen as etchant have been published and numerous graphene CVD recipes have been reported. While these efforts pointed toward finalizing the role of hydrogen in graphene CVD process, we on the other hand revisited this important conclusion, using a simple back of the envelope calculations, and determined that the partial pressure of the contaminants is comparable to the standard base pressure of the low pressure CVD chamber. That led us to postulate that these levels of oxidizing impurities can play a role not only in the growth process but also during cooling and their impact can no longer be ignored. Thus, we have opened a new chapter in this research field and shed light on the important processes involving

background impurities to the other fields such as surface science and catalysis. The results of our studies altered dramatically the knowledge shaped previously in graphene CVD field indicating the need to revisit the many conclusions drawn based on erroneous analysis with new insight.

In summary, this thesis covers the direct growth of graphene using chemical vapor deposition (CVD) on copper by exploiting the factors that directly impact its formation. All the process steps starting from substrate preparation, to graphene growth using methane and hydrogen, along with transfer of the end product are presented in details. The role of hydrogen and oxygen during growth and cooling down stages is particularly discussed and clarified.

1.2 Current challenges of graphene CVD growth on copper

Despite the great promise that graphene grown on copper has shown, little is known about the factors that determine its reproducibility, morphology, and final film quality. As we will detail in chapter 2, the main effort of the research was focused on varying the hydrogen to methane ratio in order to control the size, shape, and growth behavior of graphene domains [33, 44-49]. Moreover, the role of hydrogen-which was mainly present due to its reducing effect- became the key question. Few studies deduced that hydrogen is necessarily required for graphene CVD [50, 51], however others stated that graphene can be formed in the absence of hydrogen [44, 52]. Furthermore, Zhang el al.[53] reported hydrogen as an etchant and a growth activator for graphene. This particular conclusion was very unlikely creating a debate in the community.

Numerous articles were published on optimizing the quality of graphene films by varying the H_2 to CH_4 ratios, precursor gas flow rates, and total reactor pressure [33, 44-49] but recipes reported are inconsistent between each other. This raises the question about whether all the possible and crucial parameters or species affecting and controlling the growth are being considered. Most importantly the role of oxygen and oxidizing impurities were ignored. These impurities can mainly originate from the gas feedstock, air leaks in the chamber, and also the copper substrate which can potentially alter the growth of graphene films [54].

The next hurdle to overcome for graphene implementation in industrial applications is to grow continuous and high quality films at either low temperatures or in shorter amount of time in order

to conserve energy and lower the production cost [42, 43, 55-59]. Up to this date, numerous disparities exist in growth recipes and none shows a bright future. Although substantial efforts have been invested in this area, the question that how one can speed up the process remains.

The ultimate purpose of this thesis is to find a viable route to produce uniform graphene films having high quality compatible with industrial manufacturing standards. In order to approach the goal, we have first devised a set of systematic experiments to answer the important questions: 1) Do oxidizing impurities have an effect on graphene film? 2) What is the role of molecular hydrogen in graphene CVD growth? Or more specifically, do we need hydrogen in our growth recipe?

To answer these questions, we have used gas purifiers to minimize the amount of oxidizing impurities flowing into our growth chamber by installing them on the ultra high purity grade gas bottles. With this, we have clarified the role of hydrogen and the effect of oxidizing impurities, a significant factor that has never been considered to have a direct role in graphene CVD growth recipes answering the two important questions above. In addition, the potential role that hydrogen plays has become clear and is no longer hindered or misunderstood. Our results open the avenue for thoroughly comprehending the role of gases and most importantly the role of oxidizing impurities during the CVD growth of graphene layers. This is crucial for further improving graphene film quality and developing large single crystal graphene layers. Lastly, from the insight gained from our experimental studies, we proposed an entirely suitable method to manufacture large scale graphene films on copper in an energy and cost saving manner.

1.3 Objectives of the present work

The objectives we set out to accomplish at the beginning of this doctoral thesis project was to elucidate a viable and reproducible avenue for the production of continuous and high quality graphene films. The existence of uncertainties in this increasingly abundant literature, and the vast array of disorganized experimental results motivated us to investigate the CVD growth of graphene films on copper substrate in order to understand the interplay between the growing graphene honeycomb lattice and the role of gases, methane as the carbon precursor, and hydrogen as the reducing agent or carrier gas. In addition, finding a unique set up and recipe that

is compatible with industrial manufacturing of graphene films was desirable.

The thesis project can be summarized by the following detailed objectives:

- To establish whether molecular hydrogen is responsible for graphene etching on copper or other species such as oxidizing impurities should be accounted for this etching reaction
- To verify whether the presence of hydrogen is necessary for graphene growth on copper
- To determine the role of molecular hydrogen during the low pressure chemical vapor deposition (LPCVD) growth and post growth of graphene films on copper foils
- To implement a method to produce continuous and high quality graphene films on copper while ensuring compatibility of the process with industrial manufacturing standards.

1.4 Organization of the thesis

This work is presented in 8 chapters. In chapter 2 we introduce different methods of graphene growth and synthesis. An overview of recent advances in the field of graphene CVD fabrication is given, and includes a discussion on the role gaseous species particularly hydrogen. Moreover, graphene growth mechanisms and different processes for its large-scale production are discussed. Finally, characterization of graphene sheet morphologies and stacking order is presented. Chapter 3 provides in depth explanations of our experimental approach, covering the experimental techniques and characterization tools that were used during the course of this work.

The main body of the thesis is presented as three articles in Chapters 4-6 and an additional chapter (Chapter 7), which is dedicated to the formation of multilayers during the post growth cooling down process. In the first article (Chapter 4: "No Graphene Etching in Purified Hydrogen"), despite the common belief in literature, we have established that molecular hydrogen does not etch graphene films on copper and that oxidizing impurities are responsible for the graphene etching reaction.

The second article (Chapter 5: "Graphene CVD: Interplay between Growth and Etching on Morphology and Stacking by Hydrogen and Oxidizing Impurities") is a comprehensive investigation of the role of hydrogen and oxidizing impurities during Low Pressure CVD (LPCVD) growth of graphene films on copper.

The third article (Chapter 6: "Speeding-up graphene chemical vapor deposition") uses the insight and methodology gained in articles 1 and 2, to implement a method to grow graphene films in approximately 1 min, which is very rapid and hence beneficial for large-scale industrial production.

Finally chapter 8 contains the overall discussion, conclusions, and future perspectives of this work.

1.5 Publications and presentations by this candidate

This research has generated several results which were presented in the form of scientific journal publications, technological innovations (patent), poster and oral presentations. The three publications are embedded in the body of this thesis and the oral presentations are listed below.

PUBLICATIONS:

- Saman Choubak, Pierre L. Levesque, Philippe Gagnon, Minh Nguyen, Patrick Desjardins, and Richard Martel. *"Speeding-up Graphene Chemical Vapor Deposition."* Submitted to the Journal of Advanced Materials.
- Saman Choubak, Pierre L. Levesque, Maxime Biron, Etienne Gaufres, Patrick Desjardins, and Richard Martel. *"Graphene CVD: Interplay between growth and etching on morphology and stacking by hydrogen and oxidizing impurities. "* Journal of Physical Chemistry C, 2014, 118, 21532-21540
- Saman Choubak, Maxime Biron, Pierre L. Levesque, Richard Martel, Patrick Desjardins. "*No Graphene Etching in Purified Hydrogen*." Journal of Physical Chemistry Letters, 2013, 4, pages 1100-1103

POSTER & PRESENTATIONS

- Oral Presentation: **Saman Choubak**, Pierre L. Levesque, Etienne Gaufres, Maxime Biron, Richard Martel, Patrick Desjardins.*" Graphene CVD: Interplay between growth and etching on morphology and stacking by hydrogen and oxidizing impurities."* Fourth International Symposium of Graphene Devices, Bellevue, Washington, USA, September 21-25, 2014.
- Poster: **Saman Choubak**, Pierre L. Levesque, Maxime Biron, Richard Martel, Patrick Desjardins. "*The role of hydrogen in low pressure chemical vapor deposition of graphene films.*" RQMP Grande Conference, Montreal, Canada, May 16, 2014.
- Oral Presentation: **Saman Choubak**, Pierre L. Levesque, Maxime Biron, Richard Martel, Patrick Desjardins."*The impact of hydrogen and oxidizing impurities in chemical vapor Deposition growth of graphene films."* MRS, Fall Meeting, Boston, Massachusetts, USA, December 1-6, 2013.
- Poster: **Saman Choubak**, Pierre L. Levesque, Maxime Biron, Richard Martel, Patrick Desjardins. "*The role of hydrogen in low pressure chemical vapor deposition of graphene films.*" Gordon Research Conferences (GRC) , Thin Film and Crystal Growth Mechanism, Biddeford, Maine, USA, July 7-12, 2013.
- Poster: **Saman Choubak**, Maxime Biron, Pierre L. Levesque, Etienne Gaufres, Nicolas Cottenye, Philippe Gagnon, Francois Lapointe, Richard Martel, Patrick Desjardins. "*Graphene studies: from growth to electrical transport*." RQMP Grande Conference, Montreal, Canada, May 17, 2013.
- Oral Presentation: **Saman Choubak**, Maxime Biron, Pierre L. Levesque, Richard Martel, Patrick Desjardins. "*No evidence of graphene etching in hydrogen*." European Workshop on Epitaxial Graphene EWEG, Aussois, France, Jan 27-31, 2013.

PATENT:

- **Saman Choubak**, Pierre L. Levesque, Philippe Gagnon, Patrick Desjardins, and Richard Martel. *"Graphene Rapid Formation on Copper via Chemical Vapor Deposition."* In Preparation.

CHAPTER 2 LITERATURE REVIEW

In this chapter, we introduce graphene and Raman spectroscopy which is widely used to characterize graphene sheet morphologies and stacking order. Next, the variety of synthesis and fabrication methods that lead to graphene production is presented. Moreover, graphene growth mechanisms and different processes for its large-scale production are discussed. In addition, the controversial subject of the formation mechanism of graphene bilayer and multilayers is reviewed. Finally, an overview of recent advances in the field of graphene CVD, the role of process condition parameters, and the influence of gaseous species particularly hydrogen and oxygen are given.

2.1 Graphene

Graphene is a flat monolayer of carbon atoms tightly packed into a two-dimensional (2D) honeycomb lattice. It is also the fundamental element for graphitic materials of all other dimensionalities. As shown in Figure 1, 0D fullerenes can be envisioned as enfolded graphene, whereas 1D nanotubes can be considered as graphene rolled up on itself whereas 3D graphite are stacked up graphene layers [1, 2, 60, 61]. As illustrated in Figure 2-1, the graphene lattice consists of regular hexagons with a carbon atom at each corner. The bond length between adjacent carbon atoms is 1.42 Å and the lattice constant is 2.46 Å [1, 2, 60, 61].

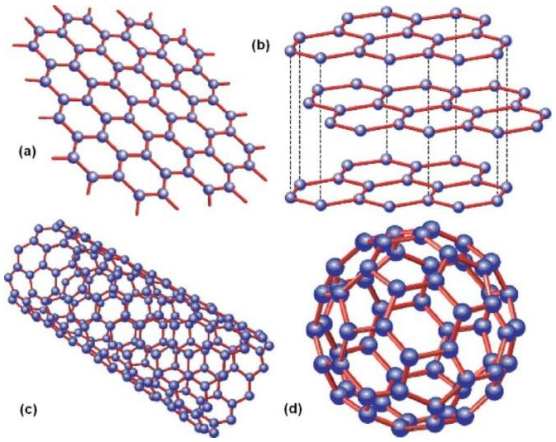

Figure 2-1. a) Mother of all graphitic forms graphene is a 2D building material for carbon materials of all other dimensionalities. b) It can be stacked in 3D to form graphite, c) rolled into a cylinder to give 1D nanotubes, and d) wrapped up into 0D to form buckyballs. Reprinted with permission from Ref. [1], © 2007, Nature Publishing Group.

2.2 Raman spectroscopy of graphene

Raman Spectroscopy is a convenient technique to identify and count the number of graphene layers. Raman fingerprints for single layers, bilayers, and few layers reflect changes in the electronic structures and allow clear, high-throughput, nondestructive identification of graphene layers [62, 63]. We have witnessed a major evolution in the understanding of Raman spectroscopy in graphene in the last six years. Indeed, new results on graphene doping, chemical functionalization, hydrogenation, interlayer coupling, and so on, considerably changed the understanding of the basic Raman processes [64]. Changes in the electronic properties due to defects, edges, doping, and multilayers can all strongly impact positions, widths, and intensities of Raman peaks [62, 64-66].

Figure 2-2 shows the 514 nm Raman spectrum of graphene deposited on SiO_2 substrate. The two most intense features are the G peak at 1580 cm^{-1} and a band at 2700 cm^{-1} historically named G' (or 2D). Uniform, single layer graphene are characterized by an integrated intensity of the 2D peak (I_{2D}) over the integrated intensity of the G peak (I_G) greater than 2 (I_{2D}/I_G >2) and a sharp, Lorentzian 2D peak with a full width half maximum (FWHM) narrower than 35 cm^{-1}. The D peak, around 1350 cm^{-1}, reveals the presence of defects. The D' band is also a disorder induced feature which appears at 1620 cm^{-1}.Overall, Raman spectroscopy allows to unambiguously determine the number of graphene sheets, up to 5 layers [62-63,70].

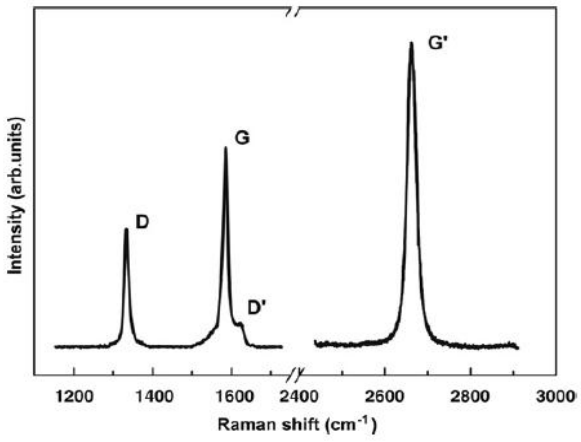

Figure 2-2. Raman Spectra of graphene acquired using an incident wavelength of 514 nm. Graphene can be identified by the position and shape of its G (1580 cm^{-1}) and G' (2700 cm^{-1}) peaks. Reprinted with permission from Ref. [70], © 2009, Elsevier.

Note that Raman spectroscopy is mainly carried out to characterize the quality of graphene films. The absence of D and D' peak in the Raman spectra is indicative of a defect free graphene layer commonly referred to as "high quality" [13,28,30,40,62,63,70]. Some graphene samples grown by chemical vapor deposition (CVD) exhibit additional peaks between 1450 $cm^{-1}$and 1525cm^{-1} (so-called R) and also above the G band at ~1620 cm^{-1} (so-called R' or D'). These bands emerge in bilayer and multilayer samples in which the individual layers are rotated with respect to another (twisted bilayer graphene (tBLG) [64, 66-70]. The D and D' bands are attributed to structural disorder. Their precise positions depend on the excitation energy (E_L); for example, they appear at 1350 cm^{-1} and 1620 cm^{-1} for E_L=2.41 eV. The R and R' bands that appear at ~1450-1525 cm^{-1} and ~ 1625 cm^{-1}, respectively, assigned to a superlattice-induced Raman process and their frequencies are independent of the laser energy. These modes have been ascribed to intervalley and intravalley interactions between two rotated graphene layers [64, 66-70]. Figure 2-3 shows a) the schematic of a rotationally stacked bilayer graphene, and b) the actual representative optical micrographs of the CVD samples transferred onto a SiO_2/Si substrate. Figure 2-3c is the Raman spectra of the samples in b in the G band range; R and R' band ranges are highlighted in yellow [66, 67].

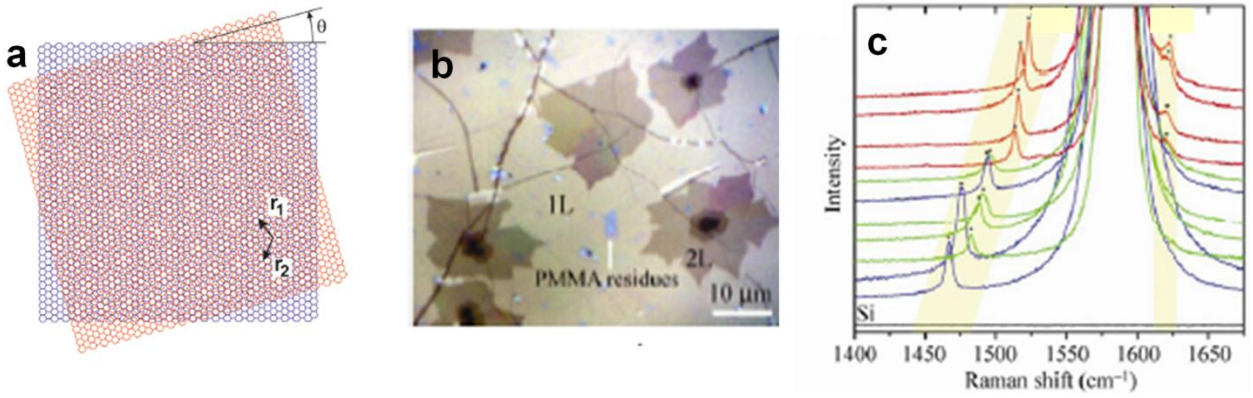

Figure 2-3. a) The schematic of a rotationally stacked bilayer graphene, and b) the actual representative optical micrographs of the CVD samples transferred onto a SiO_2/Si substrate, and c) the Raman spectra of the samples in b in the G band range where the R and R' bands are highlighted in yellow. Reprinted with permission from Ref. [67,68], © 2011,2013, American Chemical Society and Springer.

Havener el al. [65] used transmission electron microscopy along with wide field Raman imaging in order to study the correlation between the angle and Raman intensity of twisted bilayer graphene. They observed an enhancement of the G band intensity and they proposed that this

enhancement can be related to the presence of a singularity in the joint density of states of tBLG. Figure 2-4 is a representative DF-TEM image together with wide field G and 2D band maps acquired using an excitation energy of 2.33eV of one area containing 10 different tBLG domains with varying Θ values shown in Figure 2-4b. The data shows a strong enhancement of the G band integrated area (A_G) for a few specific domains, such as 12.4° domain in Figure 2-4b, while all others show similar enhancement intensity. They have further investigated this behavior and obtained full Raman spectra for each domain (Figure 2-4b) in order to quantitatively relate the G band area (A_G) and the twist angle [65].

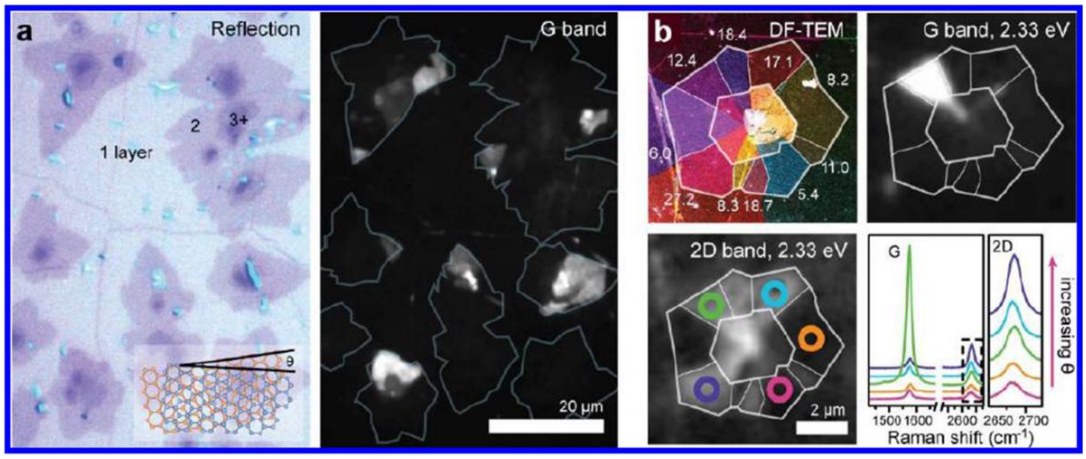

Figure 2-4. a) An optical reflection image of CVD graphene transferred to SiO2/Si and a large area widefield G band Raman image of the same region (the inset is the structure of tBLG with a twist angle Θ, b) Dark-field TEM, G band Raman images of the same multilayer tBLG sample and Raman spectra from several domains are also shown. Reprinted with permission from Ref. [66], © 2012, The American Chemical Society.

The integrated area of the G peak (acquired at a fixed laser excitation energy of E_{ex}= 2.33eV) is plotted in Figure 2-5 as a function of twist angle measured by TEM (A_G vs $Θ_G$). Twist angle in the range of 11° to 16° can be determined by the enhancement of the G peak with this specific laser excitation energy. The data presented here form a curve with strong enhancement near one specific twist angle (12.4 °) [65].

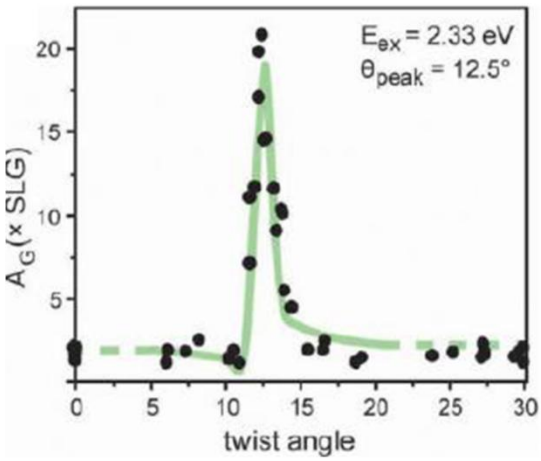

Figure 2-5. The plot of G band integrated intensity (A_G) vs Θ across many tBLG samples. Reprinted with permission from Ref. [66], © 2012, The American Chemical Society.

In this thesis, we used Raman spectroscopy and Raman imaging as a tool to characterize our samples in order to understand the CVD of graphene layer on copper and to distinguish different process condition factors that might have an effect on film quality and layer commensurability. Note that in this chapter, we have focused on Raman results that are directly relevant to the work reported in the thesis.

2.3 Graphene fabrication

To this date, graphene based electrical devices have been fabricated by a number of different methods such as 1) micromechanical cleavage of graphite (known as scotch tape technique) [14], 2) chemically reduced graphite oxide [12], 3) ultra high vacuum annealing of silicon carbide (SiC) [26], and 4) graphene synthesis on metal substrates via chemical vapor deposition (CVD). However, these techniques have downsides of central importance: the scotch tape technique for example leads to the production of very small graphene films [14], whereas the chemically reduced graphite oxide graphene electrical properties does not fully recover from its oxidized sheets [12]. Finally the graphene grown on SiC substrates is difficult to transfer to other substrates, such as Si, for integration with Si-based devices [28, 29]. Nevertheless, CVD graphene yields to a uniform graphene film whose size is limited only by the size of the substrate and the growth parameters [13, 28-30, 45]. Once a uniform graphene layer is grown, it can be

transferred onto an arbitrary substrate of choice via both wet and dry transfer techniques [13, 40, 71].

Direct growth of graphene using chemical vapor deposition (CVD) on certain metal catalysts such as Ni and Cu led to high coverage of high quality graphene, opening up a promising future for methods of this type and a large step towards commercial realization of graphene products [28, 30]. Graphene CVD offers unique aspects: first and foremost, it allows large area and uniform graphene synthesis with low defects on a wafer scale. Secondly, it permits the exploration of a wide gamut of transition metals as catalysts (substrates), and finally it enables one to develop a profound understanding of graphene nucleation and growth mechanisms on metal catalysts [13, 28, 30, 40].

Graphene CVD has been synthesized on numerous transition metals, including nickel, copper, ruthenium, iridium, silver, gold, and cobalt [29]. Graphene thermal CVD – in which the growth reaction occurs at the hot metal surface (850-1100° C) – has been achieved with a variety of hydrocarbon precursors, including methane, ethane, and acetylene. In this method, the metal substrate provides the surface for the decomposition of the carbon species and the nucleation of graphene crystals [28, 30]. Alternative CVD techniques such as hot filament CVD (HF-CVD) are also used to grow graphene on copper foils. In this method, the current is passing through a filament and reach temperatures as high as 2000 °C. Methane and hydrogen flow through a gas shower on the hot filament while the copper foil is placed right below the filament. The substrate temperature (in this case copper) depends on how far it is from the filament. Hydrocarbon gas, namely CH_4 decomposes by thermal means using the hot filament and forms carbon radicals. These carbon radicals reach the Cu surface and form graphene layers. The advantage of this technique is the fast cooling rate since the substrate can reach room temperature in seconds, however, the graphene films grown on copper are not exempt from defects. This technique has been previously used for the fabrication of diamond films and CNT. In addition, growing graphene at low temperature and directly on dielectric substrates is desirable. To achieve this goal, plasma-enhanced CVD (PE-CVD) techniques have been proposed [13]. In this method, plasma facilitates the dissociation of hydrocarbons into reactive radicals at low temperature while the substrate temperature can be held as low as 600 °C. Although graphene films are grown using this technique, the quality is not comparable to that of thermal CVD. Due to the low process temperature, graphene grain sizes are reduced since surface diffusion of carbon atoms is

limited on the substrate [13]. In addition multilayer growth is observed due to the high amount of carbon radicals generated by the plasma [72]. Thus, the graphene films grown with this technique are highly defective and lack thickness homogeneity [13, 72]. Figure 2-6 shows schematic representation of thermal, HF-, and PE- CVD.

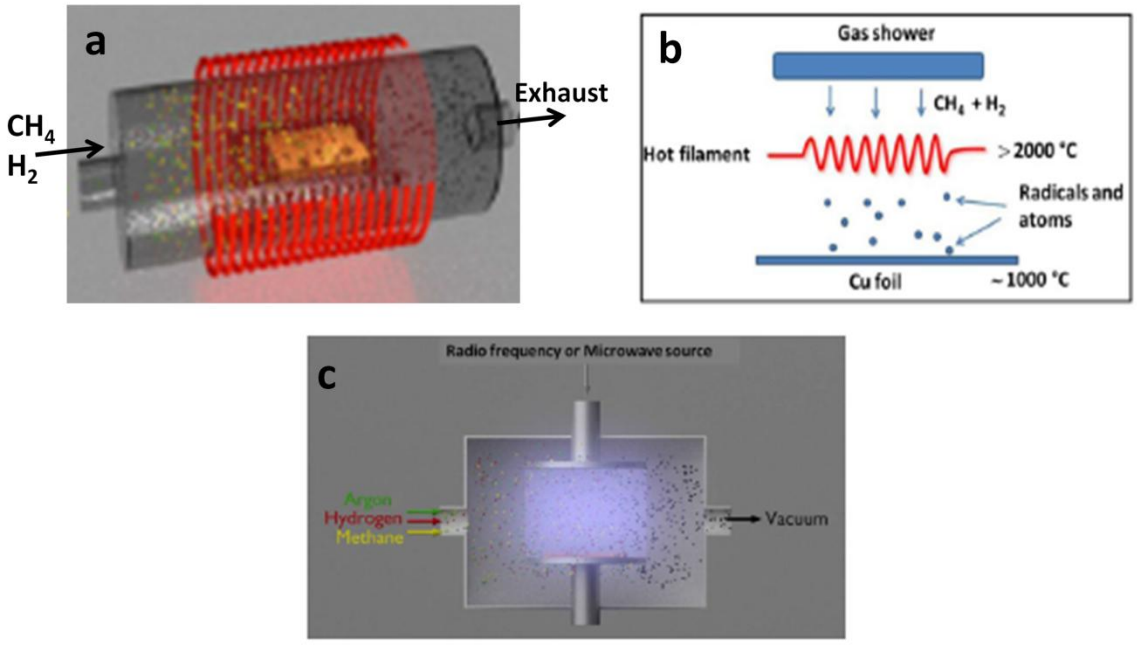

Figure 2-6. a) Schematic of typical CVD of graphene using CH_4 as a carbon precursor, b) Diagram of the hot-filament HF- CVD set up, and c) Plasma-enhanced CVD (PE-CVD) set up for graphene growth.Reprinted with permission from Ref. [14], © 2014, Wiley.

Factors such as carbon solubility limit in the metal, its lattice parameters, and crystal structure, as well as process parameters including pressure and temperature, impact the nucleation and growth mechanisms of graphene on the metal catalyst [28, 30, 45]. In general, different growth mechanisms have been ascribed mainly to the carbon solubility in the metal. In the case of catalysts having very low carbon solubilities (<0.001 atomic %) such as Cu, it has been demonstrated that the synthesis of graphene occurs only on the surface of the catalyst. In contrast, on catalyst metals having larger C solubilities (>0.1 atom %), including Co and Ni, graphene synthesis is proposed to proceed via a combination of diffusion into the metal thin film at the growth temperature, and a precipitation of carbon from the bulk to the surface of the metal

upon cooling after CVD synthesis [28-30, 45]. Figure 2-7 shows schematic diagrams of graphene growth mechanisms on Ni and Cu substrates.

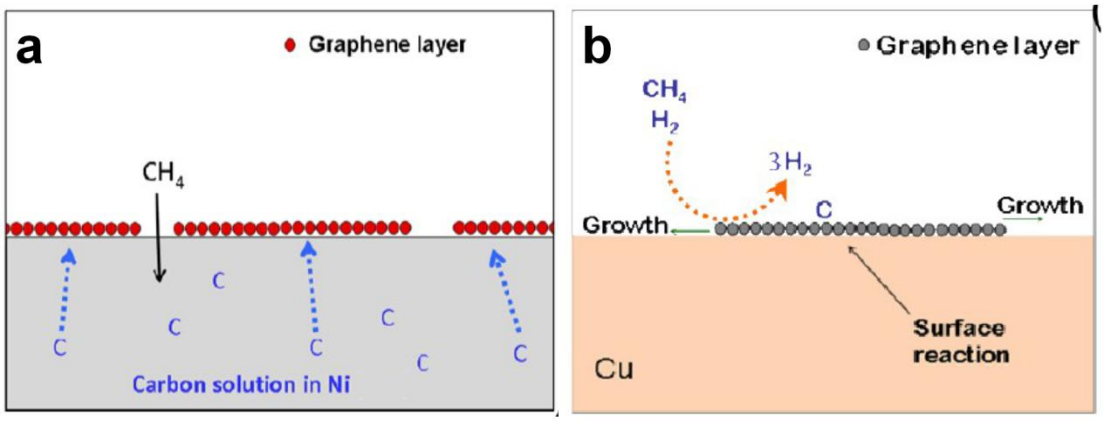

Figure 2-7. Schematic diagrams of graphene growth mechanisms on a) Ni and b) Cu. Reprinted with permission from Ref. [41], © 2013, The American Chemical Society.

As mentioned above, graphene formation on Ni is based on a segregation process; thus multilayer formation is inevitable. However, only small amounts of carbon dissolve on copper and graphene formation occurs through surface reactions. In principle copper catalyzes the decomposition reaction of hydrocarbons and once the copper is fully covered with graphene no bare copper remains and the growth stops [40].

Large area graphene synthesis on copper foils received great attention due to the few reasons summarized here: 1) the low solubility of carbon in copper limits the amount of segregated C therefore leading to a better control of graphene film growth over a reasonable temperature range (800-1000° C); 2) the absence of the copper carbide compound ensure that the Cu/C has only a binary phase diagram; 3) the ease of selecting a wet etchant that does not attack the graphene film while dissolving copper; 4) the low cost of copper relative to other metals makes the graphene production more affordable [28-30].

With all these being said, the introduction of a method to prepare free-standing graphene, single 2D carbon sheets with the same structure as the individual layers in graphite, has initiated tremendous scientific activities [1, 7]. The publication and research studies in this area are so vast that they cannot be all summarized in this review; however, the fundamental literature that is under the scope of this thesis will be covered. The attention is mostly given to the CVD growth

of graphene on copper substrates, in the low pressure growth condition, although some atmospheric pressure CVD data relevant to this thesis will also be reviewed. Our main focus is on the role of hydrogen, methane, and oxidizing species during graphene CVD and how they impact the formation of graphene sheets (i.e. shape, size) and their quality. These are largely explored in literature by altering the partial pressures of methane and hydrogen or the ratio between them during the growth. Furthermore, we discuss the latest production routes for large scale manufacturing of graphene films and their consequent integration into industrial applications.

2.4 Graphene CVD on copper

Graphene growth on copper is in principle straightforward and involves the decomposition of the hydrocarbon of choice, such as methane or ethylene gas, over a copper substrate typically held at 1000 °C [1, 2, 4, 7, 13, 28-30, 40, 46, 73]. The specific growth parameters that have been utilized for achieving the best graphene film on copper are summarized in reference 28. Most of the depositions have been on polycrystalline copper foils with thicknesses ranging from 25 to 50 μm. Although the most commonly used deposition temperature is 1000 °C, growth at temperatures ranging from 800 to 950 °C have also been reported [13, 28, 40, 73]. The CVD of graphene on copper is done under low (0.5-50 Torr) or atmospheric pressure of methane and hydrogen gas mixture at various ratios [28]. Interestingly, the size and shape of graphene domains vary in the literature with the fraction of hydrogen and methane in the gas flow; however, no clear understanding of this phenomena has emerged [45, 48, 50, 53].

The copper foils pretreatment is also crucial in getting large graphene domains. The as- received Cu foils are covered by native oxide (CuO, Cu_2O) suppressing copper surface catalytic activity [28, 30]. In order to facilitate growth of graphene sheets, before carbon deposition, the Cu substrate must be annealed in a hydrogen reducing atmosphere at 1000 °C. The annealing step prior to carbon deposition is also important because it increases the Cu grain size and rearranges its surface morphology, such as introduction of atomic steps and elimination of surface structural defects. The copper foils are annealed for 30 minutes in most cases. Figure 2-8 illustrates the three main stages of graphene growth on Cu by CVD [13, 28, 30, 40].

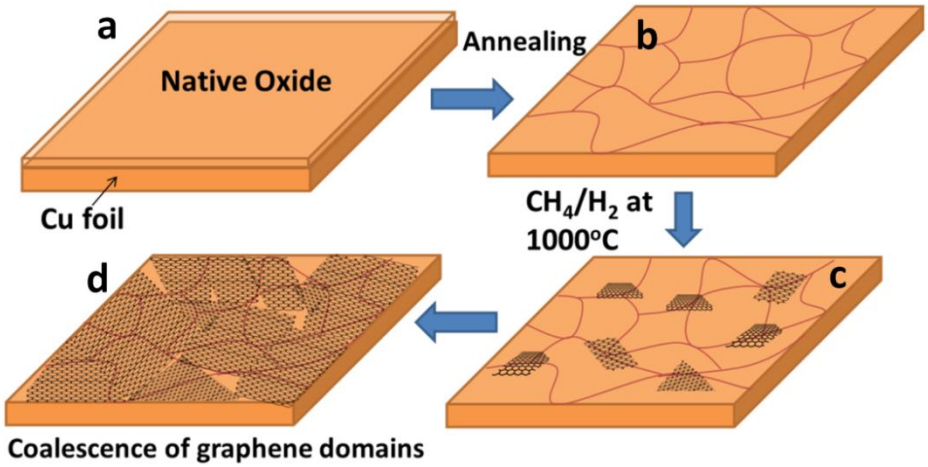

Figure 2-8. Schematic illustration of the main stages of graphene growth on copper by CVD: a) copper foil with native oxide; b) the exposure of copper foil to H_2 atmosphere at 1000° C leading to an increase in Cu grain size; c) the introduction of CH_4 along with H_2 and nucleation of graphene crystal, and d) the enlargement of graphene flakes with different in-plane lattice orientations. Reprinted with permission from Ref. [29], © 2010, Royal Society of Chemistry .

Scanning electron microscope images of the growth of single layer graphene at different times are shown in Figure 2-9. In Figure 2-9a, graphene islands of finite size (indicated by large oval) and the nucleation site of one of the other islands (indicated by smaller oval) are shown [30]. As growth proceeds, the graphene domains progressively increase in size until coalescing and forming a continuous layer. The weak interaction between graphene and the Cu substrate permits the expansion of graphene islands over the grain boundaries with minimal structural perturbation. The presence of wrinkles in the as-grown graphene is generally attributed due to the difference in the thermal expansion coefficients (TEC) between graphene and copper. The large negative graphene TEC ($\alpha_{graphene}$=(-6x10^{-6} /K)) at room temperature compare to copper TEC (α_{copper}= 24x10^{-6}/K) leads to huge shrinkage of Cu upon cooling inducing mechanical stress on graphene. This stress is released via the formation of wrinkles [28, 30, 73].

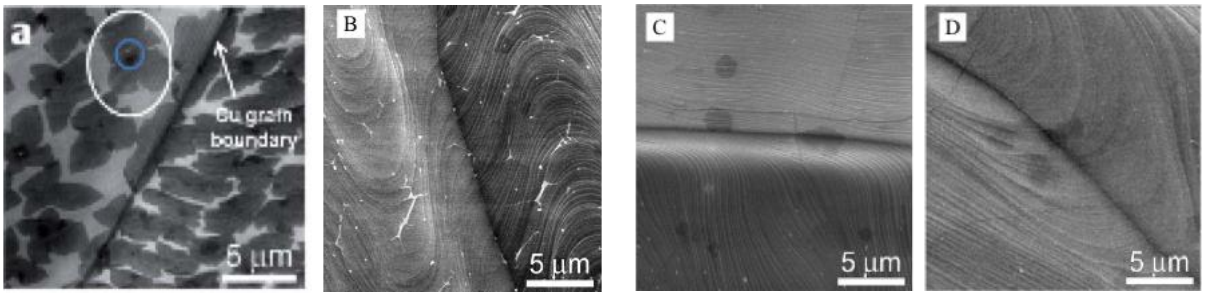

Figure 2-9. SEM images of graphene on Cu via methane/hydrogen mixture (A) 1 min, (B) 2.5 min, (C) 10 min, and (D) 60 min. Reprinted with permission from Ref. [30], © 2009, The American Association for Advancement of Science.

2.5 Industrial large scale production

In order for graphene to become useful in practical applications, its industrial scale production with good uniformity and low defect density is essential. Thus, it needs to be produced with low cost and feasible techniques. In this section, we highlight the mile stones achieved up to this date in this area.

Bae et al. [43] have developed a roll-based graphene synthesis and transfer process. They took advantage of the CVD method and the copper foil flexibility to scale up the graphene film production. They used an 8 inch tubular quartz CVD reactor for the production of monolayer graphene on a roll of copper with dimensions as large as 30 inches in the diagonal direction (Fig. 2-10). The CVD process is similar to what is common in CVD technique (i.e.: T=1000 °C, hydrogen flow for 30 min, introduction of the methane for 30 min, and finally the cooling down under hydrogen or both gases.) Once the growth step terminates, the graphene films on copper are attached to a thermal release tape by simply applying a soft pressure between the two rollers. The etching of copper foil is done in the next step where a bath of copper etchant is present. After the etching step, the transferred graphene film on the tape is rinsed with deionized water to remove the residual etchant, and thus it is ready to be transferred to any kind of surface. The graphene film on the thermal release tape is inserted between the rollers together with a target substrate while it is heated between 90-120 °C so that the tape is released and graphene can be transferred on the targeted substrate. This method is industrially scalable and fairly easy to

implement. (See Figure 2-10)

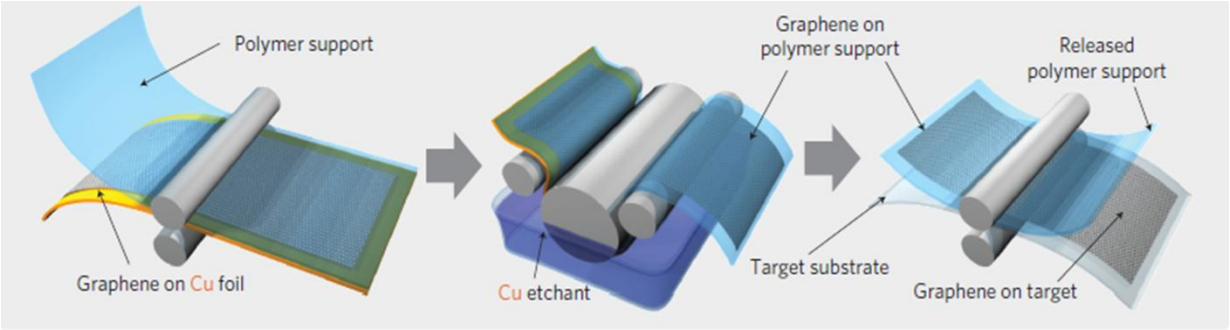

Figure 2-10. Schematic of the roll-based production of graphene films grown on copper foil. The process includes adhesion of polymer supports, copper etching (rinsing), and dry transfer-printing on a target substrate. Reprinted with permission from Ref. [44], © 2010, Nature Publishing Group.

Later on Liu et al. [74] reported graphene CVD by heating the copper foil locally using two graphite electrodes. With this system, the foil gets to high temperature at a shorter amount of time and it can also be cooled down rapidly. This method although in its infancy was beneficial in terms of energy saving. However, the quality of the films were not comparable to other existed graphene layers produced using conventional CVD method and bi - multi-layers, and sometimes holes were present on the graphene film [74]. Taking into account the roll to roll process and the local heating method, recently Kobayashi et al. [42] developed a roll to roll CVD system with a vacuum chamber, a pair on winders, and a pair of current feeding electrode rollers separated by a distance. The copper foil is suspended between the rollers and is thus heated to a temperature of 1000 °C by Joule heating. The gases are introduced to the chamber and graphene CVD process is taking place inside. This set up is advantageous as it conserves energy and the copper can be cool down to room temperature in no time. Continuous graphene coverage was observed, but it was only close to the center of the copper foil, pointing out a heat loss at the edges due to a non negligible temperature drop. Moreover, microcracks were visible on the graphene sheet lowering the quality of the film [42]. A schematic of the set up is shown in Figure 2-11.

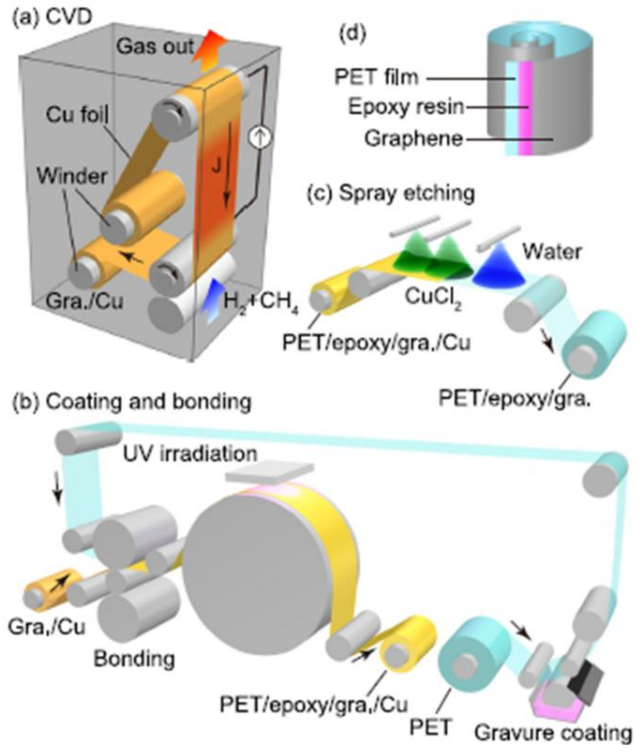

Figure 2-11. a) Continuous roll-to-roll CVD system using selective Joule heating to heat the copper foil suspended between two current feeding electrodes. b) Reverse gravure coating of a photo curable epoxy resin onto a PET film and bonding to the graphene/copper foil, followed by curing up the epoxy resin. c) Spray etching of the copper foil with a $CuCl_2$ solution. d) Structure of the fabricated graphene/epoxy/PET film. Reprinted with permission from Ref. [43], © 2013, AIP Publishing LLC.

2.6 Graphene multilayer growth mechanism on copper

The formation mechanism of graphene bilayer and multilayers during the CVD is not well understood. The graphene growth community anticipated the arrangement of graphene multilayers to be similar to that in typical crystal growth [75] where the graphene layers are stacked on top of one another meaning that the smaller sheets are grown on top of the larger layers [76, 77]. Few studies have mentioned this growth behavior (see Figure 2-12) whereas the field remained largely unexplored.

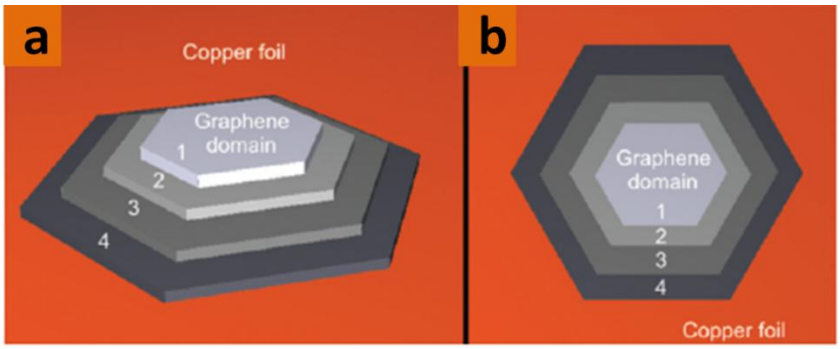

Figure 2-12. a) A 3D schematic representation of a few layer graphene domain on copper foil, and b) Top view of a. Reprinted with permission from Ref. [77], © 2012, The American Chemical Society.

Later on Nie et al. [78] reported an underlayer growth mechanism where the second and subsequent layers are grown from below. They believe that new layers nucleate and grow next to the substrate since copper is catalyzing the hydrocarbon decomposition and the graphene multilayer growth terminates once the Cu is covered with the main layer, therefore the smaller layers are formed beneath the main layer.

After their results were published, two contradictory growth models, the inverted wedding cake (IWC) or underlayer growth mechanism [78-81] and the wedding cake model (WC) or on-top growth mechanism [76, 77, 82] became subject of an intense debate in the literature. Figure 2-13 shows a cross sectional schematics of graphene layers on copper illustrating the differences between these two growth models.

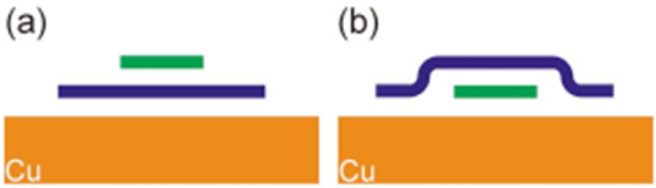

Figure 2-13. Cross sectional schematic of graphene layers on a Cu substrate. a) On-top growth, b) Underlayer growth Reprinted from Ref. [79], open access.

Li et al. [79] studied the growth of bilayer and multilayer graphene on copper by isotopic labeling of the methane precursor in order to understand the stacking order of graphene films.

They grew graphene by sequentially introducing isotopically labeled methane $^{12}CH_4$ first and then $^{13}CH_4$. They transferred the samples onto the SiO_2/Si substrate and exposed the transferred sample to oxygen plasma in order to introduce defects on the film. Based on the Raman measurements, a D_{12} defect peak at 1350 cm^{-1} associated with ^{12}C appeared on the Raman spectrum after the oxygen exposure. This clearly showed that the ^{12}C graphene layer is on the top layer in their samples since no ^{13}C defect band was detected in the Raman spectrum. Figure 2-14 shows the Raman map of the G_{12} (1560-1600 cm^{-1}) band intensity from the transferred graphene before and after oxygen exposure along with cross-section of the graphene layers at the position marked in (a,b) by a white line respectively. Lastly, the Raman spectrum of the positions indicated in c and d is shown.

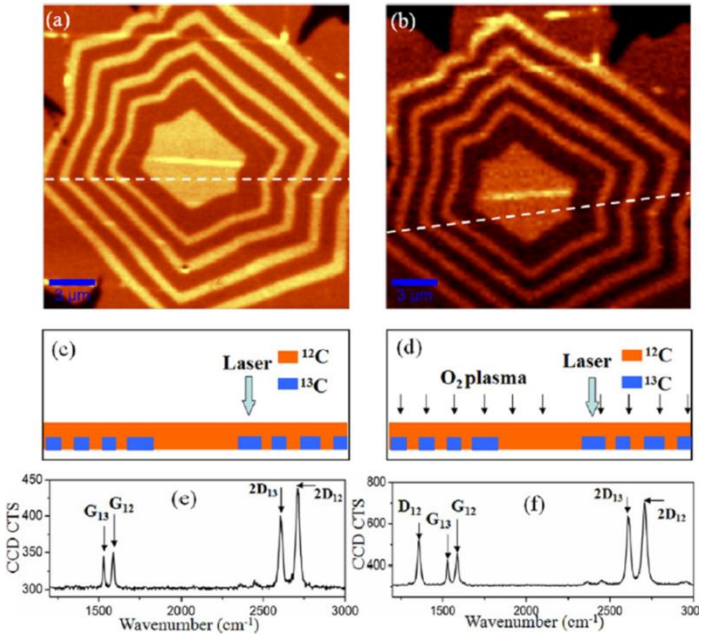

Figure 2-14. Raman isotopically labeled bilayer graphene before and after oxygen plasma etching. (a,b) The Raman map of the G_{12} (1560-1600 cm^{-1}) band intensity from the transferred graphene before and after the oxygen exposure (c,d) cross-section of the graphene layers at the position marked in (a,b) by a white line respectively (e,f) the Raman spectrum of the positions indicated in c and d. Reprinted with permission from Ref. [80], © 2013, The American Chemical Society.

Similarly, Fang et al. [80] selectively modified the top surface using a fluorination XeF_2 treatment to see whether the second layer is grown on top or at the bottom. Fluorinated C atoms

are sp^3-bonded thereby leading to drastic changes in Raman spectra. Comparing isotopic labeling and fluorination results, they concluded that the ^{13}C layer was on the bottom since no change was observed in the Raman spectrum after surface modification confirming that the ^{12}C layer was protecting it. While these observations point toward the IWC model, Kalbac et al. [82] rather suggested the on-top growth mechanisms or WC model. They believe that the graphene layers are grown on top of the main layer with different growth rates. They attribute this behavior to the presence of an excess amount of carbon leading to multilayer growth as a WC or the presence of hydrogen that etches the top layer - since top layer is more accessible to hydrogen-while the main layer is growing. Recently, Zhang et al. [81] proposed a growth model where IWC growth mechanism is possible at relatively higher hydrogen pressure whereas at low hydrogen pressure the growth is terminated and is limited to single layer. Figure 2-15 is a schematic representation of the growth mechanism proposed by a) Zhang et al. [81] and b) Li et al. [79].

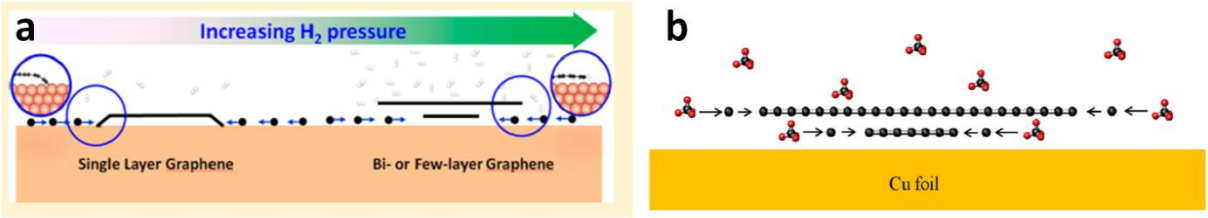

Figure 2-15. Schematic representation of the graphene growth mechanism on copper by a) Zhang et al., and b) Li et al.. Reprinted with permission from Ref. [82], © 2014, and Ref. [80], © 2013 respectively. The American Chemical Society.

Despite the most recent detailed characterization of bilayer and multilayer growths supporting the IWC model, the formation mechanism of these layers is still not well understood and remains controversial. The question of which mechanism is the most plausible or whether both case scenarios are possible in different growth conditions remains unclear. Further investigations in this area are required to further understand the graphene multilayer formation mechanisms on copper substrates. We will discuss this matter briefly based on the evidences we gathered later on in this thesis.

2.7 Review on the role of gases (H_2 and O_2) and process conditions during graphene CVD

2.7.1 Role of hydrogen

Hydrogen is mainly used in graphene CVD as a copper oxide reducer; however, a mixture of various CH_4 to H_2 ratios has been constantly reported in literature indicating an unknown role that hydrogen might play in graphene CVD growth [48, 49, 83, 84]. Investigation on the role of hydrogen were conducted by Losurdo et al. [51] and they concluded that H_2 is a kinetic inhibitor for graphene growth since it blocks Cu surface sites that would otherwise be available for C atoms attachment from methane dissociation. They also suggested that hydrogen might have an etching effect that is competing with methane dissociation, which further slows down the graphene growth rate. Vlassiouk et al. [50] have conducted growth and annealing experiments to further investigate the role of hydrogen in graphene CVD. Figure 2-16 shows SEM images of graphene grown on copper and further exposed to a flow of hydrogen. After hydrogen exposure graphene films are partially etched.

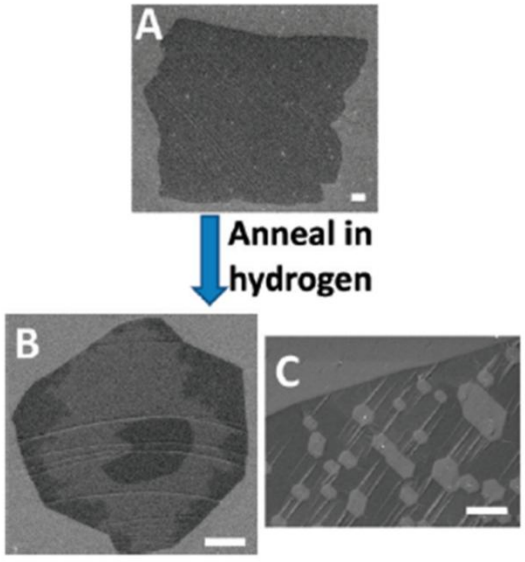

Figure 2-16. The effect of annealing in hydrogen (19 Torr H_2 in 1 atm of Ar, 1000 °C). A) as-grown graphene on copper, B) Annealed in hydrogen for 30 min and 850-1000°C) annealed after exposure of the sample to air (it is believed that dust particles deposited on the sample after their exposure to air serve as a catalyst for etching graphene). Scale bars are 1µm. Reprinted with permission from Ref. [50],© 2011, The American Chemical Society.

In addition, changing the hydrogen pressure during the growth led to different graphene morphologies as seen in Figure 2-17.

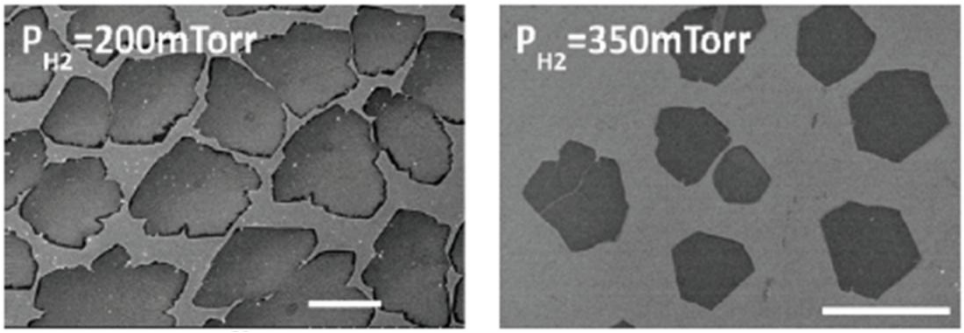

Figure 2-17. SEM images of graphene grains synthesized during 30 min in LPCVD at 1000 °C on Cu foil using 1 mTorr of methane at different hydrogen partial pressures. Reprinted with permission from Ref. [50],© 2011, The American Chemical Society.

Moreover, they did not observe graphene growth at relatively low hydrogen partial pressures concluding that hydrogen is necessarily required for graphene growth. In contrast Gao et al. have previously shown that graphene can be grown in the absence of hydrogen. Ignoring Gao et al. [44], they deduced that hydrogen serves a double role: growth activator and etching reagent. Concurrently to these studies, Zhang et al. [53] conducted systematic annealing experiments on graphene layers grown on copper at high temperature (700-1000° C) and 500 mTorr total pressure in order to discriminate the role of hydrogen from that of methane during the CVD growth. They observed anisotropic etching of graphene films on copper with the highest etch rate between 800-850 °C. Figure 2-18a shows the as-grown graphene transferred on SiO_2/Si substrate with a corresponding Raman spectrum while Figure 2-18b demonstrates the anisotropic etching of graphene film exposed to hydrogen at 500 mTorr at 800 °C. The film is transferred to SiO_2/Si after treatment. No graphene peak is observed in Raman spectra from the etched region.

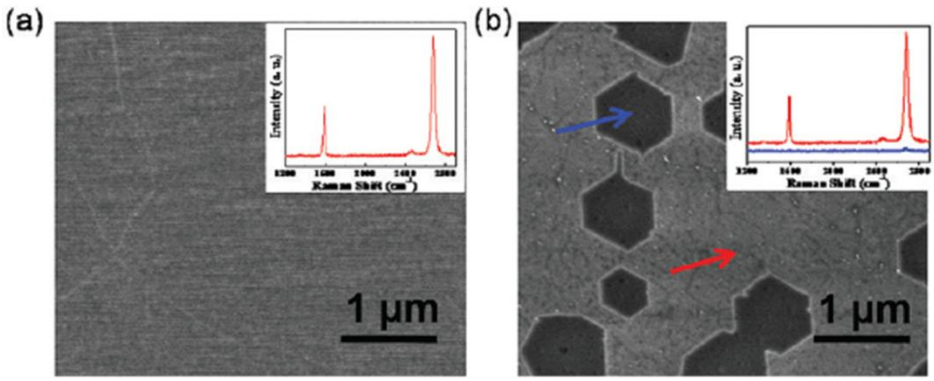

Figure 2-18. SEM images of graphene CVD before and after etching. a) As-grown graphene transferred on SiO_2/Si and the corresponding Raman spectrum, b) graphene etched by H_2 at 800 °C and transferred to SiO_2/Si. Raman spectra shows graphene remaining intact and no graphene in the etched regions. Reprinted with permission from Ref. [54],© 2012, The American Chemical Society.

Similar annealing experiments on graphene grown on copper were conducted on transferred graphene on SiO_2/Si substrate and surprisingly no evidence of graphene etching is observed. This led the authors of this study to suggest that copper catalyzes the etching reaction [53, 85]. Following these experiments, other researchers have suggested different recipes, known as "etching-aided" or "pulsed" CVD, to grow monolayer graphene films [86, 87]. A schematic diagram of this strategy is shown in Figure 2-19. In this process, after the metal catalyst (i.e. copper) is exposed to the carbon precursor, the carbon supply is cut off and hydrogen is used to etch excess carbon formed during the growth process. The sample is then cooled down under an Ar atmosphere leading to the formation of monolayer graphene film [86, 87].

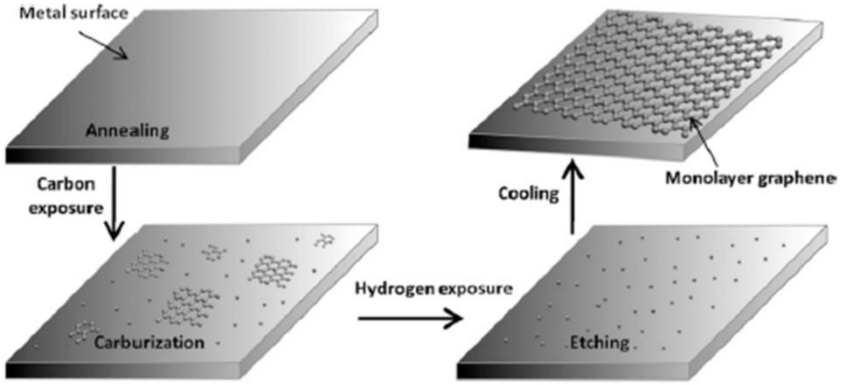

Figure 2-19. Schematic diagram of etching-aided CVD growth of monolayer graphene on metal substrates. Firstly, the metal substrates are annealed inside the quartz tube at 1000 °C for 30 min. Then, the carbon precursor is introduced into the furnace. Next, the carbon supply is stopped and a hydrogen exposure is performed. Finally, upon cooling, monolayer graphene is expected to be formed on metal surfaces. Reprinted with permission from Ref. [86],© 2012, Elsevier

The role of hydrogen and its influence on the formation of graphene on copper foil became the subject of intense current research. The total pressure of the CVD process and the methane to hydrogen ratio were altered in order to find the best recipe for graphene growth, control the shape and size of graphene domains, and understand the role of gases on the morphology of the films. These results are summarized in the next sub-section.

2.7.2 Impact of process conditions

It is possible to control the nucleation density and the size of the initial graphene crystals by tuning the partial pressure of CH_4, the total growth pressure, and the temperature [45, 46, 48, 49, 83, 84, 88, 89]. Figure 2-20 presents SEM images of partially grown graphene under different conditions such as temperature, methane flow rate, and partial pressure [46]. As seen in the figure, the density of graphene nuclei decreases with increasing growth temperature resulting in larger graphene domain sizes. Reducing the methane flow rate (J_{Me}) leads to larger graphene islands and fewer nucleation sites (Figure 2-20c). A further decrease in the methane partial pressure (P_{Me}) leads to even fewer nucleation sites (Figure 2-20d) and larger graphene islands compare to Figure 2-20c. However, growth terminates before full surface coverage if the partial pressure of methane remains below a critical value as seen in Figure 2- 20d. In this case, even

with longer methane exposure, graphene films remain incomplete [46].

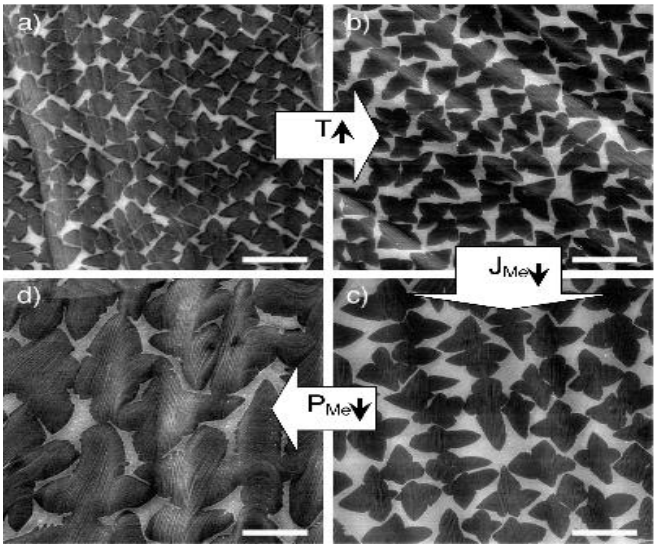

Figure 2-20. SEM images of partially grown graphene using methane/hydrogen under different growth conditions: T(°C)/J_{Me} (sccm)/P_{Me} (mTorr): a) 985/35/460, b) 1035/35/460, c) 1035/7/460, d) 1035/7/160. Scale bars are 10 μm. Reprinted with permission from Ref. [47],© 2010, The American Chemical Society.

Among all different growth parameters, the total pressure of the CVD system and the methane to hydrogen ratio appeared to have the greatest influence on graphene grain morphology [48, 49, 83, 84]. Figure 2-21 shows graphene layer morphologies obtained using various growth conditions for a 30 min reaction time at 1000 °C. As seen in the Figure 2-21 (right column) for a fixed total pressure of 150 mTorr and a gradual increase in the methane to hydrogen ratio 1:30 to 1:2, graphene islands change from hexagonal to flower to irregular shape. Moreover, the increase in methane to hydrogen ratio up to 1:2, led to a continuous film with multilayers in some areas. A similar behavior is observed when the total pressure is increased from 80 to 400 mTorr for a fixed methane to hydrogen ratio of 1:12.5. (left column) [48]. These results have suggested that graphene growth is a balance between carbon growth and hydrogen etching.

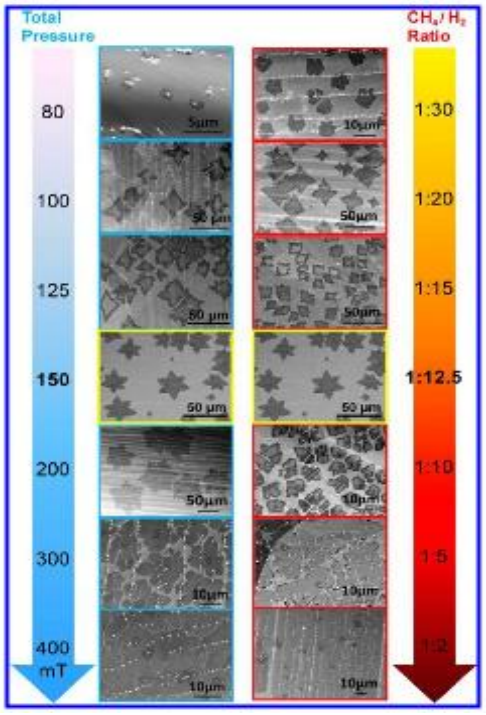

Figure 2-21. SEM images of graphene grown on copper foil at 1000 °C for 30 min. The central images in both columns are the same. The samples of the left are grown with a fixed CH_4 to H_2 ratio 1:12.5, and varied total pressure. The right-side samples are prepared using a fixed total pressure of 150 mTorr and CH_4 to H_2 ratios ranging from 1:30 to 1:2. Reprinted with permission from Ref. [49],© 2012, The American Chemical Society.

Kidambi el al. [49] have conducted a set of experiments where they changed the ratio of methane to hydrogen in both LP-CVD and AP-CVD. The SEM images reveal nearly complete graphene films with evidence of mono and multilayer growth for a 25 min growth using a CH_4 to H_2 ratio of 1:10 at low pressure (Figure 2-22b), However, the film is incomplete for 1:1 ratio and 5 min growth and multilayer growth is also observed. Similar behavior is observed in AP-CVD (Figure 2- 22g-j) [49].

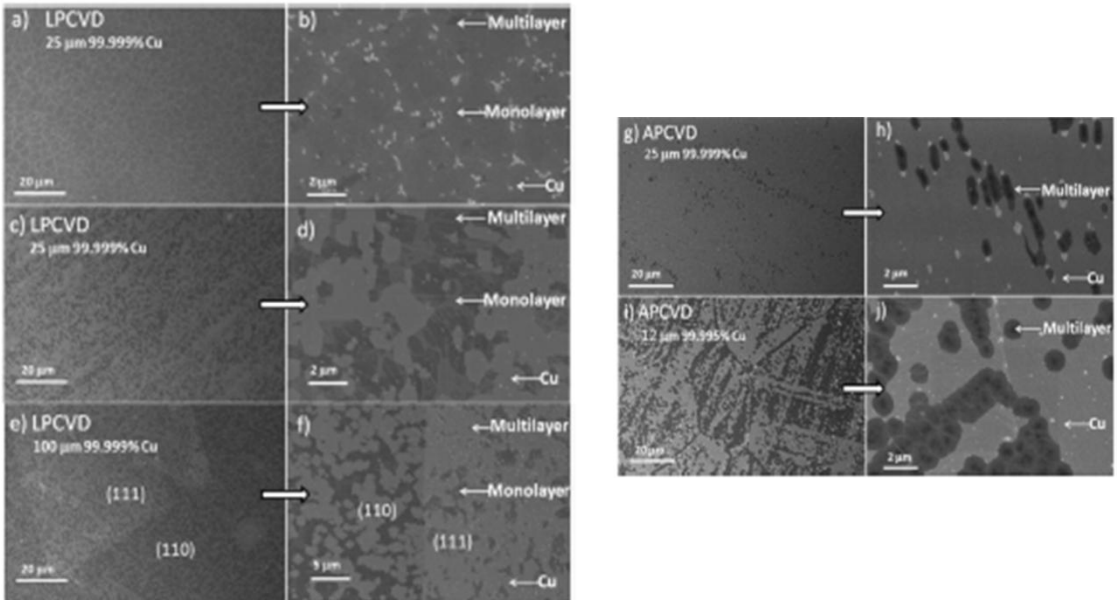

Figure 2-22. SEM images at different magnifications showing graphene nuclei on Cu before merging to form a continuous film: (a, b) monolayer nuclei, LPCVD, 4 mbar, 1000°C, 1:10 CH_4/H_2 for 25 min (c, d) multilayer nuclei, LPCVD, 4 mbar, 1000°C, 1:1 CH_4/H_2 for 5 min, (e, f) multilayer nuclei, LPCVD, 4 mbar, 1000°C, 1:1 CH_4/H_2 for 5 min, g, h) multilayer nuclei, APCVD, 1000°C, 1:25 CH_4/H_2 for 5 min, on (i, j) multilayer nuclei, APCVD, 1000°C,1:25 CH_4/H_2 for 5 min. Reprinted with permission from Ref. [50],© 2012, The American Chemical Society.

Here again they proposed that their results can be explained by a competition between carbon growth and hydrogen etching. Moreover, not only the pressure of the CVD chamber changes the graphene morphology but also the presence of higher amount of carbon (less hydrogen consequently less etching) strongly impacts graphene formation. Multilayer growth is favored when the carbon supply is greater than that of hydrogen suggesting different graphene growth pathways [49]. This behavior has also been reported by Vlassiouk et al. where elevated methane concentration led to the formation of multilayers, some of which are commensurate with one another whereas others have random stacking orders [50].

While uniform and continuous graphene films with high quality were grown on copper foil by controlling the methane to hydrogen ratio and playing with the total pressure during CVD, the origin of the disparities between different growth recipes from one group to another [13, 28, 40, 46, 48-50, 84, 87] remained puzzling and led us to suspect that impurities mainly oxygen are perhaps playing a role in graphene CVD process. We will discuss this matter in detail shortly.

2.7.3 The role of oxygen

The role of oxygen is generally not discussed explicitly in the graphene growth literature. However, its influence was sometimes questioned in passing [49, 50, 76]. The presence of oxidizing contaminants in the feed stock as well as the leaks into the chamber were mentioned in some papers [49, 50, 76], but no study permitted to decouple the role of oxygen from that of other gases present during the CVD process. Vlassiouk et al. [90] have shown that exposure of graphene films grown on copper to air at high temperatures > 400 °C results in etching, mostly starting at the interdomain boundaries. They noted that this should be avoided in order to maintain the graphene film quality. Figure 2-23 shows SEM images of graphene film etched by oxygen when the CVD furnace was opened to air at high temperature [90].

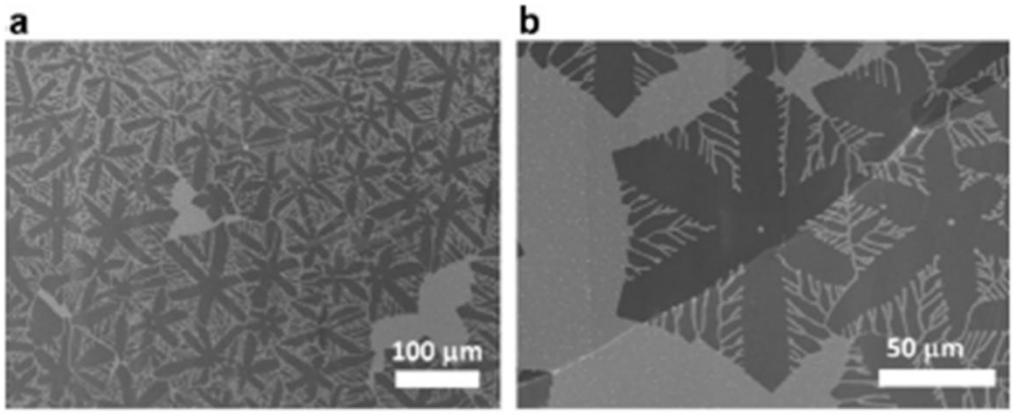

Figure 2-23. SEM images of graphene on copper foil etched by oxygen when the CVD furnace was opened to air at high temperature > 400° C. Oxidation starts at the interdomain boundaries. Reprinted with permission from Ref. [90],© 2013, Elsevier.

2.7.4 Remarks

Despite the great number of studies in literature showing that hydrogen is etching graphene films, we postulated that hydrogen is not responsible for this etching reaction. In fact, based on surface science and catalysis studies, metals of group XI are not versatile catalysts for hydrogenation reactions and fail to be active in hydrogen chemisorption. In other words, hydrogen neither dissociates nor adsorbs on copper surfaces [91, 92] .Moreover, based on a

simple back of the envelope calculation, we found that this etching reaction is evident at hydrogen pressures from which the partial pressure of contaminants becomes comparable to the standard base pressure of LP-CVD furnaces. We therefore proposed that some other parameters, most likely traces of oxidizing impurities present in the gas mixture or air leaks, are responsible for this etching reaction. This enabled us to design the experiments presented in chapters 4 and 5 for investigating the role of these oxidizing species along with hydrogen during graphene annealing and growth.

2.8 Implementing graphene CVD process into industrial manufacturing

The commercial application of graphene products is driven by the advancements made in manufacturing of graphene films with properties suitable for the particular application. This is likely to last until each of graphene's many potential applications fulfills its own requirements. Currently, the process of making graphene films is expensive mainly due to large energy consumption. The game-changing breakthrough will be the growth of graphene films at low temperature or implementation of a fast growth process that meet the industrial manufacturing standards with the films having minimal number of defects. In the next section, the progress in this area is reported.

2.8.1 Low temperature graphene CVD

In an effort to decrease energy consumption and consequently reduce the cost of the graphene fabrication process, growth studies at lower temperature were conducted [55-59, 93]. Liquid or solid precursors such as Toluene and Graphite are favored since these carbon sources have lower C-H bond dissociation energies or require fewer dehydrogenations steps to produce C species compared to methane. Isolated graphene islands have been grown on Cu at low temperatures (300-600 °C) using these precursors [56, 58, 59, 93]. The growth of continuous graphene layers was mainly possible using a two-step process – in which the second step served to graphene islands' extension and coalescence through increasing the chamber pressure by a factor of 10 in the last 5 min of the growth time [59] – thereby making the overall process too long and fairly

complex to be economically viable for mass production.

In addition the intensity of the Raman D peak from films grown at low temperature using liquid precursors was enhanced indicating the presence of structural defects [55-59, 93]. Figure 2-24 shows SEM pictures and Raman spectra of graphene films grown on copper using ethanol at different temperature. Higher growth temperatures result in a reduction of the D peak intensity [57].

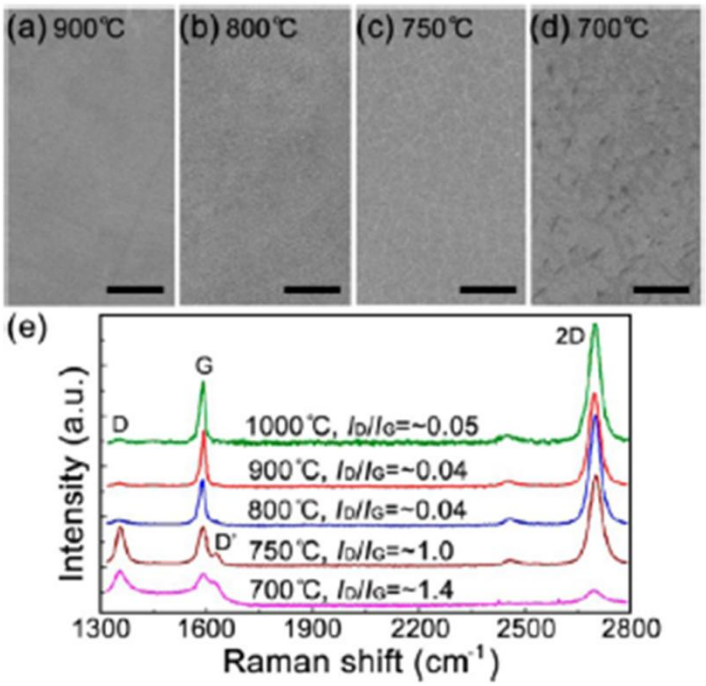

Figure 2-24. (a-d) SEM images of graphene films grown on copper foil after 10 min exposure to ethanol at CVD temperature of a) 900, b) 800, c) 750, and d) 700 °C. Scale bars are 5μm. e) Typical Raman spectra corresponding to graphene shown in (a-d). Reprinted with permission from Ref. [58],© 2013, American Chemical Society.

Recently graphene growth on copper foils at a lower temperature around 700-750 °C using CH_4 was reported by Jacobberger et al.[1]. Although the process was successful and the quality of the films was comparable to what is generally obtained at higher T, the growth process was much longer ~ 56 hrs. Such growth rates are obviously a drawback for manufacturing graphene and cannot be implemented at industrial scale.

[1] Article under revision by Journal of Physical Chemistry C

2.8.2 Rapid CVD growth

Rapid and efficient growth of graphene CVD in 20 seconds on copper using ethanol was recently reported by Lisi et al. [94]. Although fast and energy efficient, this technique still does not permit the growth of high quality graphene. As shown in the SEM images of Figure 2-25, the surface is not clean, a significant bilayer coverage and amorphous C are visible on the graphene films grown using this recipe.

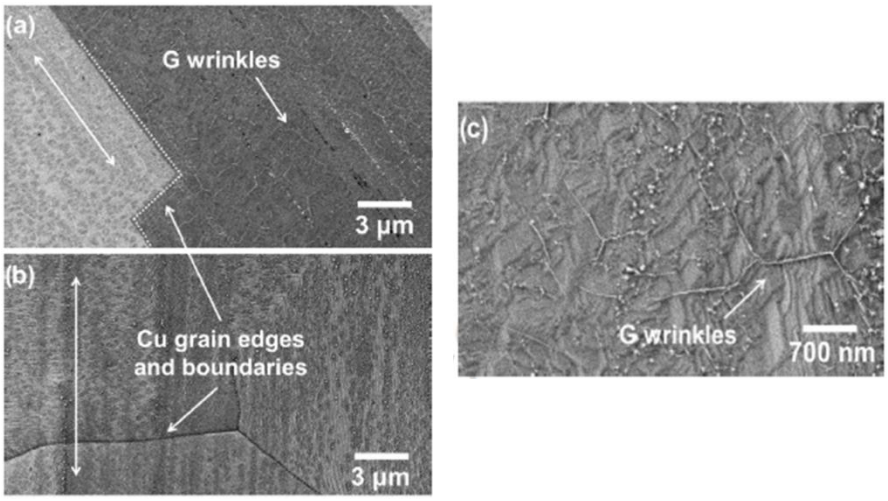

Figure 2-25. SEM images of graphene films grown on Cu at 1070 °C for durations of a) 60 s, b-c) 20 s. Reprinted with permission from Ref. [95],© 2014, Elsevier.

Despite all the efforts that have been made to minimize the fabrication cost , the films produced from these methods have yet to meet the quality required for practical applications [15]. Many questions remain unanswered, e.g. How long does it take for graphene to cover the entire surface? Do the Cu surface morphology, the gases selection or other parameter play a significant role in the growth process?

In Chapter 6 we show a promising yet simple solution for manufacturing graphene films in less than one minute. This will substantially reduce the amount of energy required to make graphene and subsequently lower the manufacturing cost.

2.9 Perspective of the work in this thesis

The existence of uncertainties in graphene CVD on copper literature, the vast array of disorganized experimental results, and notable absence of systematic studies motivated us to investigate the CVD growth of graphene films on copper substrate in order to understand the interplay between the growing graphene honeycomb lattice and the role of gases, methane as the carbon precursor, and hydrogen as the reducing agent or carrier gas. First and foremost, we intended to resolve the discrepancy on the dual functionality of hydrogen being an etchant and growth activator [50]. We tackled this strategically by conducting systematic experiments to decouple the role of hydrogen and trace amounts of oxidizing impurities such as oxygen, two separate elements which we postulated that play different roles in graphene CVD and have therefore limited further progress in this emerging field. The results of these studies are detailed in Chapter 4 and 5.

Later on, based on the fundamental insights we obtained from our previous studies, we developed a recipe or more precisely a method to engineer graphene CVD process in an energy- and cost effective- manner being entirely suitable to industrial manufacturing standards. We have also proposed a simple kinetic growth model of graphene formation on copper surface including the effect of oxygen impurities for the first time. The results of these studies are detailed in Chapter 6.

CHAPTER 3 EXPERIMENTAL TECHNIQUES

3.1 Graphene chemical vapor deposition (CVD)

Chemical vapor deposition (CVD) is a technique in which thin solid films are deposited on substrates through chemical reactions via vapor species [95]. CVD processes differ by operating pressure: (i) Atmospheric pressure CVD (AP-CVD), (ii) Low-pressure CVD (LP-CVD) which operates at reduced pressures, and (iii) Ultrahigh vacuum CVD (UHV-CVD) which is at low pressure of approximately 10^{-8} Torr. In order to minimize the undesirable gas-phase reactions and enhance the film quality, graphene CVD was performed at LP-CVD in hot wall tube furnace in this thesis. Figure 3-1 illustrates the schematic of a typical tube-furnace used in CVD systems for graphene growth. The set up is composed of a gas delivery system for the introduction of gases, a reactor where reactions occur and graphene is grown, and a gas removal system composed of vacuum pumps to remove the excess gas from the CVD reactor. The flow can be monitored and controlled by mass flow rate controllers or by the pressure and leak valves. The heaters surround the reactor to provide high temperature for reactions and the temperature ismonitored by thermocouples located on the heaters [28, 30, 33, 45, 95].

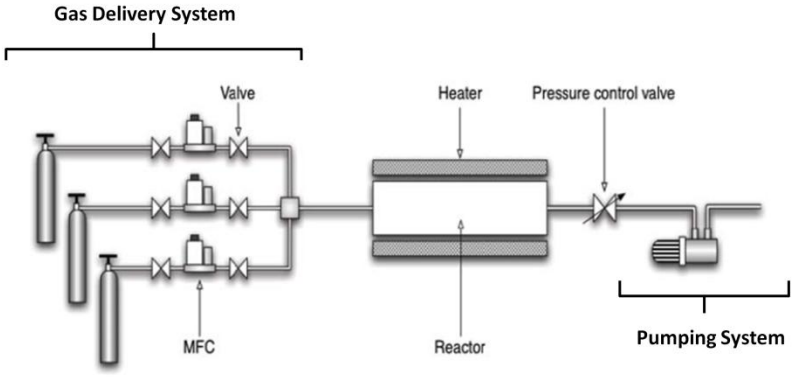

Figure 3-1. Schematic diagram of a tube furnace CVD system. It consists of a gas delivery system, mass flow controllers or leak valves, deposition chamber, pressure gauge with controller and a pumping system. Reprinted from Ref. [95], open access.

We used 25-µm-thick Cu foils (Alfa Aesar, item no. 13382) as the substrate, CH_4 (Praxair, UHP, grade 3.7, O_2 < 15ppm) as the carbon precursor, and H_2 (Praxair, UHP, grade 5, O_2 < 1ppm) as the carrier gas and copper oxide reducer. Prior to each growth, the copper foils were cut to 2 x 2 cm and were chemically cleaned (see section 3-1-3). After the cleaning procedure, the foils were placed on a quartz slide and pushed into the CVD furnace using a stainless steel rod. All the samples were placed in the middle of the reactor in the course of this thesis. Thus, all the conditions were the same throughout the experiments. The growth was performed in a 3.8-cm diameter (1.5 inch.) fused quartz tube inside a horizontal furnace (Lindberg/Blue M, Thermo Scientific) under low pressure conditions at 950-1000 ºC. The system is equipped with a manifold capable of UHV conditions. Leak valves on the manifold (gas delivery section) are used to control the pressure monitored by the gauge at the exit. Prior to each growth, the system is evacuated to a vacuum of 5 $x10^{-6}$ Torr using a turbo molecular pump. The copper foils are then heated to 1000 ºC and annealed at this temperature for 30 min under the flow of H_2. Then, CH_4 is introduced into the chamber and growth is carried out at temperatures between 950 and 1000 °C for 45 min with the reactor pressure maintained at 500 mTorr. Finally, the chamber is cooled down to room temperature.

As mentioned above, the heaters surround the reactor to provide high temperature for reactions. The temperature is monitored by thermocouples located on the heaters. There is a difference of ±10 °C between the substrate temperature and the actual temperature read by the thermocouples in the CVD reactor.

The typical graphene LP-CVD process in represented schematically in Figure 3-2. Temperature profile as well as gas sequences are presented as a function of time for the entire growth process starting from a pre-deposition annealing stage to the graphene growth itself, followed by the final cool-down phase.

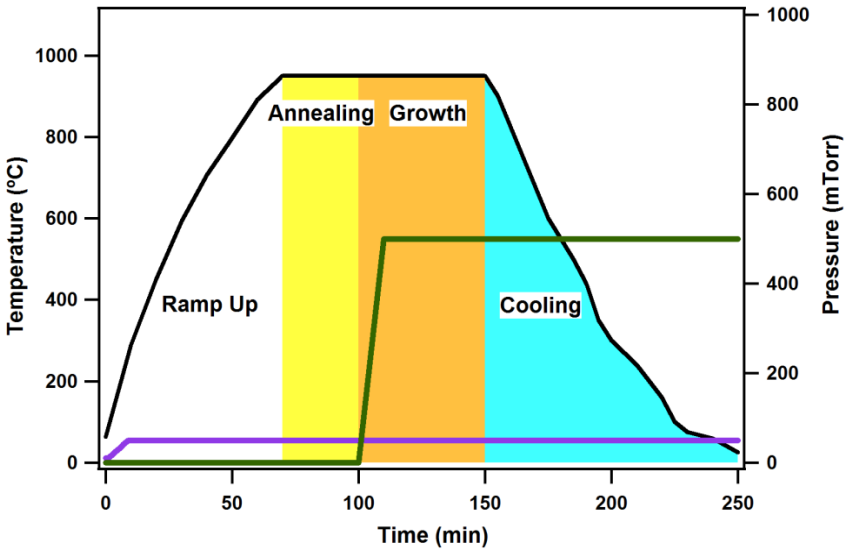

Figure 3-2. Schematic of the typical CVD growth process. Broad lines depict the temperature profile. The fine solid lines represent the partial pressure of the specific gas present during the annealing, growth, and cooling stages (i.e : H_2 purple and CH_4 green).

Our as-received ultra high purity (UHP) gas bottles (hydrogen, methane, and argon) contain approximately 1-15 ppm of oxygen if not greater. In order to minimize the amount of oxygen or oxidizing species flowing into the chamber, we used gas purifiers to reduce the level of oxygen to below 1 ppb. The use of specific gas purifiers for each lines is key to our investigations. We installed the purifiers on the same gas bottle with which the normal (unpurified gas) growth experiments were conducted. Figure 3-3 is a schematic representation of the gas line with and without purifiers and the LP-CVD furnace to clarify the method used in this thesis. It is noteworthy to mention that we have conducted experiments to quantify the amount of oxygen in the chamber using mass spectrometers. However, the results of our experiments were inconclusive and therefore are not reported in this thesis.

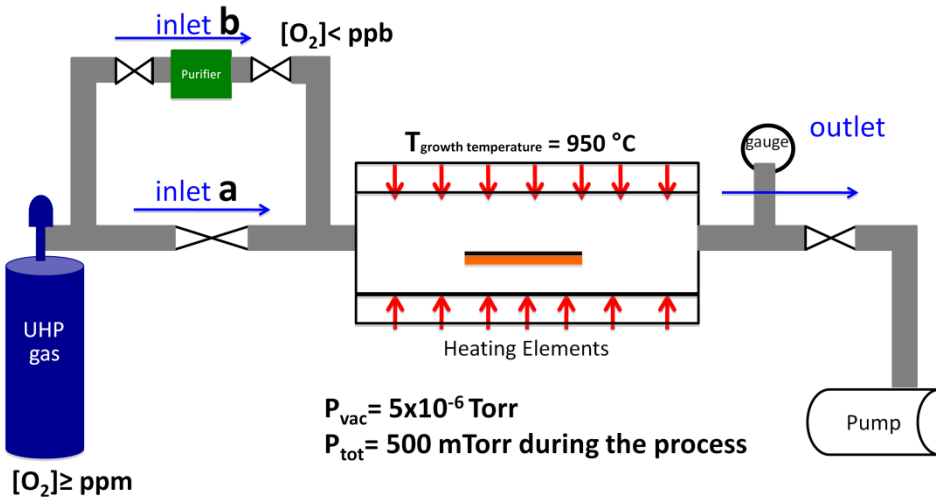

Figure 3-3. Schematic representation of the gas line and the CVD furnace without (a) and with (b) purifiers.

3.1.1 Gas grades and suppliers

We used hydrogen (Praxair, UHP, grade 5, O_2 < 1ppm), methane (Praxair, UHP, grade 3.7, O_2 < 15ppm), argon (Alfagaz, UHP, grade 2, O_2 < 1ppm), and carbon dioxide (Praxair, Anaerobic, grade 4, 99.99% purity) throughout our experiments.

3.1.2 Gas purifiers

The process of gas purification deals with the removal of unwanted species from the source. Our experiments require the gas mixtures to be free of oxygen, therefore we used specific purifiers for each UHP gas using in our experiments to minimize the level of oxidizing impurities flowing into the chamber where the CVD process was taking place.

3.1.2.1 DEOXO™ (Hydrogen purifier)

For H_2 (Praxair, UHP, grade 5, O_2 < 1ppm), we used DEOXO™ (O_2 < 1ppb). DEOXO hydrogen purifier provides pure hydrogen with less than 1<ppb of oxygen. The catalytic combination of oxygen and hydrogen is performed actively in the presence of the palladium catalyst deposited on a support of aluminum oxide and leads to the formation of water [96]. Note that the combination of hydrogen and oxygen reaction in the presence of the catalyst is extremely fast at room temperature, making the DEOXO purifier convenient and most importantly efficient to use for industrial processes [96]. Figure 3-4 is a schematic representation of the reaction occurring in the DEOXO hydrogen purifier.

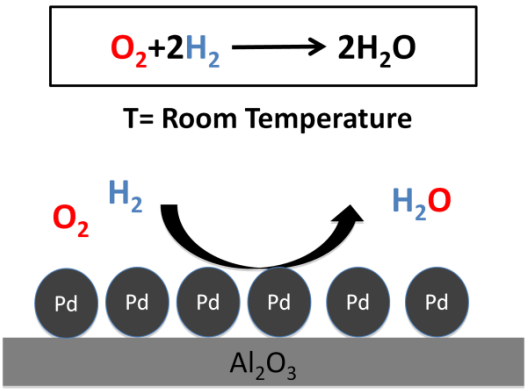

Figure 3-4. Schematic representation of the catalytic combination of oxygen and hydrogen in the presence of the palladium catalyst deposited on a support of aluminum oxide and the formation of water.

3.1.2.2 SAES Pure Gas Inc. (Methane, Argon, and CO_2 purifier)

We used SAES Pure Gas Inc. MC1-950FV (H_2O and O_2 < 1ppbV) for CH_4 (Praxair, UHP, grade 3.7, O_2 < 15ppm), MC1-902FV (H_2O and O_2 < 1ppbV) for Ar (Alfagaz, UHP, grade 2, O_2 < 1ppm), and MC1- 804FV (H_2O and O_2 < 1ppbV) for CO_2 (Praxair, Anaerobic, grade 4, 99.99% purity). These purifiers are based on a Ni-support catalyst. Due to proprietary reasons, we do not have the specific information of the purifiers. However, we know, from a private

communication, that the catalyst in the purifier works as a getter for oxygen molecules. Therefore, the production of the byproducts are either very limited or close to zero. The catalyst in the purifier saturates after approximately 2 years depending on the use, but most of the purifiers can be regenerated.

3.1.3 Water trap

In order to see the effect of water, a by-product of the DEOXO purifier, we installed a water trap after the DEOXO purifier. We cooled it down with liquid nitrogen all along the experiments.

3.1.4 Copper chemical cleaning

Prior to each growth the Cu foils (Alfa Aesar 13382, 99.8% purity, 0.025 mm thick) were chemically cleaned in 1 M acetic acid (Sigma Aldrich, Reagent Plus > 99%) at 60 ºC followed by acetone and then 2-propanol (without drying) for 10 min in each step. The Cu substrates are then blown-dried with nitrogen [97].

3.2 Graphene transfer

The transfer method is adapted from the procedure in reference 71. Once the graphene film is formed on copper and the characterization on copper foils is done, the poly methyl methacrylate (PMMA, M.W. 15000 GPC, Acros organics, 4% in chlorobenzene) solution is spin coated on one side of the graphene/ copper foils at 4000 rpm for 30 s and dried in air at room temperature for 1 hour. Next the graphene layer on the other side of the copper foil is etched away by Reactive Ion Etching (RIE) technique using 10 sccm of O_2 at 125 mTorr for 1 min at a 100W power. [Note that graphene is grown on both sides of the copper foils in the CVD furnace; in order to achieve single layer graphene on the Si substrate, the graphene grown on one side of the copper needs to be etched away]. Next, the copper is etched away using 0.1 M ammonium persulfate (Reagent, ACS 98+%, Acros Organics) at room temperature. Once the copper is etched the PMMA/graphene layer floats on the surface of the etchant solution. The PMMA/graphene is then transferred to DI water for rinsing using a glass slide. After rinsing, the

target substrate is placed in water with a tilting angle of approximately 30° underneath the floating film. Water is pulled out using a syringe to lower the film onto the substrate while positioning the film simultaneously with the syringe. After drying, the PMMA/graphene transferred on substrate in vacuum for several hours, the PMMA/graphene/substrate is then put in the acetone bath to remove the PMMA. The graphene/substrate is air dried for subsequent use and optical and electrical characterization [71]. A schematic of the graphene transfer method is shown in Figure 3-5 [71].

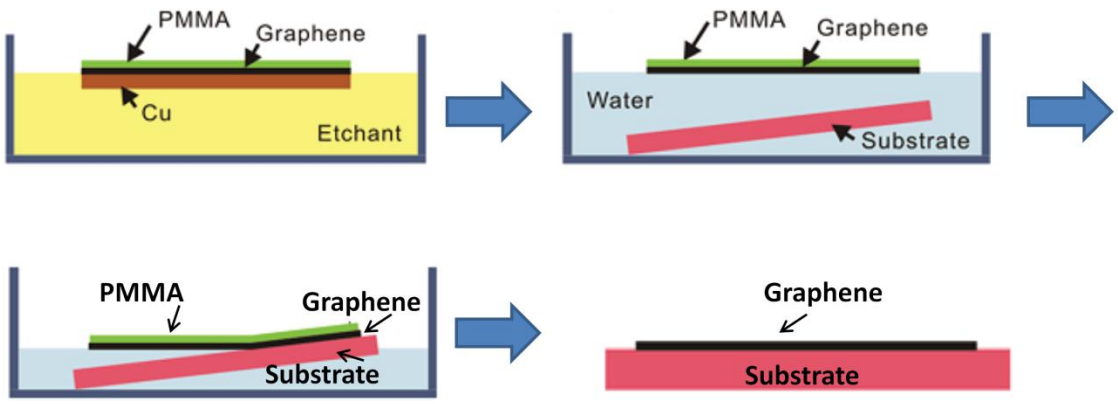

Figure 3-5. Schematic illustration of graphene transfer processes to the flat substrate. See text for the procedure. Reprinted from Ref. [71], © 2011, American Chemical Society.

3.3 Electron microscopy

In this project, we used scanning electron microscopy (SEM), scanning auger microscopy (SAM), and low energy electron microscopy (LEEM) in order to characterize our samples.

3.3.1 Scanning electron microscopy (SEM)

SEM imaging is particularly well-suited for characterizing graphene films on copper substrates as it is a rapid, non-invasive, and effective for imaging the different morphologies of graphene. SEM is also able to detect impurities, ruptures, folds, holes present on the surface of graphene films, and most importantly discontinuities of synthesized or transferred graphene on a variety of

substrates [98-101]. Special conditions are needed to image an atomic-thick graphene layer because it is highly transparent to high energy electron beams. The SEM image is simply sensitive to the morphologies of the substrate beneath the graphene rather than the graphene layer itself. Also, in some cases, graphene films are too smooth to produce sufficient contrasts. Therefore, graphene films imaging should be performed with a field emission scanning electron microscope (FE-SEM) with low voltage- small beam to specimen interaction volume- in order to enhance the contrast and capability of displaying surface details [98, 99].

We used a Hitachi S-4700 field emission microscope in order to image the graphene films grown on copper and transferred on SiO_2/Si substrate. The accelerating voltage is at 1kV and the working distance was set to 4.8-5.8 mm. The microscope has been operated in its ultra high resolution mode (resolution ~ 2 nm) and the top and side secondary electron detectors were enabled. The current of the beam was limited to 10 μA in order to avoid beam induced damage to the graphene film.

Figure 3-6 shows typical SEM images of continuous and uniform graphene films on copper, and transferred to a SiO_2/Si substrate. Based on the contrast in the images, as the number of graphene layer increases, fewer secondary electrons can escape from the surface, thus the detected signal decreases which leads to a darker contrast.

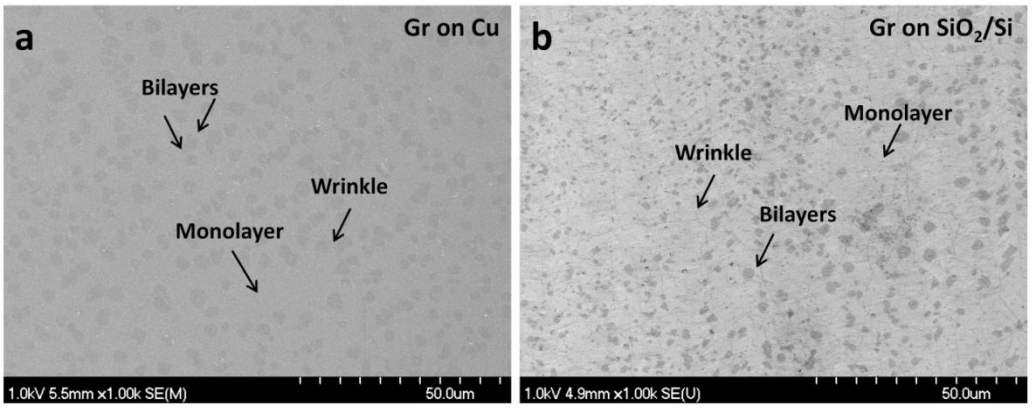

Figure 3-6. Representative SEM images of a) graphene film grown on copper foil via CVD, and b) transferred graphene on SiO_2/Si substrate.

It should be noted that we used a different field emission scanning electron microscope (SEM-JSM-7600F) for the most recent samples since the other SEM (Hitachi S-4700) was not operational. The accelerating voltage is at 1 kV and the working distance was set to ~10 mm. The lower secondary electron detector was enabled in order to get the best possible contrast and resolution. The current of the beam was limited to 7 μA. Figure 3-7 compares the images taken from the two different microscopes. There is no fundamental difference between the two images in terms of data analysis and interpretation, however, finer surface morphologies such as copper steps can be observed with the more recent JSM-7600F field emission electron microscope. Note that the narrow dark lines are graphene wrinkles being a signature of CVD graphene grown on copper foils. These are associated with the difference of thermal expansion coefficients between graphene and Cu during the CVD process. In the case of non-continuous and etched graphene films, copper is brighter and the graphene film is darker in contrast.

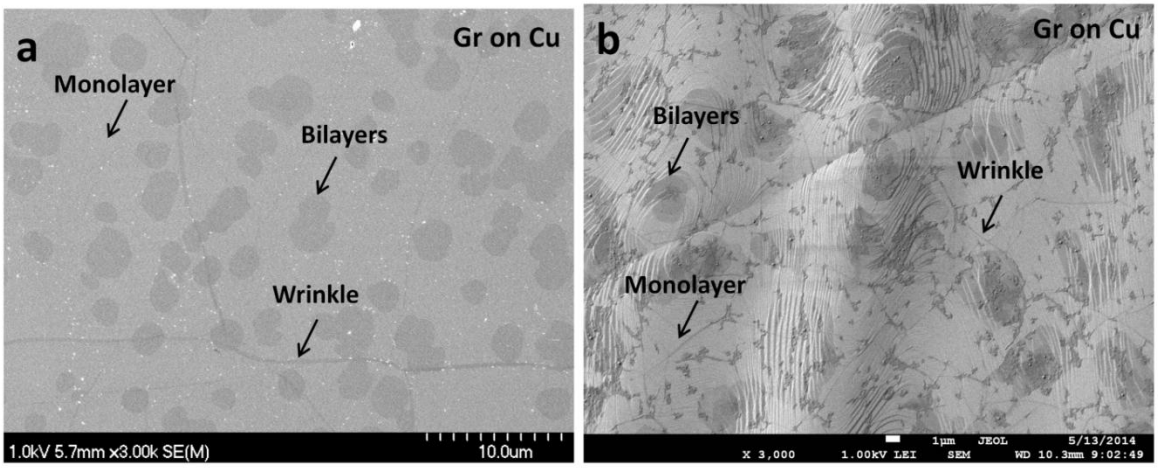

Figure 3-7. Graphene film grown on copper foil via CVD. Image taken with SEM a) Hitachi-S4700 and b) JSM-7600F.

3.3.2 Auger electron microscopy

Scanning Auger Microscopy (SAM) is a combination of the techniques of SEM and Auger Electron Spectroscopy (AES). It is an analytical method widely used to investigate the composition of thin films and solid surfaces [102-104].

We used an Omicron NanoScanning Auger Microscopy (SAM) with a thermal field emitter. The energy is 8kV and the beam current is 3.0 nA. The pressure in the chamber is $1x10^{-9}$ Torr. The survey spectra has an energy step of 1 eV with a retard ratio of 10. An important instrument limitation worth mentioning here is that the yield of Auger electrons is not great for primary electron energies outside of the range of 3-15 kV thus the 8 kV energy chosen here was the most efficient. Figure 3-8a is a representative SEM image of the graphene on copper. Figure 3-8b is a zoom in image and the square in this SEM image indicating the raster area measured in the AES spectrum (Figure 3-8c). Note that the spheres found on this sample were charging and moving during the measurement and this resulted in visible jumps in the spectrum.

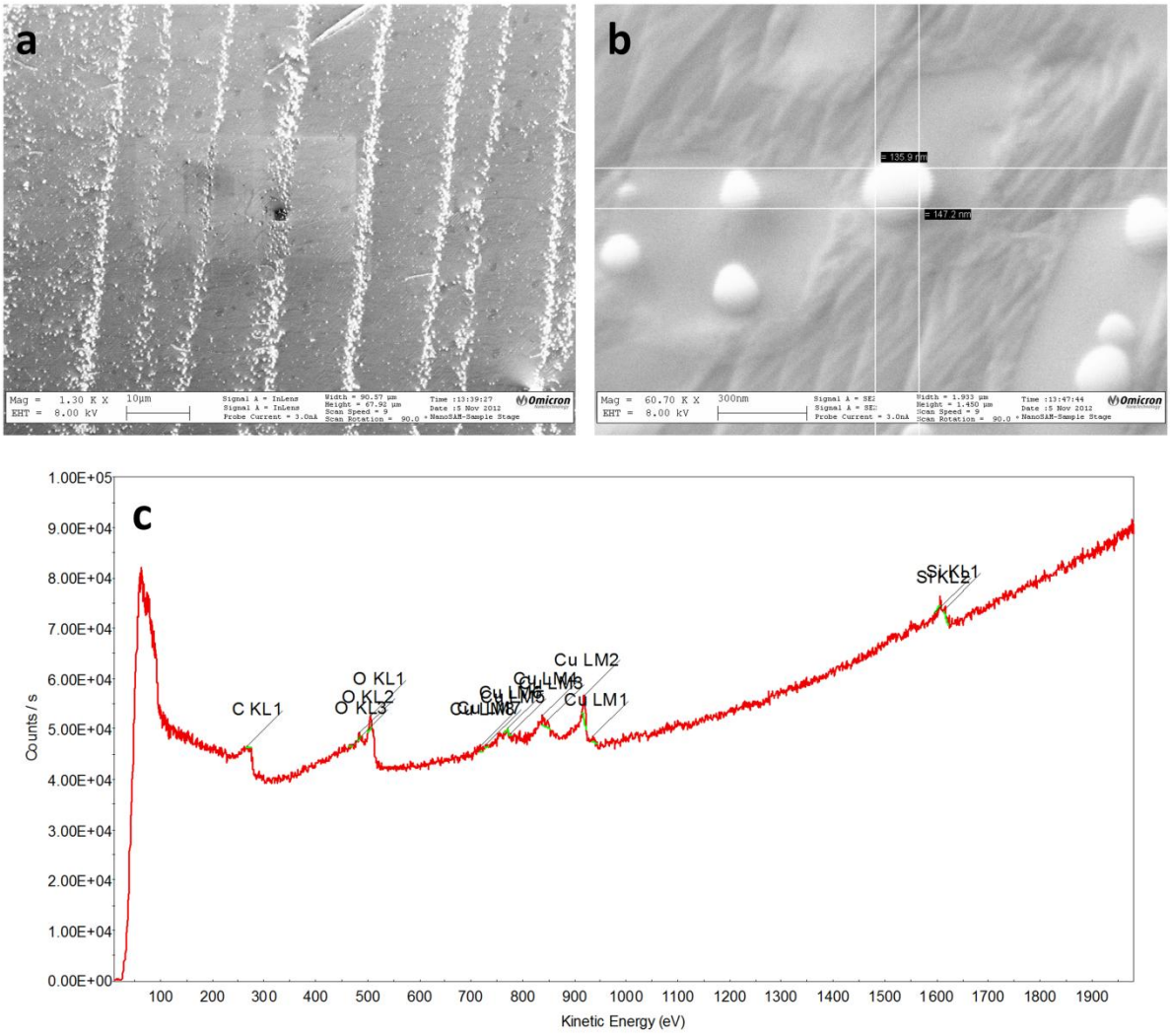

Figure 3-8. a) SEM image of graphene grown on Cu foil taken with NanoSAM, b) zoom in image of a, and c) the Auger spectrum taken from the square (raster area) in b.

In order to analyze the chemical composition of our samples, the Auger electron spectra taken from the region of interest (raster area) were differentiated using the built in software (Thermo Avantage v4.75). The ratio of the elements of interest (i.e C/Cu) were reported which is simply the ratio of the peak-to-peak height of Carbon (C) and Copper (Cu) Auger signal. Figure 3-9a is a representative SEM image of our samples. Figure 3-9b is actual Auger spectrum for the raster area and Figure 3-9c is the differentiated spectrum.

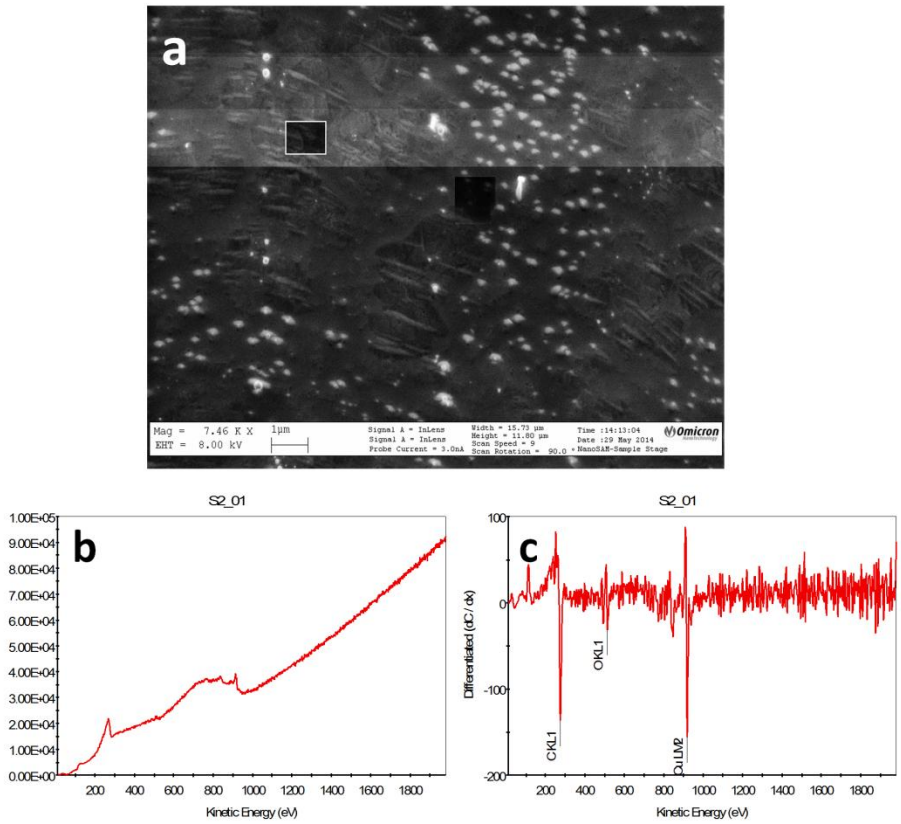

Figure 3-9. a) SEM image of graphene on Cu taken with NanoSAM, b) the actual Auger spectrum of the raster area in a and c) the differentiated spectrum.

3.3.3 Low energy electron microscopy (LEEM)

Low energy electron microscope (LEEM) is a powerful and versatile tool to characterize surfaces of thin films. Its capability to image surfaces along with good spatial and temporal resolution makes it superior to other surface imaging microscopy. In LEEM, high energy

electrons (15-20 keV) are emitted from the electron gun, however they are decelerated to an energy of a few eV since the sample is held at a potential near that of the gun. The strong interactions of these low energy electrons with the matter/specimen limit the information depth to a few atomic layer which yields extreme surface sensitivity [105].

Figure 3-10 demonstrates the basic layout of a low energy electron microscope. As shown in the image, electrons leave the electron gun at kinetic energies between 10 to 20 keV. The electron source can be thermionic or field emission one. These high-energy electrons pass through the condenser lens system responsible for focusing the electrons and positioning the beam at the entrance of magnetic prism array [106]. A point source image being formed by the condenser lens system transferred to the back focal plane of the objective lens by the prism array which deflects the beam through a 90° angle toward the surface. Note that electrons flying to the right from the prism array to the objective lens and sample chamber still have high energies. Since the sample is biased close to 15 kV, once the electrons pass through the objective lens, they are slowed down and decelerated to an energy of only a few eV and interact with the sample surface with very low kinetic energy on the order of 0-50 eV. These slow electrons are diffracted back from the sample to the objective lens. When reaching the objective lens, once again they are accelerated back due to the potential difference between the objective lens and the sample surface [105, 107]. These high-energy electrons are deflected downward into the projection column by the magnetic prism array. These projection lenses are responsible for magnifying and focusing the image or diffraction patterns onto the channel plate phosphor screen. The image become visible and is recorded using a video camera outside the vacuum chamber [105-108].

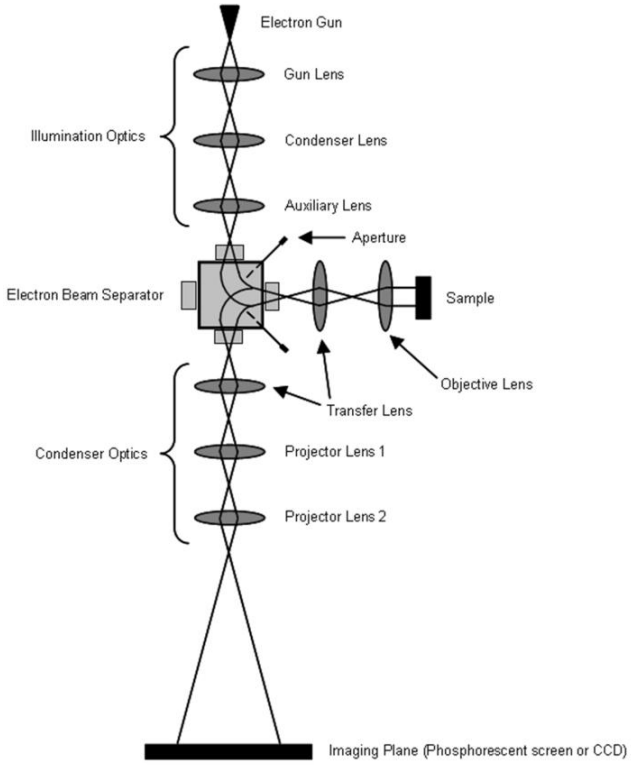

Figure 3-10. Schematic diagram of low energy electron microscope. Reprinted from Ref. [107]. Web accessible.

Image contrast is formed due to electron reflectivity variations originating from the structural, chemical, and magnetic properties of the sample surface. Once low energy electrons hit the surface, the electrons are diffracted and a low energy electron diffraction pattern (LEED) forms in the back focal plane of the objective lens. Using a contrast aperture in the imaging column, one of the diffracted beam can be chosen for imaging. If the (0,0) beam is selected, the resulting image is called a bright-field image. Images taken with any other beam are called dark-field images [105-108]. This is called diffraction contrast in LEEM [105]. Figure 3-11 shows dark and bright field images of Si (100).

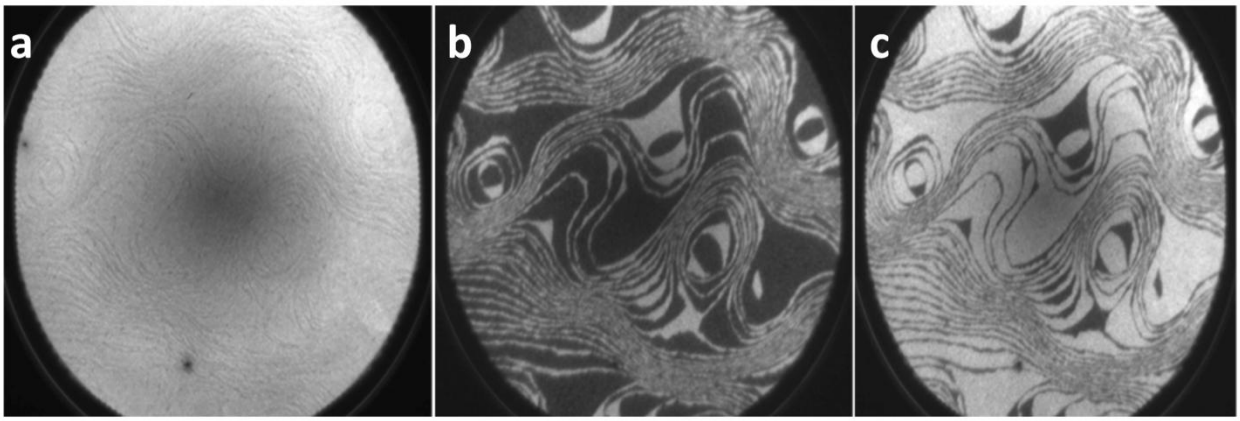

Figure 3-11. LEEM images taken with our LEEM. a) Bright field LEEM image of Si (100). The lines are indicative atomic steps that separate the (1x2) and (2x1) terraces. b and c) Dark field LEEM image of the Si (100) surface. Alternating (1x2) and (2x1) terraces appear black and white, respectively.

It should be noted that in the case of crystalline samples such as graphene, elastic electron scattering is accompanied by diffraction from the crystal lattice. Thus, along LEEM as an imaging technique, most of the samples are also studied by low energy electron diffraction (LEED) as a complementary technique to access reciprocal space information. LEED provides insight on the diffraction patterns, being a supplementary information on the crystallographic orientation of deposited films [105, 108].

In our case, LEEM was performed at 2.4 eV kinetic energy in the UHV chamber (base pressure $4x10^{-10}$ mbar) using a FE-LEEM P90 from SPECS-GmbH.

3.4 Raman spectroscopy and Raman imaging

Raman Spectroscopy is a convenient technique to identify and count the number of graphene layers [62]. This spectroscopic technique is based on inelastic scattering of monochromatic light, usually from a laser source. The laser light interacts with molecular vibrations, phonons or other excitations in the system, leading to an energy shift, the so called Raman effect. This shift provides information about vibrational, rotational and other low frequency transitions in molecules. Single layer graphene cannot be seen under the optical microscope on most

substrates; it can only become visible when deposited on oxidized Si substrates with a finely tuned thickness of oxide layer (typically, 300 nm SiO_2). Raman fingerprints for single layers, bilayers, and few layers reflect changes in the electron bands and allow clear, high-throughput, nondestructive identification of graphene layers [62, 109].

Our Raman microspectroscopy measurements are performed at room temperature with a Renishaw Invia spectrometer with a laser wavelength of 514 nm. A 50X objective (N.A.= 0.55) focuses a 4 mW laser beam to a probe spot about 1 μm in diameter. Figure 2-2 of chapter 2 shows the 514 nm Raman spectrum of graphene layer transferred on SiO_2/Si substrate. The two most intense features are the G peak at 1580 cm^{-1} and a band at 2700 cm^{-1} historically named G' (or 2D). An additional peak observed in the spectrum is the D peak, which can be seen around 1350 cm^{-1}. The absence of a D peak in the spectrum can be a proof of the absence of significant number of defects.

Raman imaging was carried out using a widefield hyperspectral Raman imager RIMA^{TM} based on a Bragg Tunable Filter (BTF) technology [110]. In order to guarantee a uniform illumination over the entire field of view of the microscope objective, a single mode laser passes through a custom beam shaping module. In our measurements, a continuous wave (cw) laser line at λ=532 nm illuminates a 100 x 100 μm^2 sample surface area through a 100X microscope objective (N.A=0.9). The light emitted from the sample is collected and collimated with the same objective and is sent to the Bragg tunable filter where a single wavelength of the whole image is reflected. This reflected beam is then focalized by a lens on a charge couple device (CCD) camera. Turning the Bragg filter allows to scan over wavelengths with a step of 0.05-0.1 nm and thus form a series of monochromatic images. The combination of these images provides access to the spectral information. In this configuration, the sample is excited with a fluence of 150 $\mu W.\mu m^{-2}$, the acquisition time is 120 sec per step and the resolution is diffraction limited.

CHAPTER 4: Article 1: "No Graphene Etching in Purified Hydrogen."

Saman Choubak,[a] Maxime Biron,[a] Pierre Levesque,[b] Richard Martel,[b] Patrick Desjardins[a]

a Regroupement Québécois sur les Matériaux de Pointe (RQMP) and Département de Génie Physique, Polytechnique Montréal, C.P. 6079, Succursale Centre-ville, Montréal, Québec H3C 3A7, Canada

b Regroupement Québécois sur les Matériaux de Pointe (RQMP) and Département de Chimie, Université de Montréal, C.P. 6128, Succursale Centre-Ville, Montréal, Québec H3C 3J7, Canada

Reprinted with permission from Journal of Physical Chemistry Letters, 2013, 4, 1100-1103

Authors' Contribution: S. Choubak designed and conducted the experiments. Characterized, analysed, and interpreted the data. Drafted the manuscript and revised it accordingly. M. Biron transferred the graphene samples from Cu to SiO_2/Si and carried out some Raman spectroscopy measurements. P.L. Levesque provided advice during the course of experiments and revised the manuscript. P. Desjardins and R. Martel revised the manuscript critically for important intellectual content, approved the final version to be published and agreed to be responsible for all aspects of the work in ensuring that questions related to the accuracy or integrity of any part of the work are appropriately investigated and resolved.

CHAPTER 4: ARTICLE 1: "NO GRAPHENE ETCHING IN PURIFIED HYDROGEN."

4.1 Abstract

A systematic study has been conducted to investigate the role of hydrogen in the etching reaction of graphene films grown on copper foils. The results at 825 °C and 500 mTorr showed no evidence of graphene etching by purified Ultra High Purity (UHP) grade hydrogen, whereas graphene films exposed to unpurified UHP grade hydrogen have been considerably etched due to the presence of oxygen or other oxidizing impurities. This finding reveals not only the major impact of oxidizing impurities in the graphene etching reaction, but also entails understanding and controlling the graphene chemical vapor deposition mechanism on copper substrates.

4.2 Introduction

Commercial developments of graphene-based devices require a technique to produce high quality films over large areas.[1-3] To this date, graphene Chemical Vapor Deposition (CVD) growth on copper foils exhibits great potential for mass-producing large area graphene films in a controllable and effective way.[4,5] In graphene CVD, carbon-rich gaseous species, most commonly methane, react with the metal substrate at high temperature (900-1050 °C) in the presence of hydrogen, leading to the decomposition of carbon species and the nucleation of graphene crystals.[4-6] Recently, studies demonstrated that hydrogen and pressure are crucial parameters impacting the CVD growth of graphene.[7-11] However, the role of hydrogen, the concentration of which has been altered enormously in literature from zero [8] to thousands times the amount of hydrocarbon precursor, raises fundamental skepticism thus far. [7-15] Indeed, studies on the role of hydrogen in graphene CVD growth concluded that hydrogen not only has a significant influence on the size and morphology of the resulting graphene domains, but can also etch graphene films.[15-17]Apart from UHV-CVD growth[18-20], these experiments along with a growing number of articles in the last year suggest that molecular hydrogen is an etchant in graphene low pressure LP-CVD and atmospheric pressure AP-CVD, yet its presence is required

for the growth.[7-12] This dual functionality as etching agent and growth activator [13-17,21] appears contradictory and improbable, since molecular hydrogen neither dissociates nor adsorbs on clean copper surfaces.[22,23] Surface science and catalysis experiments established that metals of group XI with filled *d*-levels are not versatile catalyst for hydrogenation reactions because they fail to be active in hydrogen chemisorption.[23-25] Taking these into account and examining thoroughly the results of graphene etching experiment conditions, one can realize a common point: the etching becomes apparent at a hydrogen pressure where the partial pressure of contaminants, (considering Ultra High Purity (UHP) grade hydrogen) becomes comparable to the standard base pressure of LP-CVD furnaces. One might then question whether the small amount of oxidizing impurities in the feedstock could be responsible for the etching reaction. We have then devised a set of experiments to address this crucial question.

In this communication, we show using annealing experiments that hydrogen is not the culprit for graphene etching under controlled atmosphere. Instead, small amounts of oxidizing impurities are found to be responsible for graphene etching through the catalytic action of copper. In our systematic study, we have monitored graphene morphologies following annealing treatments performed under vacuum, in UHP grade H_2 (99.999%, O_2<1ppm) and in purified UHP grade H_2 (O_2<1ppb) atmosphere. Following each treatment, the graphene samples were imaged with a scanning electron microscope (SEM) and their quality assessed by Raman spectroscopy.

4.3 Experimental methodology

Graphene films were grown on 25 μm thick Cu foils (Alfa Aesar, item no. 13382) at 1000 °C in a 1.5 inch. diameter fused quartz tube at low pressure. The system consists of a manifold capable of UHV conditions where the gases are introduced into the chamber. The system's base pressure prior to gas insertion is below $5x10^{-6}$ Torr. The Cu foils were heated to 1000 °C and annealed at this temperature for 30 min under the flow of H_2 at 50 mTorr. In order to grow graphene, CH_4 was introduced into the chamber and the total pressure reached 500 mTorr. After 45 min (growth time), the chamber was cooled down to room temperature under the flow of H_2 and CH_4.[5] Graphene samples were examined under SEM (Hitachi S-4700) prior to any treatment.

4.4 Results

All the annealing experiments were conducted in the same CVD system at the specific temperature and pressure, (825 °C and 500 mTorr), for which the highest graphene etch rate has been reported in literature.[17] In order to confirm that the vacuum level of $5x10^{-6}$ Torr of our system has no effect on graphene samples at the process temperature, a control annealing experiment has been conducted. Figures 4-1 a and b show the SEM images of the as-grown graphene film on copper and the vacuum annealed samples, respectively, demonstrating continuous, uniform, and large area graphene films in both cases. Samples were then exposed to a flow of as-received UHP hydrogen at 825 °C for 30 minutes maintaining a system pressure of 500 mTorr during the process. SEM images from the samples exposed to the flow of unpurified UHP grade hydrogen show etched areas similar to what has been previously reported by Zhang *et al.*[17] (Figure 1c). In order to observe the true effect of hydrogen and test our hypothesis on the role of oxidizing impurities, a hydrogen purifier (DEOXO^{TM}, O_2<1 ppb) was installed to provide purified hydrogen from the same hydrogen bottle used in the previous process. The same H_2 treatment described above was then conducted with purified UHP grade hydrogen on as-grown graphene films. Samples examined under the SEM showed no evidence of graphene etching from purified UHP grade hydrogen (Figure 4-1d).

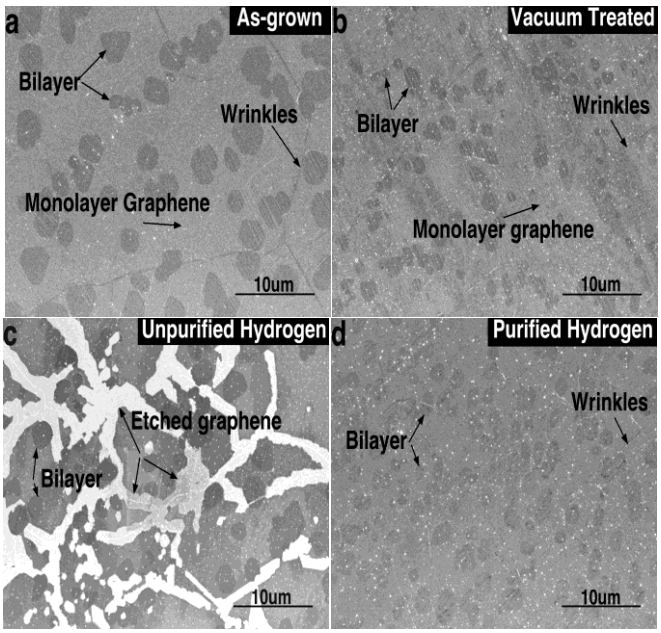

Figure 4-1. SEM images of (a) as-grown graphene film on copper foils, and annealed samples at 825°C for 30 min (b) under vacuum, (c) in unpurified UHP grade H_2, and (d) in purified UHP grade H_2.

To further examine the results and confirm our hypothesis, as-grown, vacuum, unpurified, and purified UHP grade hydrogen treated samples were transferred onto a 100 nm SiO_2/Si substrate using the transfer technique reported in reference 26. Figures 4-2 (a-c) are SEM images from the transferred as-grown, vacuum, and unpurified UHP grade hydrogen treated samples, respectively. As shown previously in Figure 4-1c, it is evident that graphene film annealed in unpurified UHP hydrogen has been etched from some areas, mostly along the wrinkles. We have also observed anisotropic etching similar to what has been previously reported by Zhang *et al.* [17] Figure 4-2d is an SEM image from a graphene film annealed in purified UHP grade hydrogen and then transferred on a Si/SiO_2 substrate. The graphene layer is uniform and continuous over a large area, and has not been substantially modified by the annealing treatment.

Micro-Raman spectroscopy measurements (Renishaw Invia, λ=514 nm) have been carried out on the transferred graphene to determine the number of layers as well as the quality of graphene films. Figure 4-2e presents typical Raman spectra averaged from 400 points collected over the entire surface of each sample. The intensity ratio of peak 2D over G (I_{2D}/I_G) is ~ 3.2 and the 2D peak has a full width at half maximum (FWHM) of ~ 27.5 cm^{-1}, confirming the formation of single layer graphene (SLG).[5,14,26] The D peak, associated with the presence of defects in the graphene, has a very low intensity, indicating that the graphene film maintains high quality after transfer. [26] The Raman spectrum from the purified UHP grade hydrogen treated graphene film exhibits a broadened D peak at ~ 1350 cm^{-1}, which is indicative of the presence of disorder [27] and amorphous carbon.[28] However, no significant change has been observed in the case of films treated in unpurified UHP grade hydrogen. This phenomenon further highlights the presence of oxidizing impurities in the feedstock, which led to etching of excess amorphous carbon and growth-induced defects, potentially making graphene films less defective.

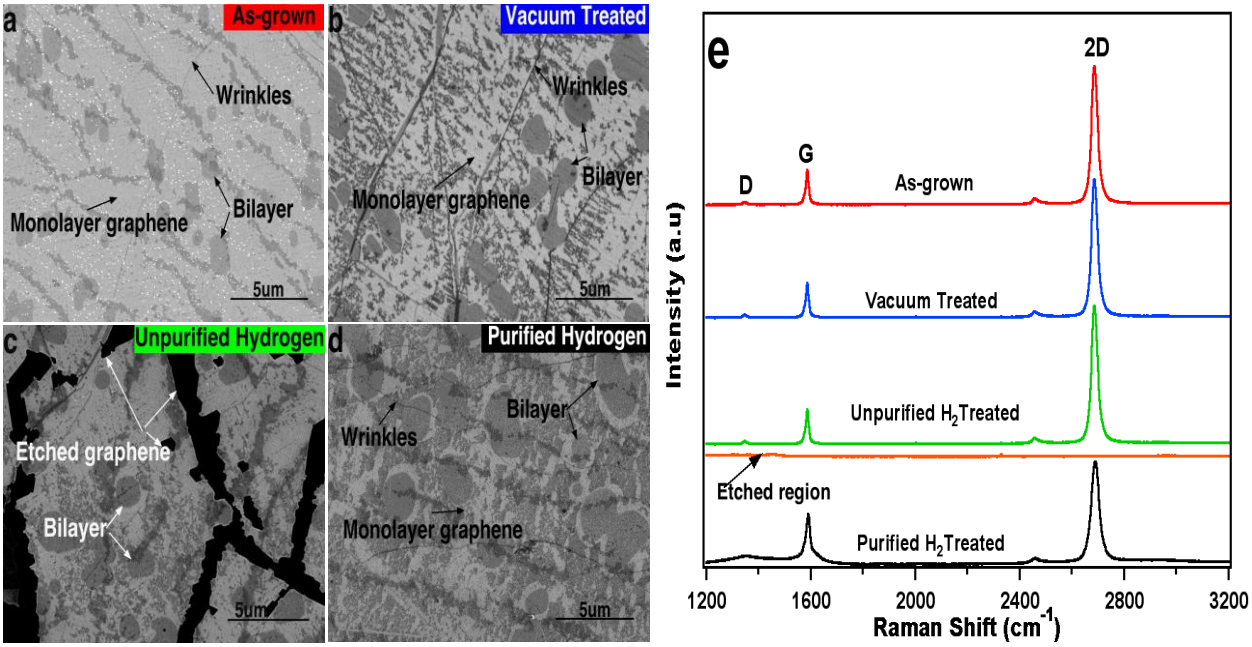

Figure 4-2. SEM images from CVD graphene transferred on SiO_2/Si substrate. a) as-grown, b) vacuum, c) unpurified, and d) purified UHP grade H_2 treated samples. e) Raman spectra (λ=514 nm) from as-grown, vacuum treated, unpurified and purified UHP grade H_2 treated samples.

To highlight the role of copper, we have also conducted identical annealing studies with unpurified hydrogen for graphene films transferred on SiO_2/Si substrate. No etching was observed, which is in agreement with studies reported in the literature.[14,17] This phenomenon suggests that oxidizing impurities do not etch graphene films directly at this temperature (825 °C) and that the substrate plays an active role in the etching process. The oxidation mechanism of graphene on metals have been elucidated on Ru and Ir.[29-31] It is been observed that preferential etching of graphene point defects and edges become visible on metals due to their catalytic activity, which facilitate the dissociation of oxygen.[29-31] On copper, the etching mechanism appear similar although further investigation is required to indentify the differences in graphene etching pathways on copper substrates.

4.5 Discussion

Our findings show that the existence of various graphene CVD growth recipes can be explained by considering differences in conditions from furnace to furnace. Various sealing conditions, different level of contaminants in gas lines, and most importantly, process gas purity are key parameters in defining the optimum growth conditions. The implication of these growth parameters is evident in the original graphene CVD growth recipes,[5] where a continuous flow of methane and hydrogen is kept during cooling down in order to yield uniform and continuous graphene films.[5,6,16,17] Considering the role of oxidizing impurities identified here, the CH_4/H_2 flow appears necessary for preventing etching, most likely by the means of a competitive action with carbon growth. This surprising chemistry was investigated further by performing additional experiments in which the methane was turned off during cooling down, leaving only purified UHP grade hydrogen in the CVD system. As expected, the SEM images showed continuous, uniform, and large area graphene. Moreover, we have performed similar CVD growth studies with solely methane, serving a double role: Copper oxide reducer and carbon supply for growth. The results showed non-continuous and etched films of graphene. This can be explained considering graphene etching by oxidizing impurities in UHP grade methane bottle (O_2< 15 ppm). These results, to be reported in details elsewhere, further confirm the significant impact of the presence of oxidizing impurities in the feedstock for the growth of graphene on copper substrates.

4.6 Conclusion

In summary, our results show no evidence of graphene etching in purified hydrogen. On the contrary, they prove that oxidizing impurities are responsible for etching reactions. We also report that the catalytic role of copper is not only essential in the growth process but also during etching. The amount of oxidizing impurities can no longer be ignored in the future growth recipes since they control the balance between growth and etching, which is crucial for further improving graphene film quality and developing large single crystal graphene layers.

Acknowledgements

The authors thank Nathalie Tang and François Lapointe for discussions, Khalid Laaziri for the help with the CVD system setup and Joel Bouchard for technical support.

4.7 Supporting information

Since water is the byproduct of the DEOXO^{TM} hydrogen purifier, we have installed a water trap after the purifier and conducted the graphene annealing experiments with purified hydrogen. In the figure below, we compared the SEM image of as-grown graphene sample on copper with the one annealed in purified hydrogen at 825 °C for 30 min. As seen in the image, the graphene film stays intact after the annealing with the presence of water trap and no etching is observed. This confirms that the presence or absence of the purifier byproduct does not affect the graphene morphology.

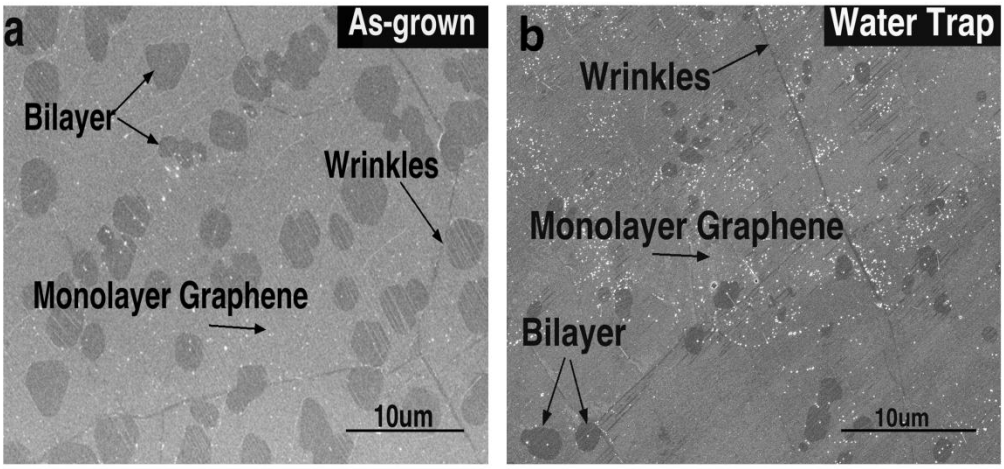

Figure S1. SEM images of graphene films grown on copper foil a) as-grown, and b) annealed in purified H_2 for 30 min at 825 °C in the presence of the water trap.

Moreover, SEM images (Figure S2) of our samples show an excess amount of white particles present on the surface. We used scanning auger microscopy (SAM) to analyze the chemical composition of these particles. The Auger spectra of the particles shows elements such as Cu, C, O, and Si. The existence of Cu and C is obvious since the sample is graphene grown on copper. Oxygen can also be present. The Si and O peak indicate that these particles are composed of SiO. These particles are believed to come from the quartz tube in the CVD chamber during annealing and growth experiments. This is in agreement with the measurements conducted by Zhang et al [17]. Figure S2 is an SEM image of the graphene grown on copper with the particles. The square in this SEM image indicates the raster area measured in the AES spectrum below. Note that the spheres found on this sample were charging and moving during the measurement and this resulted in visible jumps in the spectrum.

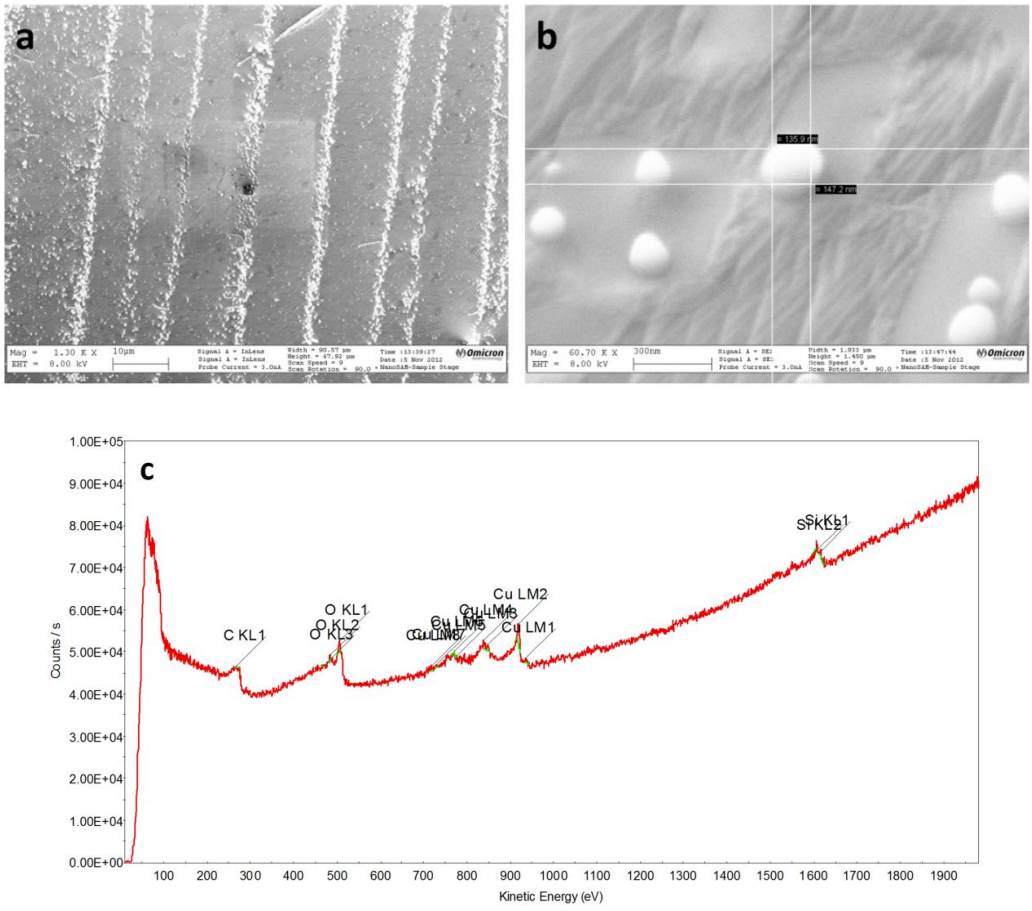

Figure S2. a) SEM images of graphene grown on Cu foil taken with scanning auger microscopy (SAM), b) zoom in image of a, and c) the Auger spectrum taken from the square (raster area) in b.

4.8 References

(1). Geim, A.K.; Novoselov, K.S. The Rise of Graphene. *Nat. Mater*. **2007**, *6*, 183-191.

(2). Novoselov, K. S.; Geim, A. K.; Morozov, S. V.; Jiang, D.; Zhang, Y.; Dubonos, S. V.; Grigorieva, I. V.; Firsov, A. A. Electric Field Effect in Atomically Thin Carbon Films. *Science* **2004**, *306*, 666–669.

(3). Geim, A. K. Graphene: Status and Prospects. *Science* **2009**, *324*, 1530–1534.

(4). Bae, S.; Kim, H.; Lee, Y.; Xu, X.; Park, J.-S.; Zheng, Y.; Balakrishnan, J.; Lei, T.; Kim, H. R. Roll-to-Roll Production of 30-in. Graphene Films for Transparent Electrodes. *Nat. Nanotechnol*. **2010**, *5*, 574.

(5). Li, X. S.; Cai, W.W.; An, J.H.; Kim, S.; Nah, J.; Yang, D.X.; Piner, R.; Velamakanni, A.; Jung, I.; Tutuc, E.; Banerjee, S.K.; Colombo, L.; Ruoff, R.S. Large Area Synthesis on High Quality Graphene Films on Copper Foils. *Science* **2009,** *324*, 1312- 1314.

(6). Mattevi, C.; Kim, H.; Chhowalla, M. A Review of Chemical Vapor Deposition of Graphene on Copper. *J. Mater. Chem.* **2011,** *21*, 3324-3334.

(7). Li, X.; Cai, W.; Colombo, L.; Ruoff, R. S. Evolution of Graphene Growth on Ni and Cu by Carbon Isotope Labeling. *Nano Lett*. **2009**, *9*, 4268.

(8). Gao, L.; Ren, W.; Zhao, J.; Ma, L. P.; Chen, Z; Cheng, H. M. Efficient Growth of High-quality Graphene Films on Cu Foils by Ambient Pressure Chemical Vapor Deposition. *Appl. Phys. Lett*. **2010**, *97*, 183109.

(9). Bhaviripudi, S.; Jia, X.; Dresselhaus, M.; Kong, J. Role of Kinetic Factors in Chemical Vapor Deposition Synthesis of Uniform Large Area Graphene Using Copper Catalyst. *Nano Lett*. **2010**, *10*, 4128.

(10). Li, X.; Magnuson, C. W.; Venugopal, A.; An, J.; Suk, J. W.; Han, B.; Borysiak, M.; Cai, W.; Velamakanni, A.; Zhu, Y.; Graphene Films with Large Domain Size by a Two-Step Chemical Vapor Deposition Process. *Nano Lett.* **2010**, *10*, 4328–4334.

(11). Li, X.; Magnuson, C. W.; Venugopal, A.; Tromp, R. M.; Hannon, J. B.; Vogel, E. M.; Colombo, L.; Ruoff, R. S. Large- Area Graphene Single Crystals Grown by Low-Pressure Chemical Vapor Deposition of Methane on Copper. *J. Am. Chem. Soc.* **2011**, *133*, 2816.

(12). Bhaviripudi, S.; Jia, X.; Dresselhaus, M.; Kong, J. Role of Kinetic Factors in Chemical Vapor Deposition Synthesis of Uniform Large Area Graphene Using Copper Catalyst. *Nano Lett.* **2010**, *10*, 4128.

(13). Zhang, Y.; Zhang, L.; Kim, P.; Ge, M.; Zhen, L.; Zhou, C. Vapor Trapping Growth of Single-Crystalline Graphene Flowers: Synthesis, Morphology, and Electronic Properties. *Nano Lett*. **2012**, *12*, 2810-2816

(14). Yao, Y.; Wong, C. Monolayer graphene growth using additional etching process in atmospheric pressure chemical vapor deposition. *Carbon*. **2012**, *50*, 5203-5209

(15). Ago, H.; Ogawa, Y.; Tsuji, M.; Mizuno, S.; Hibino, H. Catalytic Growth of Graphene: Toward Large-Area Single Crystalline Graphene. *J. Phys. Chem. Lett*. **2012**, *3*, 2228-2236

(16). Vlassiouk, I.; Regmi, M; Fulvio, P.; Dai, S; Datskos, P; Eres, G.; Smirnov, S. Role of Hydrogen in Chemical Vapor Depostion Growth of Large Single Crystal Graphene. *ACS Nano* **2011**, *5(7)*, 6069-6076.

(17). Zhang, Z.; Li, Z.; Kim, P.; Zhang, L.; Zhou, C. Anisotropic Hydrogen Etching of Chemical Vapor Deposition Graphene. *ACS Nano* **2012**, *6 (1)*, 126-132.

(18). Gao, L.; Guest, J. R.; Guisinger, N. P. Epitaxial Graphene on Cu (111). *Nano Lett.* **2010**, *10 (9)*, 3512-3516.

(19). Zhao, L.; Rim, K. T.; Zhou, H.; He, R.; Heinz, T. F.; Pinczuk, A.; Flynn, G. W.; Pasupathy, A. N. Influence of Copper Crystal Surface on the CVD growth of Large Area Monolayer Graphene. Solid State Commun. **2011**, *151*, 509-513.

(20). Robinson, Z.; Tyagi, P.; Mowll, T. R.; Ventrice Jr, C. A.; Hannon, J. B. Argon-Assisted Growth of Epitaxial Graphene on Cu (111). *Phys. Rev. B.* **2012**, *86*, 235413-235420.

(21). Kidami, P.; Ducati,C.; Dlubak,B.; Gardiner,D.; Weatherup, R.; Martin, M.; Seneor, P.;Coles, H.; Hofmann, S. The Parameter Space of Graphene Chemical Vapor Deposition on Polycrystalline Cu. *J. Phys. Chem. C* **2012**, *116*, 22492-22501

(22). Madix, R.J.; Benziger, J. Kinetic Processes on Metal Single-Crystal Surfaces. *Ann. Rev. Phys. Chem.* **1978**, *29*, 285-306.

(23). Balooch, M.; Cardillo, M.J.; Miller, D.R.; Stickney, R.E. Molecular Beam Study of the Apparent Activation Barrier Associated with Adsorption and Desorption of Hydrogen on Copper. *Surf. Sci.* **1974**, *46(2)*, 358-392.

(24). Bond, G.C.; Louis, C.; Thompson, D.T.; *Catalysis by Gold, Catalytic science series*, Volume 6, Imperial College press, 2006.

(25). Sachtler, W. M. H.; Van Der Plank, P. The Role of Individual Surface Atoms in Chemisorption and Catalysis by Nickel-Copper Alloys. *Surf. Sci.* **1969**, *18*, 62-79.

(26). Suk, J.W.; Kitt, A.; Magnuson, C.W.; Hao, Y.; Ahmed, S.; An, J.; Swan, A.K.; Goldberg, B. B.; Ruoff, R.S. Transfer of CVD-Grown Monolayer Graphene onto Arbitrary Substrates. *ACS Nano* **2011**, *5 (9)*, 6916-6924.

(27). Dresselhaus, M. S.; Jorio, A.; Hofmann, M.; Dresselhaus, G.; Saito, R. Perspectives on Carbon Nanotubes and Graphene Raman Spectroscopy. *Nano Lett*. **2010**, 10, 751–758.

(28). Chu, P.K.; Li, L. Characterization of amorphous and nanocrystalline carbon films. *Mat. Chem. Phys.* **2006**, 96, 253-277.

(29). Cui, Y.; Fu, Q.; Zhang, H.; Tan, D.; Bao, X.; Dynamic Characterization of Graphene Growth and Etching by Oxygen on Ru (0001) by Photoemission Electron Microscopy. *J. Phys. Chem. C* **2009**, 113, 20365-20370.

(30). Sutter, P.; Sadowski, J.T.; Sutter, E.A.; Chemistry under Cover: Tuning Metal-Graphene Interaction by Reactive Intercalation. *J. Am. Chem. Soc*. **2010**, 132, 8175-8179.

(31). Starodub, E.; Bartlet, N.C.; McCarty, K.F.; Oxidation of Graphene on Metals. *J. Phys. Chem. C* **2010**, 114, 5134-5140.

CHAPTER 5 : Article 2: "Graphene CVD: Interplay Between Growth and Etching on Morphology and Stacking by Hydrogen and Oxidizing Impurities."

Saman Choubak[¶], Pierre L. Levesque[¥], Etienne Gaufres[¥], Maxime Biron[¶], Patrick Desjardins[¶]*, and Richard Martel [¥]*

[¶] Regroupement Québécois sur les Matériaux de Pointe (RQMP) and Département de Génie Physique, Polytechnique Montréal, C.P. 6079, Succursale Centre-ville, Montréal, Québec H3C 3A7, Canada

[¥] Regroupement Québécois sur les Matériaux de Pointe (RQMP) and Département de Chimie, Université de Montréal, C.P. 6128, Succursale Centre-Ville, Montréal, Québec H3C 3J7, Canada

* Correponding Authors

Reprinted with permission from Journal of Physical Chemistry C, 2014, 118, 21532-21540

Authors' Contribution: S. Choubak designed and conducted the experiments. Characterized, analysed, and interpreted the data. Drafted the manuscript and revised it accordingly. M. Biron transferred the graphene samples from Cu to SiO_2/Si and carried out some Raman spectroscopy measurements. P.L. Levesque provided advice during the course of experiments, characterized the sample using LEEM, and revised the manuscript. E. Gaufres characterized the samples using Raman imaging. P. Desjardins and R. Martel revised the manuscript critically for important intellectual content, approved the final version to be published and agreed to be responsible for all aspects of the work in ensuring that questions related to the accuracy or integrity of any part of the work are appropriately investigated and resolved.

CHAPTER 5: ARTICLE 2: "GRAPHENE CVD: INTERPLAY BETWEEN GROWTH AND ETCHING ON MORPHOLOGY AND STACKING BY HYDROGEN AND OXIDIZING IMPURITIES."

5.1 Abstract

The growth of high quality graphene layers by chemical vapor deposition (CVD) has been found to strongly depend on growth conditions with results varying greatly from one laboratory to another for nominally identical conditions. We report the results of a systematic investigation of the role of hydrogen and oxidizing impurities present in the gas feedstock during the growth and cooling stages in low-pressure CVD on copper. First, we show that for a partial pressure of oxidizing impurities below 1 ppb, hydrogen is not required for graphene growth from methane. Secondly, we demonstrate that purified hydrogen does not etch graphene films at typical growth temperatures. Third, a flow of purified hydrogen during cooling counterbalances graphene etching by oxygen, thus protecting the films. Films grown under high purity conditions (low level of oxidizing impurities) exhibit a higher bilayer and multilayer coverage; Surprisingly some of these bi- and multi-layer graphene islands are twisted with respect to the first graphene layer as revealed by hyperspectral Raman imaging. Overall, this growth behavior suggests a competitive action between film growth from the carbon precursor and etching by the oxidative species. Our results provide new fundamental insights on the graphene CVD growth, highlighting the important yet indirect role of hydrogen and its major influence on controlling the action of oxidizing impurities on nucleation and etching during the growth process.

5.2 Introduction

Chemical vapor deposition (CVD) of graphene on copper substrates demonstrates great potential for its large-scale production and its integration in industrial applications [1-4]. The most popular route for graphene growth was first presented by Li et al. [2]; it involves a low-pressure mixture of methane and hydrogen flowing over a copper substrate heated to a temperature of ~1000 °C, a value slightly below its melting point. Ever since, a plethora of publications investigating a vast array of graphene synthesis conditions has followed [3-13]. Notably, considerable efforts have been invested on varying the hydrogen and methane flow ratio in order to control the shape and

growth of graphene domains [6-12,14]. In particular, the role of hydrogen, which is often considered to be essential for growth, became the subject of intense research [15-19]. While most studies conclude that hydrogen is required for graphene CVD [15,18], few groups reported hydrogen-free growth in the sole presence of methane as the carbon source [10,20,21].

Consequently, several articles report experiments designed to investigate the role of H_2 on the etching of graphene films at high temperature [11,15,16,19,22]. A careful analysis of these articles reveals numerous inconsistencies which we recently attributed to the presence of traces of oxidizing species in the gas feedstock [21]. Indeed, the fact that many publications define H_2 as an etchant during growth and post-growth processing appears improbable since H_2 neither dissociates nor adsorbs on clean Cu surfaces [23,24]. Moreover, straightforward calculations reveal that the levels of oxidizing impurities in mixtures of commercially available ultra-high purity (UHP) gases are of comparable magnitude to the standard base pressure of the low pressure CVD (LP-CVD) chamber and that they are sufficient to play a significant role during the thermal treatment [21]. We thus devised systematic annealing experiments, similar to those reported by Zhang et al. [16], but with a fundamental difference: Gas purifiers were added on the existing UHP grade hydrogen gas bottle in order to minimize the amount of oxidizing impurities flowing into the annealing chamber. We revealed that, contrary to common belief, H_2 does not etch graphene during post growth anneals [21]. Indeed, we found the films to be perfectly stable when annealed at 825 °C under a flow of purified UHP H_2 whereas etching occurs during anneals in unpurified UHP H_2. We also showed, by carrying out experiments on as-grown graphene on Cu as well as on layers transferred on SiO_2, that Cu plays a catalytic role not only for growth but also for etching [21].

In practice, it is very difficult to completely eliminate the presence of oxidizing impurities during graphene CVD. These impurities – which originate from the gas feedstock, air leaks into the chamber, and the copper substrate [25] – can significantly impact graphene growth conditions by altering the balance between growth and etching [21,26]. Many articles report major efforts for optimizing the quality of graphene films by varying, for example, H_2 to CH_4 ratios, precursor gas flow rates and total reactor pressure [9,11,22]. Based on the above discussion, we believe that the wide range of reported growth conditions in this increasingly abundant literature is linked to the presence of oxidizing impurities in the CVD chamber before, during, or after growth. Whether the hydrogen reducing agent acts to suppress the etching effect of oxygen on graphene films or to

promote it, as suggested in many papers, is an important question that requires further investigation.

We report in this article the results of experiments designed for clarifying the role of H_2 and oxidizing impurities during graphene growth from CH_4 on copper foils at 500 mTorr pressure and at high temperature (in the 950-1000 ºC range). We first show that high purity molecular hydrogen does not etch graphene films on copper even at the growth temperature of 950 °C. Taking advantage of gas purifiers, we designed a series of experiments to decouple the role of oxidizing impurities, methane, argon, and hydrogen during the growth and post-growth process steps. For extremely low levels of oxidizing impurities, the presence of H_2 is not required for growing high quality graphene layers. That is, continuous and uniform graphene films were successfully grown using solely purified CH_4 ($O_2 < 1$ ppbV), which serves a double role as a copper oxide reducer and carbon supply for growth. Under standard conditions (unpurified gases), however, a flow of CH_4/H_2 was necessary during cooling for preventing etching. These results reveal a competitive action between oxidative etching and carbon growth, which balance, for a given CH_4/H_2 ratio, depends on the partial pressures of oxidative impurities in the gas feedstock. Following the growth stage, the graphene films can be protected from the detrimental effect of oxygen in the absence of CH_4 by flowing purified UHP H_2 during cooling. Our study confirms the etching effect of oxidizing impurities introduced from as-received gas bottles and by leaks at high temperature, and establishes their determining role for the optimum conditions of graphene low-pressure CVD (LP-CVD). It also demonstrates that oxidizing impurities are responsible for the observed graphene etching and that the primary role of hydrogen is to suppress and counter-balance this etching reaction.

5.3 Experimental details

5.3.1 Graphene growth

Graphene films were grown on 25-µm-thick Cu foils (Alfa Aesar, item no. 13382) at 950-1000 ºC in a 3.8-cm diameter (1.5 inch.) fused quartz tube inside a horizontal furnace (Lindberg/Blue M, Thermo Scientific) under low pressure conditions using H_2/CH_4, purified

UHP H_2/unpurified CH_4, and purified Ar/CH_4 gas mixture, as well as unpurified CH_4 and purified CH_4 gas. The system is equipped with a manifold capable of ultra high vacuum (UHV) conditions. Prior to each growth, the system is evacuated to a vacuum of 5 $x10^{-6}$ Torr using a turbo molecular pump. The copper foils are then heated to 1000 ºC and annealed at this temperature for 30 min under the flow, at 50 mTorr, of the specific gas used in each recipe. Then, growth is carried out at temperatures between 950 and 1000 °C for 45 min. with the reactor pressure maintained at 500 mTorr. Finally, the chamber is cooled down to room temperature, which takes about 100 minutes.

The Cu foils were chemically cleaned in 1 M acetic acid (Sigma Aldrich, Reagent Plus > 99%) at 60 ºC followed by acetone and then 2-propanol (without drying) for 10 min in each step. The Cu substrates are then blown-dried with nitrogen.

The use of specific gas purifiers for each gas line is key to this investigation. We selected purifiers that allowed to decrease the residual O_2 content in UHP gases to less than 1 ppbV: (i) For H_2 (Praxair, UHP, grade 5, O_2 < 1ppm), we use DEOXO^{TM} (O_2 < 1ppb), (ii) for CH_4 (Praxair, UHP, grade 3.7, O_2 < 15ppm), we use SAES Pure Gas Inc. MC1-950FV (H_2O and O_2 < 1ppbV), and (iii) for Ar (Alfagaz, UHP, grade 2, O_2 < 1ppm), we use SAES Pure Gas Inc. MC1-902FV (H_2O and O_2 < 1ppbV). In order to carefully control the growth experiments, the purifiers are installed on the same gas bottles with which experiments with as-received gases were conducted.

5.3.2 Graphene annealing experiments

In order to permit comparison of the results of the annealing experiments with our previous work [21] and with the recent literature [9,15,16], graphene layers were grown using unpurified 450 mTorr CH_4 and 50 mTorr H_2 at 1000°C. The sample cleaning and growth procedures were those described in section 2.1. This procedure yields continuous and uniform films.

The as-grown films were analyzed by scanning electron microscope (SEM) to verify that they were complete graphene layers. The samples were then placed inside the CVD chamber for carrying out the annealing experiments. The chamber was pumped down to 5x10^{-6} Torr. Samples were then exposed to a flow of either as-received or purified UHP hydrogen at 950 °C for 30 minutes maintaining a system pressure of 500 mTorr during the process. The morphology of

each annealed graphene sample was examined using SEM and, in some cases, low-energy electron microscopy (LEEM).

5.3.3 Graphene transfer

Graphene layers were transferred onto SiO_2 (100-nm-thick)/Si wafers by the commonly used method based on poly-methyl methacrylate (PMMA) support [27]. First, a PMMA (M.W. 15000 GPC, Acros organics, 4% in chlorobenzene) layer is spin-coated at 4000 rpm for 30 sec over the front side of the graphene/copper sample and dried in air at room temperature for 1 hour. After protecting the top graphene layer with PMMA, graphene grown on the back face is removed using an oxygen plasma (100 W for 1 min). The copper foil is then etched by immersing the copper-graphene-PMMA stack in 0.1 M aqueous ammonium persulfate (Reagent, ACS 98+%, Acros Organics). After complete Cu removal, the floating PMMA/graphene film is rinsed in DI water, transferred onto a SiO_2/Si substrate, and dried in vacuum for approximately 1 hour. Finally, the PMMA is dissolved in acetone, and the sample is rinsed in isopropyl alcohol and blown-dried with nitrogen.

5.3.4 Characterization

Electron Microscopy: SEM was carried out using a Hitachi S-4700 microscope operated at 1 kV. Low Energy Electron Microscopy (LEEM) was performed at 2.4 eV kinetic energy in the UHV chamber (base pressure $4x10^{-10}$ mbar) using a FE-LEEM P90 from SPECS-GmbH.

Raman Spectroscopy and imaging: Raman microspectroscopy measurements are performed at room temperature with a Renishaw Invia spectrometer with a laser wavelength of 514 nm. A 50X objective (N.A= 0.55) focuses a 4 mW laser beam to a probe spot about 1 µm in diameter. Raman imaging was carried out using a hyperspectral Raman imager RIMA^{TM} based on a Bragg Tunable Filter (BTF) technology [28]. In these measurements, a continuous wave (cw) laser line at λ=532 nm illuminates a 100 x 100 μm^2 sample surface area through a 100X microscope

objective (N.A=0.9). In this configuration, the sample is excited with a fluence of 150 $\mu W.\mu m^{-2}$, the acquisition time is 120 sec per frame and the resolution is diffraction limited.

5.4 Results

5.4.1 Graphene annealing experiments

As indicated above, we have already demonstrated that purified UHP hydrogen does not etch graphene films deposited on Cu substrates when annealed at 825 °C [21], whereas films were significantly etched by oxidizing impurities when treated in as-received UHP H_2. Building upon these results, we have conducted further annealing studies for investigating the effects of H_2 and oxidizing impurities at 950 °C, a value within the range of typical graphene growth temperatures. Figure 5-1a shows a SEM image from an as-grown graphene layer. The film is continuous with small areas exhibiting the growth of a 2nd graphene layer. These films are comparable to the best reported data [2]. Films annealed for 30 min at 950 °C in unpurified UHP H_2 are considerably etched, as depicted in the SEM micrograph of Figure 5-1b. Only small patches of graphene remain visible on the surface. The samples were transferred on SiO_2/Si for further analysis and it is confirmed by Raman spectra and SEM contrast that the small patches are indeed graphene (see supplemental information, Figure 1S). In stark contrast, Figure 5-1c reveals that the same annealing procedure carried out in purified UHP H_2 has virtually no effect on the graphene films.

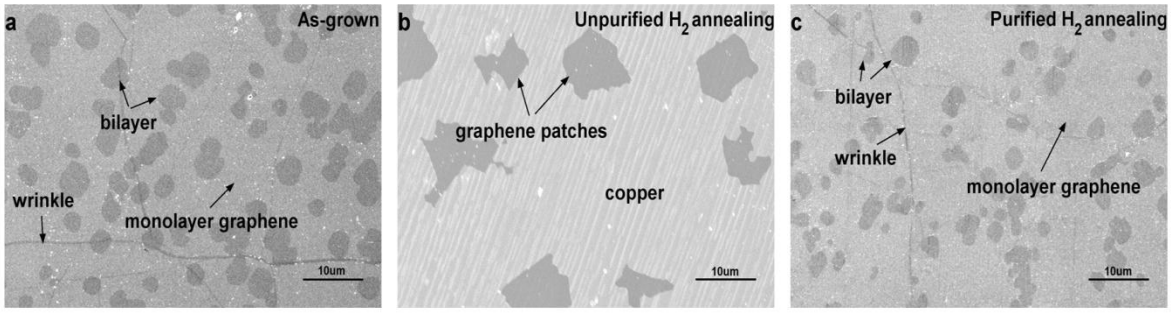

Figure 5-1. SEM images of (a) as-grown graphene film on a copper foil, and annealed samples at 950 °C for 30 min in 500 mTorr of (b) unpurified UHP-grade H_2, and c) purified UHP-grade H_2.

These observations confirm that molecular hydrogen does not etch graphene films on Cu at typical growth temperatures and partial pressures. These results also highlight that partial pressures of oxidizing impurities found in typical growth conditions are sufficient to activate a competing etching reaction pathway during graphene LP-CVD, even during the actual growth stage and sample cool-down.

5.4.2 Graphene growth experiments

We have carefully designed a series of experiments for clarifying the role of H_2 and oxidizing impurities during graphene LP-CVD from CH_4/H_2 mixtures on copper foil. The typical graphene LP-CVD process in represented schematically in Figure 5-2. Temperature profile as well as gas sequences are presented as a function of time for the entire growth process starting from a pre-deposition annealing stage to the graphene growth itself to the final cool-down phase. Figure 5-3 depicts the complete set of experiments reported in this study. Each and every growth is conducted at least three times in the same conditions to confirm the results.

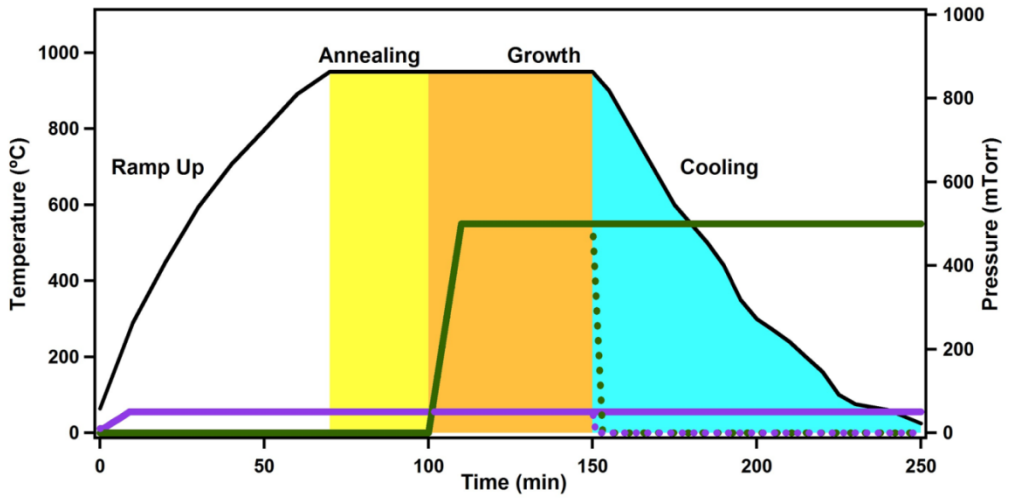

Figure 5-2. Schematic of the typical CVD growth process. Broad lines depict the temperature profile. The fine solid lines represent the partial pressure of the specific gas present during the annealing, growth, and cooling stages (i.e : H_2 purple and CH_4 green) while the dashed lines are used to emphasize the fact that, for some experiments, gas flows were interrupted during the cool down period. Figure 3 presents the detailed gas sequences for all samples investigated in this study.

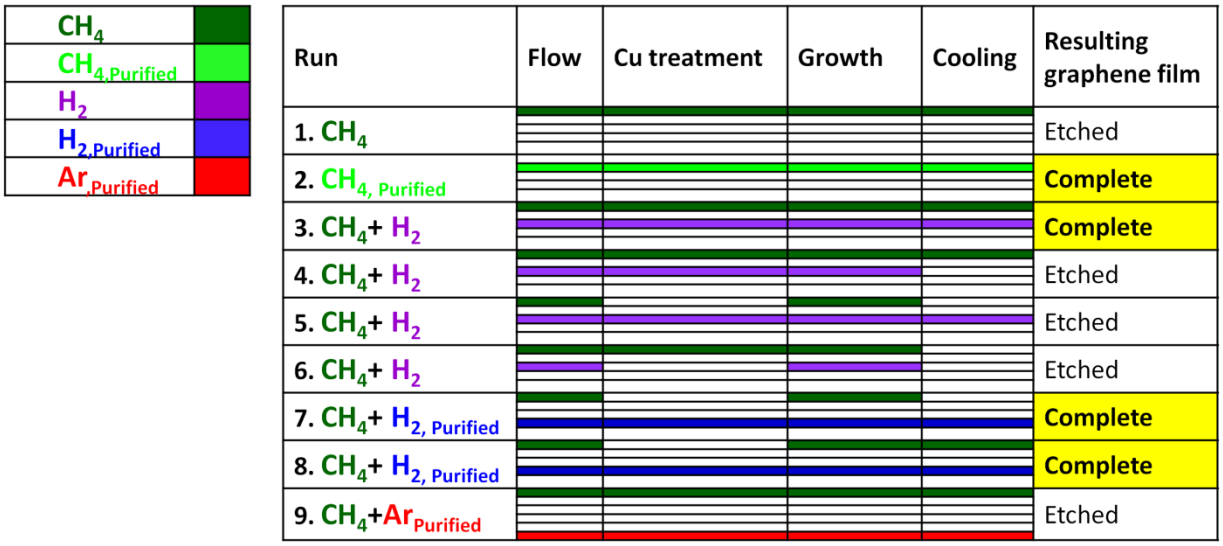

Figure 5-3. Growth experiments conducted in this study. Filled lines indicate the gas mixture used in each experiment.

5.4.2.1 Growth from unpurified and purified methane

In a first series of experiments, we wanted to establish if, as suggested by some authors [15,18], hydrogen is required for growing complete graphene layers. These experiments are also motivated by the fact that methane is used to reduce the copper oxide in chemical looping combustion for the production of carbon dioxide [29].

The SEM image in Figure 5-4a, corresponding to a film grown with only unpurified methane present during all stages of the process (including the cool-down period), reveals that the graphene layers are incomplete when grown under these conditions. In stark contrast, the micrograph in Figure 5-4b corresponding to a film grown with only purified methane present during all stages of the process (including cool-down), clearly demonstrates that hydrogen is not required for obtaining complete graphene layers. These results indicate (i) that hydrogen is not required for graphene growth and (ii) that low level of oxidizing impurities in the absence of hydrogen are essential for achieving continuous and uniform graphene films.

5.4.2.2 Effects of methane and hydrogen during post-growth cooling

Since the experiments described above reveal that graphene can be grown from methane alone, we wanted to investigate the role played by hydrogen when added to the gas mixture. The experiments, summarized in lines 3 to 8 of Figure 5-3, were devised to enable us to decouple the effects during the growth and cool-down stages.

We begin with the original graphene recipe where unpurified hydrogen and methane are both present during growth and cooling. These films are complete as shown in Figure. 5-4c (Figure 5-3, Run #3). In comparison, non-continuous films are obtained for samples grown with unpurified methane and hydrogen whether only hydrogen (Figure 5-3, Run #4) or methane (Figure 5-3, Run #5) are present during cool down (Figure 5-4d and e, respectively). Layers are also etched when cool down is carried out under vacuum as shown in Figure 5-4f (Figure 5- 3, Run #6). However, samples grown from unpurified methane and purified hydrogen but with only purified hydrogen during cool down (Figure 5- 3, Run #7) are continuous and uniform (Figure 5-4g). Graphene layers are also continuous and uniform (Figure 5-4h) when both purified hydrogen and unpurified methane are present during cool down (Figure 5-3, Run #8).

We attribute this overall behavior to the presence of residual oxidizing impurities in UHP-hydrogen at levels sufficiently high to etch graphene at high temperature. The use of purified UHP hydrogen during cooling, when no methane is present, prevents graphene etching and leads to uniform and continuous films on the copper substrate. Moreover, the use of unpurified hydrogen and methane gases, taken separately, which contain a low level of oxidizing impurities (~1-15 ppm), readily leads to etching of graphene on copper at these high temperatures. Finally, we believe that the sample cooled under vacuum is etched as a result of small air leaks into the vacuum system, inherent to the O-ring type of sealing of LP-CVD setups.

5.4.2.3 Growth (methane and purified argon)

Since some growth experiments reported in the literature were conducted in Ar/H_2 mixtures [14,15], a third set of experiments is performed by replacing hydrogen with purified argon (Figure 5-3, Line 9). This procedure aims to test the effects of inert gases, but also to exclude any steric effect

(occupying surface sites on copper) brought by hydrogen gas on the surface in graphene LP-CVD. The SEM image in Figure 5-4i reveals that samples grown from unpurified methane and purified Ar are etched and non-continuous.

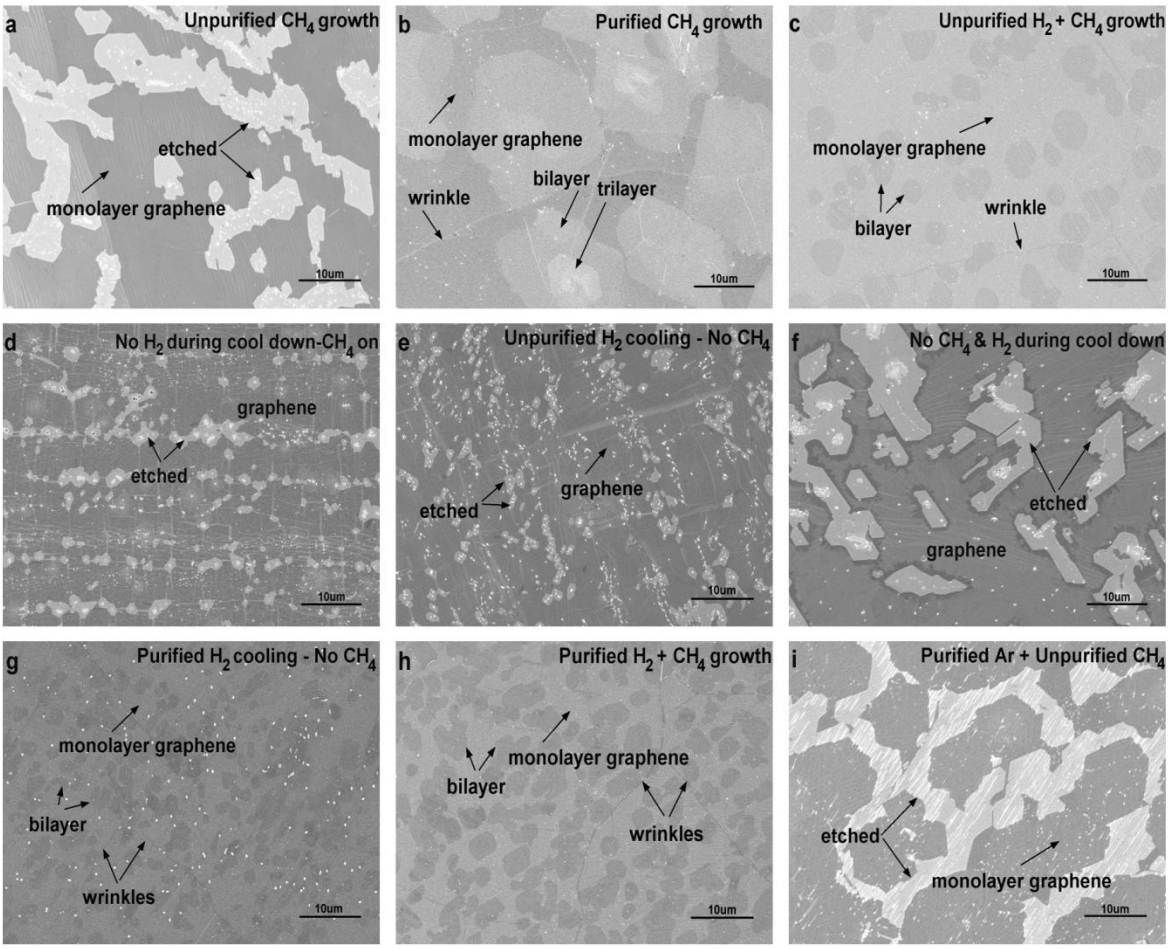

Figure 5-4. SEM images of graphene films grown on copper foils at a temperature of 1000 ºC and a total pressure of 500 mTorr. a) unpurified methane (Fig. 5-3, Run #1), b) purified methane (Fig. 5-3, Run #2), c) unpurified methane and UHP hydrogen (based on the original CVD recipe) (Fig. 5-3, Run #3), d) unpurified methane and UHP hydrogen during growth but only unpurified methane during cool down (Fig. 5-3, Run #4), e) unpurified UHP hydrogen and methane during growth but only unpurified UHP hydrogen during cool down (Fig. 5-3, Run #5), f) unpurified UHP hydrogen and methane during growth but both stopped during cool down (Fig. 5-3, Run #6), g) purified UHP hydrogen and unpurified methane during growth but only purified hydrogen during cool down (Fig. 5-3, Run #7), h) purified UHP hydrogen and unpurified methane growth both on during cool down (Fig. 5-3, Run #8) and i) purified argon and unpurified methane (Fig. 5- 3, Run #9).

5.4.3 Graphene multilayer growth in purified conditions

The results presented in section 5.4.2 and summarized in Figure 5-4 demonstrate that continuous graphene films can be obtained in several ways. A careful analysis of SEM images nevertheless reveals that samples grown under purified conditions exhibit a higher density of graphene bilayer domains, a higher overall coverage of bilayers, and most importantly multilayers when solely purified methane is used for growth.

We begin by comparing the samples grown using the original graphene growth recipe - unpurified methane and unpurified UHP hydrogen (Fig. 5-3, Run #3 & Fig.5-4c) - with samples grown using unpurified methane but purified UHP hydrogen (Fig.5-3, Run #8 & Fig.5-4h). The only difference between the two growth recipes is the gas purity level. A detailed analysis of SEM images of three batches of each growth recipe shows that the surface coverage of bilayer domains increases by a factor of ~2 (from 25±6.2 to 54±6.3%), while the number of nucleation raises by a factor of ~ 2.5 when purified UHP hydrogen is used. Furthermore, graphene growth using purified methane (Fig.5-3, Run #2 & Fig.5-4b) reveals even greater differences. Comparing the results in Fig.5-4c and Fig.5-4b, we note a higher density of graphene bilayer domains, a higher overall bilayer coverage, and most importantly several areas of multilayers growth (bilayers, trilayers, etc.) when solely purified methane is used.

Moreover, graphene films grown on copper foils in a reducing environment, using purified methane and purified UHP hydrogen (Fig.5-5b), in which the levels of oxidizing impurities are very low compared to the original graphene growth recipe (Fig.5-5a), exhibit multilayer growth. This is similar to the case where purified methane is used solely during the growth and cool down phases (Fig.5-4b). Figure 5c is a LEEM image of a similar sample shown in the SEM image of Fig.5-5b. The contrast in the LEEM image unambiguously differentiates multiple layers of graphene films grown on copper [30].

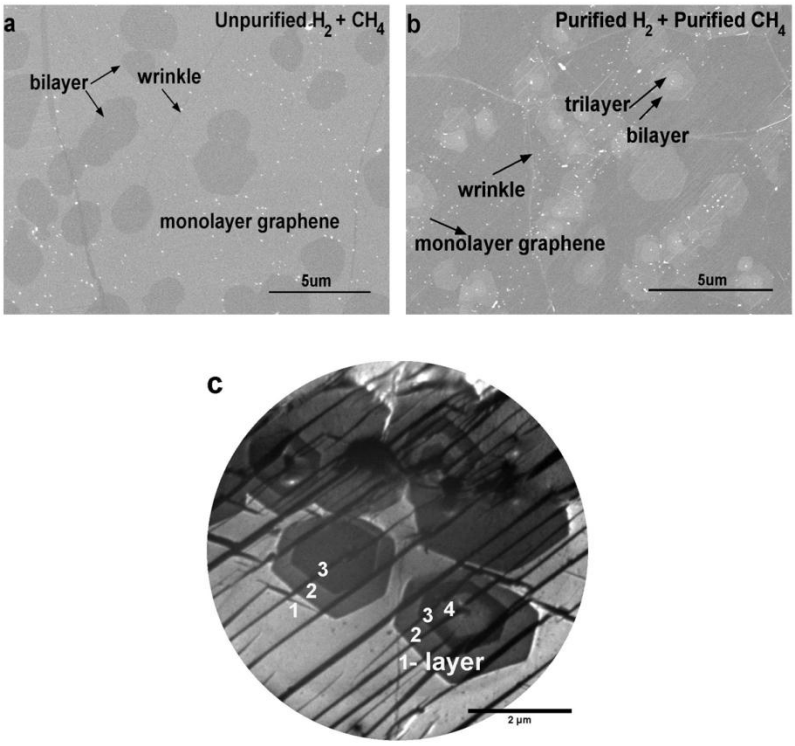

Figure 5-5. SEM images of graphene films grown on copper foils based on original graphene growth recipe at 1000° C and 500 mTorr using a) unpurified UHP hydrogen and unpurified methane, b) purified UHP hydrogen and purified methane, and c) bright field (BF) LEEM image of graphene films grown on Cu foil in the same condition as b.

5.4.4 Raman characterization

Raman spectroscopy is a nondestructive and powerful technique for evaluating the structural properties of graphene, which allows graphene to be distinguished from graphite and to determine the number of graphene layers and their structural quality [31]. Raman microspectrometry measurements were carried out on all samples following the transfer of the graphene films onto a 100 nm SiO_2 layer on Si (See section 5.3.3 for the transfer procedure). Spectra from five representative spectra of graphene samples, together with a reference spectrum from an etched region, are presented in Figure 5-6. Spectra from samples corresponding to Runs #4 to 6 are nearly identical to that from Run #3 (Fig.5-6c) and are omitted for clarity.

Overall, the spectra reveal that samples are high quality graphene layers as indicated by strong 2D and low D band intensities. The full width at half-maximum (FWHM) intensity of the 2D band is approximately 28 cm^{-1} for all samples and the ratio of the 2D to G band peak intensity (I_{2D}/I_G) is ~ 3.2. These measurements confirm the presence of single layer graphene (SLG) [2,21,32] and the low intensity of the D peak, associated with the presence of defects in graphene, indicates that the films maintain high quality after the transfer process [27].

The Raman spectrum from the film grown using purified methane (Fig. 6b) exhibits two additional peaks at approximately 1455 cm^{-1} (the so-called R mode) and 1625 cm^{-1} (the so-called D' mode). These modes have been ascribed to intravalley and intervalley interactions between two rotated graphene layers [33-35], thereby providing strong evidences that our grown samples contain twisted bilayer graphene (BLG) or/and multilayer graphene (MLG). In other words these Raman modes indicate that bi- , tri- and even thicker multilayer graphene films are formed with random rotational angles between them and that those MLG appear to grow without the directionality expected from the strong interlayer coupling. The presence of these multilayers is consistent with SEM and LEEM observations presented in Fig.5-4b and 5-5b-c.

We have used hyperspectral Raman imaging to further investigate this behavior and to determine whether these Raman peaks (R and D' mode) are also present in graphene films grown in unpurified conditions. We focused on two extreme scenarios corresponding to highly oxidative and highly reductive growth conditions: i.e. growth using the original graphene recipe with unpurified hydrogen and methane mixture (Fig.5-3, Run #3) and growth with solely purified methane (Fig.5-3, Run #2).

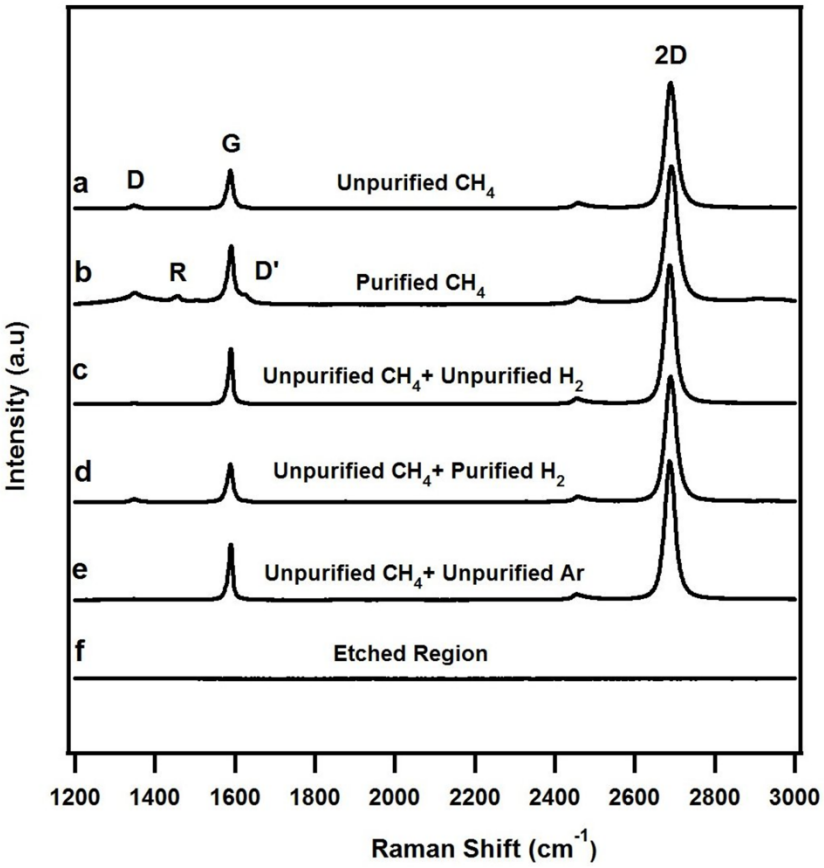

Figure 5-6. Raman spectra (λ = 514 nm) of graphene films grown on copper foils at a temperature of 1000 ºC and a total pressure of 500 mTorr using the following gas mixtures: a) purified methane (Fig.5-3, Run #1), b) unpurified methane (Fig.5-3, Run #2), c) unpurified methane and unpurified UHP hydrogen-based on the original CVD recipe (Fig.5-3, Run #3), d) unpurified methane and purified UHP hydrogen (Fig.5-3, Run #8), e) unpurified methane and purified argon (Fig.5-3, Run #9). Curve f) presents for reference a Raman spectrum from an etched region of unpurified methane growth. Note that the Raman spectrum of Run #4-6 from Figure 2 were similar to Run # 3 and Run #7 was identical to Run #8 (c-d) but are not shown in this graph

Figure 5-7 (a-b) displays Raman images from both samples at the G-mode frequency extracted from the hyperspectral Raman data taken using an illumination wavelength of 532 nm. The intensity variations of the G-mode provide indications on the emergence and stacking of the bi- and tri-layers [35]. These Raman images corroborate reasonably well with the SEM and LEEM (Fig. 5-4b-c and Fig. 5-5c) shown previously. Moreover, we notice a strong enhancement of the

G band intensity in Fig.5-7b (bright spots) in few BLG regions of the layers grown in purified methane conditions. This phenomenon on Raman intensity was described by Havener et al. as the emergence of a resonance due to a new singularity in twisted BLG joint density of state [35]. The energy position of this singularity is directly governed by the twist angle of the BLG. According to their work, the enhanced areas in Figure 5-7b correspond to BLG with a twisted angle of about 13,5° for our laser wavelength (λ=532 nm).

Selected local spectra, extracted from the hyperspectral images at locations indicated in Fig.5-7a-b, are presented in Fig.5-7c-d. In addition to the common shape of the D band at 1350 cm^{-1} and the G band at 1590 cm^{-1}, some of the spectra taken in the BLG regions - (bright spots 8-9 in Fig. 7b) - exhibit additional Raman features near 1550 cm^{-1} (R mode) and 1640 cm^{-1} (the D' mode). The presence of these modes provide further evidence that these BLG areas are twisted (i.e. rotated orientation relative to each other). Finally, note that the G band intensity enhancement and the emergence of the additional peaks in local Raman spectra indicate that twisted graphene layers are mostly present in purified conditions.

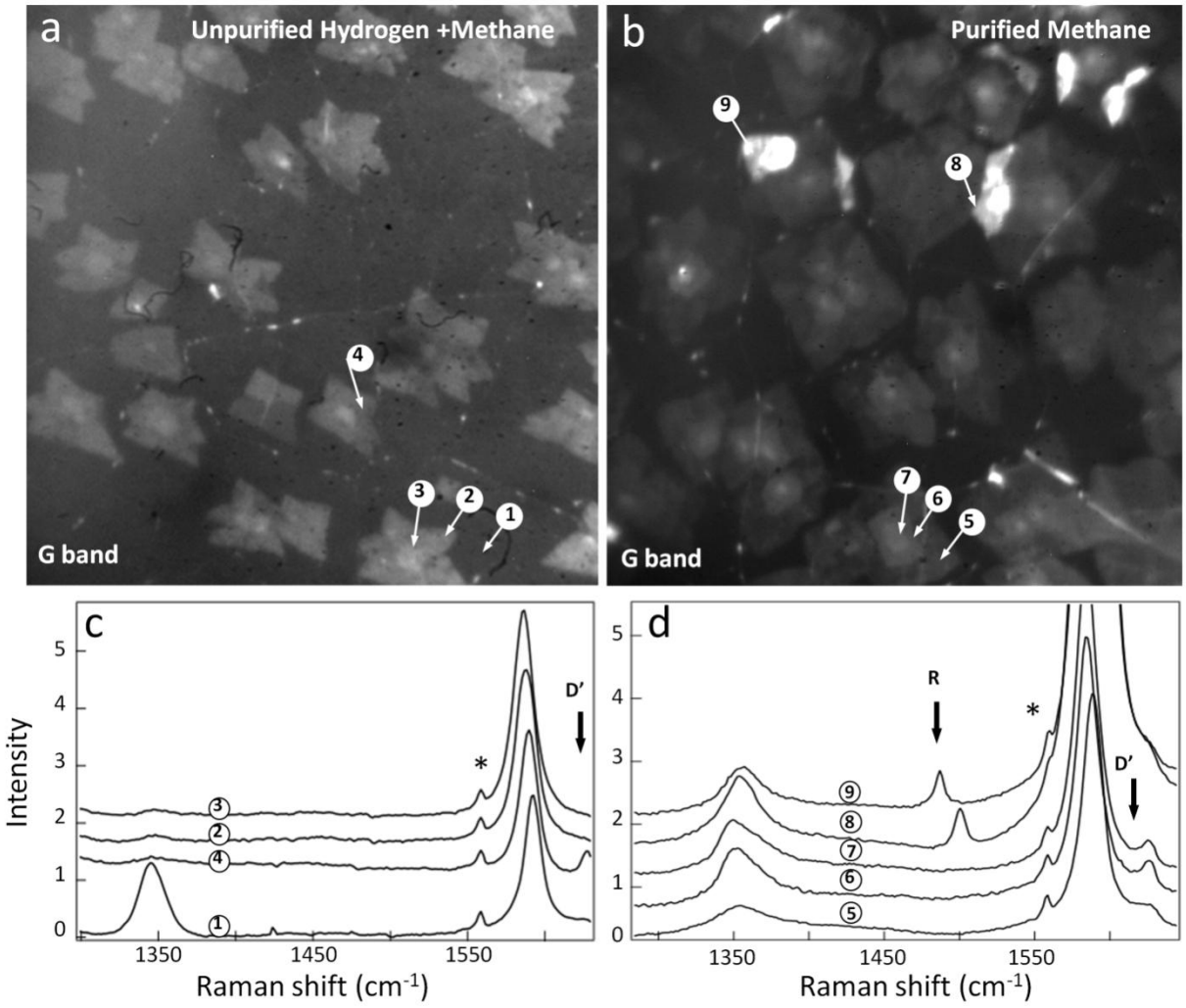

Figure 5-7. Raman hyperspectral images of the G band intensity of layers grown on copper foils at a temperature of 1000 ºC and a total pressure of 500 mTorr using (a) the original graphene growth recipe (unpurified UHP hydrogen and methane) (Fig.5-3, Run #3) and (b) purified methane only (Fig.5-3, Run #1). (c-d), Raman spectra from specific areas of the samples indicated in (a) and (b). The peak highlighted by an asterisk is an instrument artifact.

5.5 Discussion

The experimental results presented in the previous section clearly demonstrate that continuous and uniform graphene films can be grown in the sole presence of purified methane (O_2 < 1 ppbV). This indicates that methane serves the dual role of copper oxide reducer [29] and carbon supplier for growth. In addition, the need of having purified methane present in the chamber during cooling for obtaining complete graphene films suggests that small amounts of oxidative impurities can leak into typical low-pressure CVD systems fitted with O-ring seals. Adding a flow of purified methane during the cooling stage provides a reducing environment that is sufficient to protect the films against oxidation and to help maintain the overall conditions required for graphene stability and growth at high temperature.

The CH_4/H_2 mixture, as reported in the original graphene LPCVD growth recipe [2], provides similar but enhanced reducing conditions that prevent etching from background impurities. Besides supplying carbon for growth, the chemistry most likely involves additional reductive reaction paths against the oxidizing species introduced into the chamber. Once growth is complete, however, it is only required to prevent etching from air leaks during cool-down; this could be achieved by flowing merely purified UHP hydrogen. Our results show that purified UHP hydrogen works as well as a mixture of unpurified CH_4/H_2, which precise composition appears to depend on the oxygen level introduced into the CVD chamber.

By replacing hydrogen with purified Argon, the results confirmed our hypothesis that Ar, an inert gas, plays no direct role in graphene low pressure CVD growth. Thus, in conditions where the level of oxidizing impurities is typical of UHP gases, purified UHP hydrogen appears to be the best option for establishing reductive conditions and preventing etching of growing or previously grown graphene films on copper. The growth and annealing experiments described above and in reference [21] strongly support that hydrogen does not etch graphene on Cu in LPCVD, even at high temperatures. We therefore conclude that the role played by hydrogen is to protect the film against oxidative etching reactions. Further investigations will be required to elucidate the detailed reaction mechanism for this effect.

While our results demonstrate that complete graphene layers can be obtained using a variety of growth conditions (see Figure 5-3), they also reveal important differences in the resulting films. Namely, we observed that films grown from purified gases exhibited a significantly higher

bilayer and multilayer coverage, as shown by LEEM and SEM (Fig.5-5 and Fig.5-4h&4b), compared to films grown using the "standard" recipe involving as-received UHP precursors.

Based on literature, there is a consensus that catalytic decomposition of methane by Cu generates mobile intermediate species, such as C_mH_n: (e.g. CH_3, CH_2, CH, C, C_2H_n, etc.) on the Cu surface, which are growth precursors for the multilayers [36,37]. The mechanism of formation of these multilayers is however not well understood and is even controversial. Nie et al. [30] reported an underlayer growth mechanism where the second layer and subsequent layers are grown from below. They believe that new layers nucleate and grow next to the substrate and the graphene multilayer growth terminates once the Cu is covered with the main layer. Other groups have concluded using Raman investigation of isotope-labeled bilayer films that these multilayers are indeed underneath the first or main graphene layer [36,38]. On the contrary, other studies proposed that the multilayers are rather grown on top of previously formed domains and this is mostly due to the excess supply of methane [39-41].

Our entire set of results reveals that multilayer growth occurs primarily in highly reducing environments, when the level of oxidizing impurities during LP-CVD is low. Moreover, our results indicate that Cu is an active interface not only for the growth but also for the etching [16,19,21] and that etching is not occurring via hydrogen, but from oxygen impurities. Therefore, in the absence of oxidizing species, the films cannot be etched and the carbon precursors cannot be burnt at the Cu interface, leading to an excess amount of carbon species and further multilayer growth. The top growth mechanism appears therefore inconsistent with these conclusions because the Cu catalyst providing growth and etching of the graphene edges is blocked as the main graphene layer becomes larger than the multilayer islands. Note that etching by impurities is not observed on graphene layers on SiO_2 (i.e. no Cu) [16,19,21]. Thus, we believe that the most plausible growth mechanism is from below since multilayers can grow/etch as long as the bare Cu surface is available for dissociating CH_4 to grow graphene layers and impurities to etch them. When the main layer is complete, however, the growth/etching rates of these multilayers drop significantly, even after longer exposure time, due to a lack of new supply of carbon and impurities.

Furthermore, in the original graphene growth recipe – in which methane and UHP hydrogen are both unpurified – the surface coverage of bilayer domains is reduced by a factor of ~2 while the number of nuclei is decreased by a factor of ~ 2.5, compared to the case where purified UHP

hydrogen and unpurified methane is used. We believe that in the presence of higher amounts of oxidizing impurities, graphene islands are etched and that growth precursor's species are captured; therefore the number and size of graphene islands decreases. Consequently, few bilayer and multilayer areas remain at the end of the growth process. This implies that controlling the level of oxygen during the growth is a powerful mean to tailor the morphology of the film.

Lastly, Raman imaging has shown that MLG films grown in the sole presence of purified methane contains twisted bilayers whereas no evidence of such incommensurability is observed on the films grown based on the original graphene growth recipe [2]. This is consistent with the above growth behavior where a highly reduced environment, in which etching is minimized, favors multilayer growth. Due to the absence of oxidizing impurities, the overall "effective" attachment rate of carbon species to the graphene edge, the mere nature of the methane intermediate species as well as their mobility are likely to be modified since nothing is blocking or interfering with them during the growth process. The presence of incommensurate graphene multilayers is therefore evidence that these changes lead to different growth kinetics. In the unpurified growth conditions, graphene nucleation and growth occur while the competition between carbon atoms impinging the surface and attaching to graphene edges, and oxidizing impurities etching some of these C species remains active. These oxidative species thus slow down the kinetics and add more freedom to the carbon atoms to be placed in accordance with each other, which direct consequence is the formation of more commensurate BLG and MLG.

5.6 Conclusion

We have shown that hydrogen is not required for graphene growth from methane in the absence of oxidizing impurities. We also confirmed that purified UHP hydrogen does not etch graphene in low pressure CVD conditions and that small amounts of oxidizing species are responsible for this etching reaction. Using carefully designed graphene growth experiments, we have decoupled the role of hydrogen and oxidizing species during the growth and cooling stages. We revealed that oxidizing impurities clearly play a significant role in graphene CVD and that a flow of hydrogen can counterbalance the graphene etching reaction. Furthermore, films grown under high purity conditions (low level of oxidizing impurities) exhibit a higher bilayer and multilayer coverage, as observed with low energy electron microscope (LEEM) and scanning electron

microscope (SEM). Surprisingly, some of these bi- and multi-layer graphene islands are twisted with respect to the first graphene layer as revealed by hyperspectral Raman imaging.

In light of these experiments, further investigation of the growth mechanism will be possible by taking into account the impact of oxidizing species, which may reveal to be the key elements to influence the growth kinetics and to identify new routes towards large scale fabrication of high quality single crystalline graphene films.

Acknowledgment

The authors thank Dr. Nicolas Cottenye for fruitful discussions and Mr. Joël Bouchard for technical support and discussions. This research was financially supported by the Natural Sciences and Engineering Research Council of Canada (NSERC), the Canada Research Chair program and the Selenium Tellurium Development Association. Sample characterization was carried out in the Thin Film Research Laboratories at Polytechnique/UdeM, which are partially supported by grants from NanoQuébec and the Fonds de Recherche du Québec.

5.7 Supporting information

1. Graphene sample annealed in unpurified hydrogen at 950 °C transferred on SiO_2/Si

Figure S1 is the SEM image of the transferred graphene sample presented in Fig 1b. It also shows the Raman spectra for this sample. Based on the SEM image contrast and Raman measurement, it is confirmed that the small patches are indeed the remaining graphene.

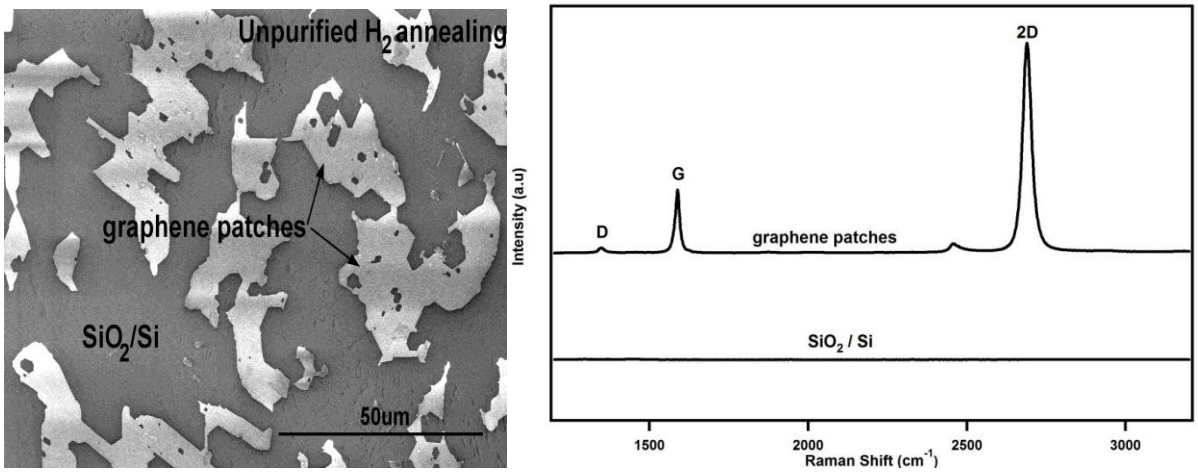

Figure S1. SEM image and Raman spectra of the unpurified hydrogen annealed sample as shown in Fig. 5-1b at 950 °C for 30 min transferred on SiO_2/Si.

5.8 References

(1) Bae, S.; Kim, H.; Lee, Y.; Xu, X. F.; Park, J. S.; Zheng, Y.; Balakrishnan, J.; Lei, T.; Kim, H. R.; Song, Y. I.; et al. Roll-to-Roll Production of 30-inch Graphene Films for Transparent Electrodes. *Nat. nanotechnol.* **2010**, *5*, 574-578.

(2) Li, X.; Cai, W.; An, J.; Kim, S.; Nah, J.; Yang, D.; Piner, R.; Velamakanni, A.; Jung, I.; Tutuc, E.; et al. Large-Area Synthesis of High-Quality and Uniform Graphene Films on Copper Foils. *Science* **2009**, *324*, 1312-4.

(3) Mattevi, C.; Kim, H.; Chhowalla, M. A Review of Chemical Vapour Deposition of Graphene on Copper. *J. Mater. Chem.* **2011**, *21*, 3324.

(4) Li, X. S.; Magnuson, C. W.; Venugopal, A.; An, J. H.; Suk, J. W.; Han, B. Y.; Borysiak, M.; Cai, W. W.; Velamakanni, A.; Zhu, Y. W.; Fu, L. F.; et al. Graphene Films with Large Domain Size by a Two-Step Chemical Vapor Deposition Process. *Nano Lett.* **2010**, *10*, 4328-4334.

(5) Bhaviripudi, S.; Jia, X. T.; Dresselhaus, M. S.; Kong, J. Role of Kinetic Factors in Chemical Vapor Deposition Synthesis of Uniform Large Area Graphene Using Copper Catalyst. *Nano Lett* **2010**, *10*, 4128-4133.

(6) Fan, L. L.; Zou, J.; Li, Z.; Li, X.; Wang, K. L.; Wei, J. Q.; Zhong, M. L.; Wu, D. H.; Xu, Z. P.; Zhu, H. W. Topology Evolution of Graphene in Chemical Vapor Deposition, A Combined Theoretical/Experimental Approach Toward Shape Control of graphene domains. *Nanotechnology*, **2012**, *23*,115605.

(7) Fan, L. L.; Li, Z.; Li, X.; Wang, K. L.; Zhong, M. L.; Wei, J. Q.; Wu, D. H.; Zhu, H. W.: Controllable Growth of Shaped Graphene Domains by Atmospheric Pressure Chemical Vapour Deposition. *Nanoscale* **2011**, *3*, 4946-4950.

(8) Li, X.; Magnuson, C. W.; Venugopal, A.; Tromp, R. M.; Hannon, J. B.; Vogel, E. M.; Colombo, L.; Ruoff, R. S. Large-area Graphene Single Crystals Grown by Low-Pressure Chemical Vapor Deposition of Methane on Copper. *J. Am. Chem. Soc.* **2011**, *133*, 2816-9.

(9) Jacobberger, R. M.; Arnold, M. S. Graphene Growth Dynamics on Epitaxial Copper Thin Films. *Chem. Mater.* **2013**, *25*, 871-877.

(10) Gao, L. B.; Ren, W. C.; Zhao, J. P.; Ma, L. P.; Chen, Z. P.; Cheng, H. M. Efficient Growth of High-Quality Graphene Films on Cu Foils by Ambient Pressure Chemical Vapor Deposition. *Appl. Phys. Lett.* **2010**, *97*, 183109.

(11) Zhang, Y.; Zhang, L.; Kim, P.; Ge, M.; Li, Z.; Zhou, C. Vapor Trapping Growth of Single-Crystalline Graphene Flowers: Synthesis, Morphology, and Electronic Properties. *Nano Lett.* **2012**, *12*, 2810-2816.

(12) Liu, L. X.; Zhou, H. L.; Cheng, R.; Chen, Y.; Lin, Y. C.; Qu, Y. Q.; Bai, J. W.; Ivanov, I. A.; Liu, G.; Huang, Y.; Duan, X. F. A Systematic Study of Atmospheric Pressure Chemical Vapor Deposition Growth of Large-Area Monolayer Graphene. *J. Mater. Chem.* **2012**, *22*, 1498-1503.

(13) Vlassiouk, I.; Fulvio, P.; Meyer, H.; Lavrik, N.; Dai, S.; Datskos, P.; Smirnov, S. Large Scale Atmospheric Pressure Chemical Vapor Deposition of Graphene. *Carbon* **2013**, *54*, 58-67.

(14) Celebi, K.; Cole, M. T.; Choi, J. W.; Wyczisk, F.; Legagneux, P.; Rupesinghe, N.; Robertson, J.; Teo, K. B. K.; Park, H. G. Evolutionary Kinetics of Graphene Formation on Copper. *Nano Lett.* **2013**, *13*, 967-974.

(15) Vlassiouk, I.; Regmi, M.; Fulvio, P. F.; Dai, S.; Datskos, P.; Eres, G.; Smirnov, S. Role of Hydrogen in Chemical Vapor Deposition Growth of Large Single-Crystal Graphene. *ACS Nano* **2011**, *5*, 6069-6076.

(16) Zhang, Y.; Li, Z.; Kim, P.; Zhang, L. Y.; Zhou, C. W. Anisotropic Hydrogen Etching of Chemical Vapor Deposited Graphene. *ACS Nano* **2012**, *6*, 126-132.

(17) Losurdo, M.; Giangregorio, M. M.; Capezzuto, P.; Bruno, G. Graphene CVD Growth on Copper and Nickel: Role of Hydrogen in Kinetics and Structure. *Phys. Chem. Chem. Phys.* **2011**, *13*, 20836-43.

(18) Ago, H.; Ogawa, Y.; Tsuji, M.; Mizuno, S.; Hibino, H.: Catalytic Growth of Graphene: Toward Large-Area Single-Crystalline Graphene. *J. Phys. Chem. Lett.* **2012**, *3*, 2228-2236.

(19) Yao, Y.; Wong, C.-P. Monolayer Graphene Growth Using Additional Etching Process in Atmospheric Pressure Chemical Vapor Deposition. *Carbon* **2012**, *50*, 5203-5209.

(20) Shin, Y. C.; Kong, J. Hydrogen-Excluded Graphene Synthesis via Atmospheric Pressure Chemical Vapor Deposition. *Carbon* **2013**, *59*, 439-447.

(21) Choubak, S.; Biron, M.; Levesque, P. L.; Martel, R.; Desjardins, P. No Graphene Etching in Purified Hydrogen. *J. Phys. Chem. Lett.* **2013**, *4*, 1100-1103.

(22) Kidambi, P. R.; Ducati, C.; Dlubak, B.; Gardiner, D.; Weatherup, R. S.; Martin, M.-B.; Seneor, P.; Coles, H.; Hofmann, S. The Parameter Space of Graphene Chemical Vapor Deposition on Polycrystalline Cu. *J. Phys. Chem. C* **2012**, *116*, 22492-22501.

(23) Balooch, M.; Cardillo, M. J.; Miller, D. R.; Stickney, R. E.: Molecular Beam Study of the Apparent Activation Barrier Associated with Adsorption and Desorption of Hydrogen on Copper. *Surf. Sci.* **1974**, *46*, 358-392.

(24) Madix, R. J.; Benziger, J.: Kinetic Processes on Metal Single-Crystal Surfaces. *Annu. Rev. Phys. Chem.* **1978**, *29*, 285-306.

(25) Hao, Y.; Bharathi, M. S.; Wang, L.; Liu, Y.; Chen, H.; Nie, S.; Wang, X.; Chou, H.; Tan, C.; Fallahazad, B.; et al. The Role of Surface Oxygen in the Growth of Large Single-Crystal Graphene on Copper. *Science* **2013**, *342*, 720-3.

(26) Reckinger, N.; Felten, A.; Santos, C. N.; Hackens, B.; Colomer, J.-F. The Influence of Residual Oxidizing Impurities on the Synthesis of Graphene by Atmospheric Pressure Chemical Vapor Deposition. *Carbon* **2013**, *63*, 84-91.

(27) Suk, J. W.; Kitt, A.; Magnuson, C. W.; Hao, Y. F.; Ahmed, S.; An, J. H.; Swan, A. K.; Goldberg, B. B.; Ruoff, R. S. Transfer of CVD-Grown Monolayer Graphene onto Arbitrary Substrates. *ACS Nano* **2011**, *5*, 6916-6924.

(28) Marcet, S.; Verhaegen, M.; Blais-Ouellette, S.; Martel, R. Raman Spectroscopy Hyperspectral Imager Based on Bragg Tunable Filters. *Proc. SPIE, Photonics North* **2012,** *8412*; 84121J

(29) Monazam, E. R.; Siriwardane, R.; Breault, R. W.; Tian, H.; Shadle, L. J.; Richards, G.; Carpenter, S. Kinetics of the Reduction of CuO/Bentonite by Methane (CH4) during Chemical Looping Combustion. *Energy Fuels* **2012**, *26*, 2779-2785.

(30) Nie, S.; Wu, W.; Xing, S.; Yu, Q.; Bao, J.; Pei, S.-s.; McCarty, K. F. Growth From below: Bilayer Graphene on Copper by Chemical Vapor Deposition. *New. J. Phys.* **2012**, *14*, 093028.

(31) Ferrari, A. C.; Meyer, J. C.; Scardaci, V.; Casiraghi, C.; Lazzeri, M.; Mauri, F.; Piscanec, S.; Jiang, D.; Novoselov, K. S.; Roth, S. et al. Raman Spectrum of Graphene and Graphene Layers. *Phys. Rev. Lett.* **2006**, 187401.

(32) Chu, P. K.; Li, L. Characterization of Amorphous and Nanocrystalline Carbon Films. *Mater. Chem. Phys.* **2006**, *96*, 253-277.

(33) Carozo, V.; Almeida, C. M.; Ferreira, E. H.; Cancado, L. G.; Achete, C. A.; Jorio, A. Raman Signature of Graphene Superlattices. *Nano Lett.* **2011**, *11*, 4527-34.

(34) He, R.; Chung, T. F.; Delaney, C.; Keiser, C.; Jauregui, L. A.; Shand, P. M.; Chancey, C. C.; Wang, Y. N.; Bao, J. M.; Chen, Y. P. Observation of Low Energy Raman Modes in Twisted Bilayer Graphene. *Nano Lett.* **2013**, *13*, 3594-3601.

(35) Havener, R. W.; Zhuang, H. L.; Brown, L.; Hennig, R. G.; Park, J. Angle-Resolved Raman Imaging of Inter layer Rotations and Interactions in Twisted Bilayer Graphene. *Nano Lett.* **2012**, *12*, 3162-3167.

(36) Li, Q. Y.; Chou, H.; Zhong, J. H.; Liu, J. Y.; Dolocan, A.; Zhang, J. Y.; Zhou, Y. H.; Ruoff, R. S.; Chen, S. S.; Cai, W. W. Growth of Adlayer Graphene on Cu Studied by Carbon Isotope Labeling. *Nano Lett.* **2013**, *13*, 486-490.

(37) Zhang, W.; Wu, P.; Li, Z.; Yang, J. First-Principles Thermodynamics of Graphene Growth on Cu Surfaces. *J. Phys. Chem. C* **2011**, *115*, 17782-17787.

(38) Fang, W.; Hsu, A. L.; Caudillo, R.; Song, Y.; Birdwell, A. G.; Zakar, E.; Kalbac, M.; Dubey, M.; Palacios, T.; Dresselhaus, M. S. et al. Rapid Identification of Stacking Orientation in Isotopically Labeled Chemical-Vapor Grown Bilayer Graphene by Raman Spectroscopy. *Nano Lett.* **2013**, *13*, 1541-1548.

(39) Robertson, A. W.; Warner, J. H. Hexagonal Single Crystal Domains of Few-Layer Graphene on Copper Foils. *Nano Lett.* **2011**, *11*, 1182-9.

(40) Yan, K.; Peng, H.; Zhou, Y.; Li, H.; Liu, Z.: Formation of Bilayer Bernal Graphene: Layer-by-Layer Epitaxy via Chemical Vapor Deposition. *Nano Lett.* **2011**, *11*, 1106-10.

(41) Kalbac, M.; Frank, O.; Kavan, L. The Control of Graphene Double-Layer Formation in Copper-Catalyzed Chemical Vapor Deposition. *Carbon* **2012**, *50*, 3682-3687.

CHAPTER 6 : Article 3: "Speeding- up Graphene Chemical Vapor Deposition"

Saman Choubak[¶], Pierre L. Levesque[¥], Philippe Gagnon[¶], Minh Nguyen[¥], Patrick Desjardins[¶]*, and Richard Martel [¥]*

[¶] Regroupement Québécois sur les Matériaux de Pointe (RQMP) and Département de Génie Physique, Polytechnique Montréal, C.P. 6079, Succursale Centre-ville, Montréal, Québec H3C 3A7, Canada

[¥] Regroupement Québécois sur les Matériaux de Pointe (RQMP) and Département de Chimie, Université de Montréal, C.P. 6128, Succursale Centre-Ville, Montréal, Québec H3C 3J7, Canada

* Corresponding Authors

Submitted to Journal of Advanced Material

Authors' Contribution: S. Choubak designed and conducted the experiments. Characterized, analysed, and interpreted the data. Solved problems related to the growth kinetic model. Drafted the manuscript and revised it accordingly. P.L. Levesque provided advice during the course of experiments, characterized the sample using LEEM and LEED, contributed substantially to the evolution of the kinetic model and revised the manuscript. M. Nguyen transferred the graphene samples from Cu to SiO_2/Si. P. Gagnon provided the growth kinetic model. P. Desjardins and R. Martel revised the manuscript critically for important intellectual content, approved the final version to be published and agreed to be responsible for all aspects of the work in ensuring that questions related to the accuracy or integrity of any part of the work are appropriately investigated and resolved.

CHAPTER 6: ARTICLE 3: "SPEEDING-UP GRAPHENE CHEMICAL VAPOR DEPOSITION."

6.1 Abstract

Chemical vapor deposition (CVD) of graphene films on copper foils is one of the most promising and widely employed methods to produce large graphene sheets of high quality. However, continuous monolayer coverage of graphene on copper requires high temperatures and long growth times therefore making this process unsuitable for industrial manufacturing. Here, we report on how to maximize the growth efficiency of high quality single layer graphene films using methane CVD. We show that graphene formation on copper within 1 min is possible in the absence of oxidizing impurities in the gas feedstock and furnace atmosphere. Our results highlight a competitive action between adsorbed methane intermediate species as carbon precursors and surface oxygen as the growth inhibitor. Removing traces of oxygen in the feedstock is key to graphene fast growth and impurity level of less than 5 ppm O_2 with respect to H_2 allows the continuous growth of graphene films on copper. Our method is entirely suitable for large scale manufacturing of graphene films on copper, thereby opening the door to viable synthesis of graphene materials in an energy and cost saving manner.

6.2 Introduction

The low-pressure chemical vapor deposition (LP-CVD) of graphene films, demonstrated for the first time less than six years ago, is viewed as a potentially scalable and efficient process compatible with industrial requirements.[1-4] Despite substantial efforts, obtaining continuous monolayer graphene coverage with low defect density remains a challenge and can generally only be achieved at high temperatures and after long growth times.[3, 5, 6] Indeed, the large scale manufacturing of graphene films by CVD has so far been hindered by these constraints. Thus, the crucial questions in graphene LP-CVD growth remain unresolved: Why is the growth of graphene on copper so slow? More specifically how can one speed up the process while maintaining or even improving film quality?

Up to this date, many milestones have been achieved by introducing roll-to-roll production and also by adapting growth recipes with a local heating of the copper substrate in order to reduce cost and save energy.[1, 4] While roll-to-roll approaches are potentially interesting in terms of scalability and manufacturing volume, they still require long growth times and high temperature; thus the associated energy cost remains prohibitive.[1] Local heating synthesis routes, although much more cost- and time-effective, currently result in lower quality films with microcracks.[4] Others have investigated graphene CVD growth at lower temperature in an attempt to reduce the energy cost and make the graphene synthesis more suitable for industrial manufacturing processes.[6-11] However, the resulting processes are still too long and generally fail to enhance the economical viability of the mass production of graphene material.[10]

A careful analysis of the recent literature on LP-CVD of graphene on Cu reveals numerous apparent inconsistencies in terms of optimal growth parameters. In particular, growth duration for CVD from a methane/hydrogen mixture ranges from 5 to 45 min or even higher with no specific reasoning behind it.[1, 2, 5, 6, 12-20] Although Li et al. reported full coverage of copper with graphene after 1.5 min at a pressure of 285 mTorr, their recipe maintains methane and hydrogen gas flow during cool-down, implying effectively longer growth time.[15] Much longer growth time have however been used in literature afterwards,[5] which might indicate poor graphene reproducibility at such short growth time.

We recently showed that oxygen impurities, not hydrogen, are responsible for graphene etching on copper and that there is a competitive action between oxidation and carbon growth during graphene formation in LP-CVD reactor.[21, 22] The presence of different levels of impurities in the furnace atmosphere and gas feedstock explains the discrepancies in growth recipes from one group to another. In the absence of these oxidizing impurities, we hypothesize here that oxidation and etching is minimized and copper is covered by graphene film in virtually no time.

Here, we report the accelerated formation of continuous, high quality single graphene film on copper foil from a methane/hydrogen mixture. This is accomplished by carrying growth in a controlled environment where the level of oxidative impurities is greatly reduced compared to standard LP-CVD growth conditions.[2] In a series of experiments where growth time is decreased from 45 min down to 1 min, no clear difference in the quality and morphology of the film is observed. In contrast, control growth experiments carried out in standard conditions,

where the level of oxidative species are typical of graphene LP-CVD, show that more than 20 min are required to achieve full graphene coverage and high quality films. We develop a rate-equation kinetic model describing this graphene growth process, which includes a competitive reaction between the carbon species and the oxidizing impurities, while considering also the effect of hydrogen gas for inhibiting the oxidizing etching reaction and protecting the film. By including the effects of hydrogen and oxidizing impurities, our kinetic model is qualitatively in agreement with the general trends reported in literature on the growth of graphene films on copper and readily explains the faster growth rate reported here.

6.3 Experimental section

Graphene films were grown on 25 μm thick Cu foils (Alfa Aesar, item no. 13382) at 1000 °C in a 1.5 inch fused quartz tube at low pressure. The system consists of a manifold capable of UHV conditions where the gases are introduced into the chamber. The system's base pressure prior to gas insertion is below $5x10^{-6}$ Torr. Gas purifiers were installed on as-received gas bottles in order to decrease the residual O_2 content in UHP gases to less than 1 ppbV. We used DEOXO^{TM} (O_2 < 1ppb) for H_2 (Praxair, UHP, grade 5, O_2 < 1ppm), and SAES Pure Gas Inc. MC1-950FV (H_2O and O_2 < 1ppbV) for CH_4 (Praxair, UHP, grade 3.7, O_2 < 15ppm). The Cu foils were chemically cleaned in 1 M acetic acid (Sigma Aldrich, Reagent Plus > 99%) at 60 ºC followed by acetone and then 2-propanol (without drying) for 10 min in each step. The Cu substrates are then blown-dried with nitrogen. They were heated to 1000 °C and annealed at this temperature for 30 min under the flow of *purified* H_2 at 50 mTorr. In order to grow graphene, *purified* CH_4 was introduced into the chamber and the total pressure reached 500 mTorr. After the desired growth time (45, 30, 20, 10, 5, and 1 min), *purified* methane exposure was stopped and evacuated from the furnace. The chamber was cooled down to room temperature under the flow of *purified* H_2 solely. The growth in standard conditions – where the level of oxidative species are relatively higher than in the purified conditions – were conducted using as-received CH_4 (Praxair, UHP, grade 3.7, O_2 < 15ppm) as the carbon source.

Graphene samples were examined by scanning electron microscopy (SEM-JSM-7600F) operated at 1 kV and in some cases low energy electron microscopy (FE-LEEM P90 from SPECS-GmbH) performed at 4.4 eV kinetic energy in the UHV chamber (base pressure $4x10^{-10}$ mbar). Their

quality is assessed using Raman Spectroscopy (Renishaw Invia) with a laser wavelength of 514 nm. A 50X objective (N.A= 0.55) focuses a 4 mW laser beam to a probe spot about 1 μm in diameter. The graphene films grown on copper were transferred onto SiO_2 (100-nm-thick)/Si wafers by a liquid phase method based on poly-methyl methacrylate (PMMA) support. [23]

6.4 Results

Figure 6-1 shows SEM images of graphene films grown on copper for different growth times and gas purity levels. Figure 1(a-f) are images for growth in purified conditions starting from 45 min growth time down to 1 min. The lower growth time limit was dictated by limitations of our experimental set up. Continuous, hole-free, monolayer graphene films are formed on copper foil even down to 1 min. Interestingly, no significant difference was observed between all the films grown under purified conditions.

In order to validate these results and compare them with previous literature results, we removed the methane purifier from the line and conducted growth studies using as-received *UHP* methane (O_2 < 15ppm) and *purified* hydrogen (O_2 < 1ppb). Except for the methane purifier being removed, all the growth conditions are exactly the same as the previous experiments discussed above. We chose three different growth times 5, 20, and 45 min to investigate the graphene film growth evolution and behavior until a complete layer is observed (Figure 1(g-i)). The impact of the oxidizing impurity is evident; the growth for 5 and 20 min leads to an incomplete coverage of graphene film on copper whereas the film is complete after 45 min. These results further reveal the importance of a competitive action between growth and growth inhibition by oxidation during graphene synthesis in LP-CVD reactor. In the absence of oxidizing impurities, graphene films can be formed on copper foil in less than 1 min.

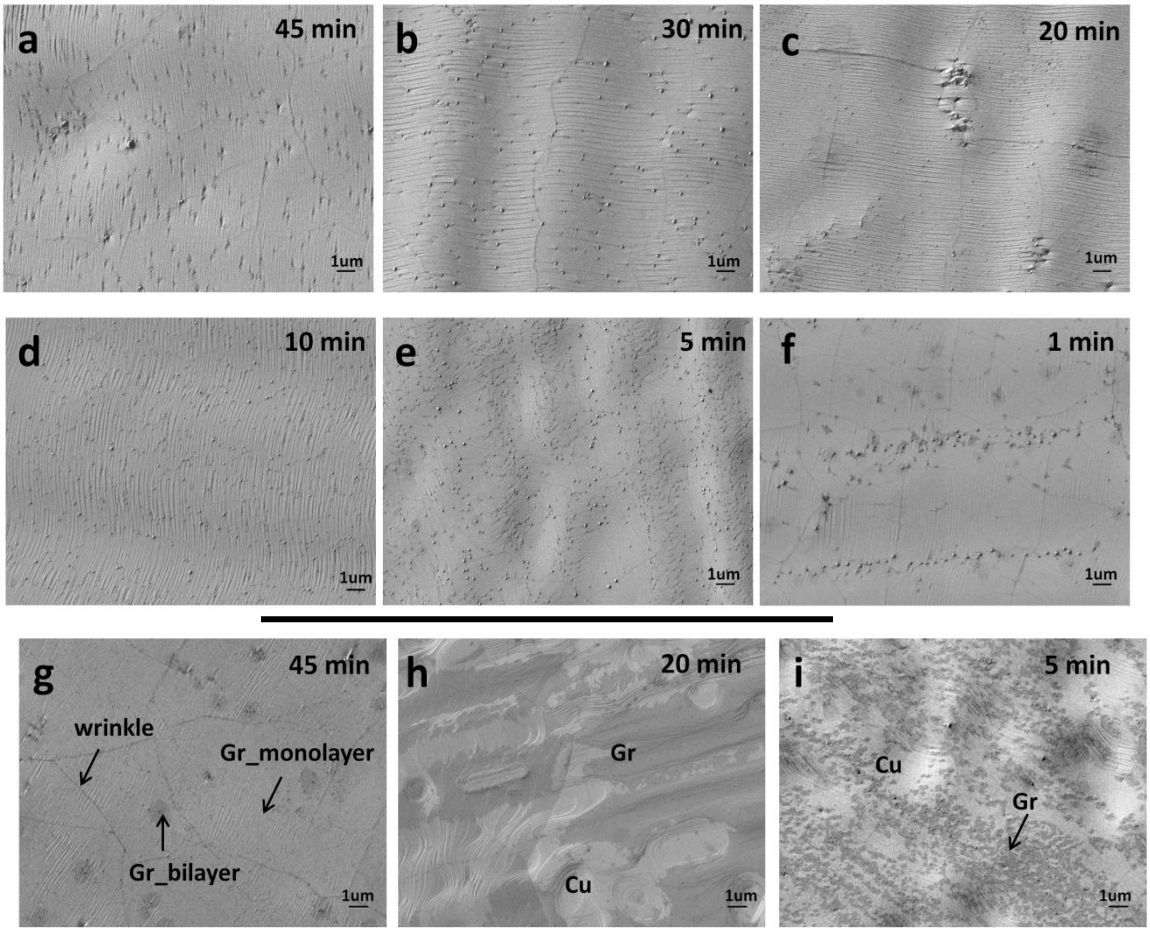

Figure 6-1. SEM images of graphene films grown on copper for different growth times. Purified methane exposure at 1000° C for a) 45 min, b) 30 min, c) 20 min, d) 10 min, e) 5 min, and f) 1 min, and unpurified methane exposure for g) 45 min, h) 20 min, and i) 5 min.

Micro-Raman spectroscopy measurements were carried out on graphene layers prepared using purified methane after transferring them on SiO_2 in order to determine the number of layers and film quality. Raman spectra from films grown for different times are presented in Figure 6-2. They reveal that films grown from purified methane are high quality graphene layers, as indicated by strong 2D and low D band intensities. The full width at half-maximum (FWHM) intensity of the 2D band is approximately 28 cm^{-1} for all samples and the ratio of the 2D to G band peak intensity (I_{2D}/I_G) is ~ 3.2. These measurements confirm the presence of single layer graphene (SLG) [2, 21, 24] and the low intensity of the D peak, associated with the presence of defects in graphene, indicates that the films is of high quality. [23]

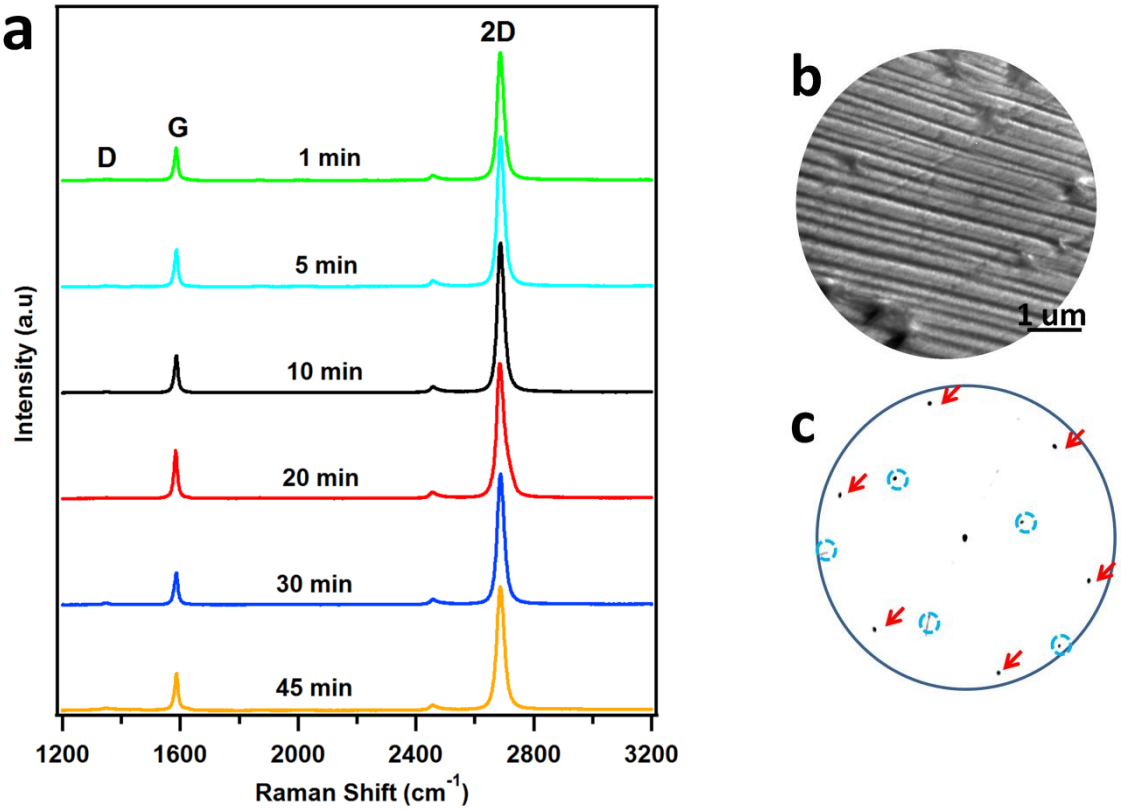

Figure 6-2. a) Raman spectra of graphene films grown from purified methane on copper for different growth times after transfer on 100nm SiO_2/Si substrate, b) Bright field LEEM image of the graphene film grown on copper for 1 min (acquired at an incident electron energy of 4.4 eV), and c) LEED pattern acquired at 65eV in the area depicted in b). The pattern is from a single layer graphene domain. The spots marked by red arrows are from the smooth regions in the LEEM and the shifted spots circled in blue are from the same graphene domain but sitting on the copper facets (darker lines in the LEEM image). A Fast Fourier Transform high pass filter has been applied to the LEED image in order to remove background ascribed to diffuse scattering and secondary electrons.

Figure 6-2b is a LEEM image of a 1 min graphene sample grown on copper from purified methane. The graphene film covers the whole surface and, as the film is uniform, the contrast arises from copper structures. The bright areas and dark lines are graphene covered copper terraces and facets, respectively. LEED pattern in Figure 6-2c shows sharp single layer graphene diffraction spots indicating the good crystallinity of the graphene sheet. The diffraction spots marked by red arrows are from a single layer graphene domain lying on the copper terraces while the diffraction spots circled in blue are from the same graphene domain lying on the copper

facets. The angle between the facet and the principal Cu(001) plane is 16.5±1 deg. which corresponds to the Cu (632) surface reported previously on copper foil.[25] LEED patterns have been acquired at various locations on the sample surface and several orientations, random in appearance, have been found. The sample can be moved slightly to shifted locations exhibiting only one LEED pattern within the illuminated area of 10 µm, which implies that the graphene film is polycrystalline and the grain sizes are larger than 10 µm.

Our entire set of results could be assembled into a simple rate-equation kinetic model of graphene CVD on Cu in the presence of oxygen impurities and solved using quasi-steady state approximation. Based on data in literature,[18, 19, 26, 27] we assume that methane adsorbs and dissociates on copper by forming Growth Intermediate Species (GIS) that can then be converted to graphene or alternatively react with adsorbed oxidizing impurities and desorb. The model considers also an inhibition channel to GIS oxidation-desorption through a reaction with gaseous hydrogen molecules. We assume that only the free Cu surface sites (no graphene) are reactive and exposed to constant gas pressure. As detailed in the supplementary information (SI), the model yields the following overall graphene growth rate equation:

$$\frac{d\theta_{Graphene}}{dt} = k_{diss(CH_4^*)} K_{ads(CH_4)} \frac{P_{CH_4}}{1 + k_{inhib} \frac{P_{O_2}}{P_{H_2}} \theta_*^2} \theta_*^{(n+1)} \left(1 - \theta_{Graphene}\right) f\left(\theta_{\mathrm{Graphene}}\right),$$

here P_X is the partial pressure of the gas X in the furnace, $\theta_{Graphene}$ is the coverage of graphene, θ_* is the fraction of free sites on the surface, θ_X is the fraction of surface sites occupied by X and n is the order of reaction for CH_4 dissociation. $k_{diss(CH_4^*)}$ and $K_{ads(CH_4)}$ are the dissociation reaction and the adsorption equilibrium constants of CH_4, respectively. As presented in SI, k_{inhib} regroups several kinetic constants of the system and $f(\theta_{\mathrm{Graphene}})$ is an evolving factor that accounts for geometric and diffusion considerations, such as nucleation, that are not explicitly included in our model. For example, $f(\theta_{\mathrm{Graphene}})$ is expected to increase with $\theta_{\mathrm{Graphene}}$ for a given number of nuclei because the perimeter of the islands increases. This effect provides more attaching sites and also shortens the average diffusion length with decreasing active area of bare Cu. As indicated in the SI, Cu sites remain nearly unoccupied during growth ($\theta_* \cong 1$) at all times and these Cu sites vacancies are therefore assumed to vary only slightly with changing pressure conditions.

Our model which is based on competitive reactions with hydrogen and oxidizing impurities correctly predicts most, if not all, experimental trends reported in the literature on graphene growth on copper. More specifically: the growth rate increases with both P_{CH_4} and P_{H_2} and decreases with P_{O_2} and $\theta_{Graphene}$.

6.5 Discussion

Our experimental results demonstrate that oxidizing impurities are currently limiting graphene growth kinetics in a typical LP-CVD environment. By simply minimizing the oxygen level in the gas feedstock, continuous and uniform monolayer graphene film can be reliably grown on copper from methane within 1 min, which is between 5 to 45 times faster than what is reported up to this date.[1, 2, 5, 6, 12-20] The installation of gas purifiers is entirely compatible with industrial manufacturing processes and is beneficial as it can lower graphene production cost by reducing process time and saving energy. The quality and uniformity of the graphene films are maintained even for the shortest growth times reported here, as demonstrated by SEM and Raman spectroscopy.

The fact that the SEM images in Figure 1 do not show evidences of bi- and multi- layer formation, demonstrates that once a complete graphene layer is formed on copper, the layer is sealed and graphene formation terminates. Since Cu plays a catalytic role in decomposing methane, this observation is in line with previous growth studies in which graphene growth stops when no bare Cu remains.[28] Furthermore, we believe that minimum graphene growth time for complete layer can be further decreased below 1 min, but this could not be explored due to limitations of our CVD system.

Based on the growth model presented above, the graphene growth rate is controlled by the partial pressure of CH_4 and the ratio $\frac{P_{O_2}}{P_{H_2}}$. For a given level of oxidizing impurities, increasing P_{H_2} helps to maximize the growth rate - the growth rate reaches 50% of its maximum value, r_{MAX} , when $\frac{P_{O_2}}{P_{H_2}} = \frac{1}{k_{inhib}}$ and then saturates, even after further increase of P_{H_2}. Based on our observed relative growth rates in purified and standard conditions and estimated levels of oxidizing impurities, a lower limit for k_{inhib} is found to be 200 000 (see SI). This value sets the total level of oxidizing

impurities with respect to H_2 to below 5×10^{-6} in order to reach 50% of r_{MAX}, since $\frac{P_{O_2}}{P_{H_2}} = \frac{1}{k_{inhib}}$ in the rate equation yields the criterion $\frac{r_{MAX}}{2}$. More importantly, lowering the impurity level by two orders of magnitude (i.e. down to $\frac{P_{O_2}}{P_{H_2}} = 5 \times 10^{-8}$) would be required to reach 99% of r_{MAX}.

In standard LP-CVD systems, only three sources of oxidizing impurities can be identified: i) H_2 gas bottle, ii) CH_4 gas bottle and iii) air leaks into the CVD chamber from flanges and fittings. For instance, a standard CVD systems with 10^{-6} Torr base pressure requires a minimum of 40 mTorr of pure H_2 to compensate to oxygen leaks and to provide minimum conditions for $\frac{r_{MAX}}{2}$ because the oxygen base pressure is roughly 2×10^{-7} Torr (note: 20% O_2 in air). Our UHP grade of H_2 has however less than 1 ppm of O_2 and CH_4 feedstock contains less than 15 ppm of O_2, leading to $\frac{P_{O_2}}{P_{H_2}} \cong 1 \times 10^{-4}$ using P_{H_2}= 0.05 Torr and $P_{CH_4} = 0.5$ Torr. Without further purification of the gas, only 3% of r_{MAX} can be reached in those conditions. To reach the criterion $\frac{r_{MAX}}{2}$, the hydrogen partial pressure has to be further increased to at least 1.5 Torr of pure H_2. From this simplified model, it appears clear that one can always compensate for the presence of O_2 impurities using a proportional level of pure H_2, but increasing further the pressure will eventually hinder the availability of reactive Cu sites and hence slow down the growth.

The results in our previous reports [21, 22] show that oxidizing impurities play a significant role in graphene CVD and these new results reveal now their dramatic effect on the growth rate. Slight changes in impurity level due to modification of the CVD chamber or sources of feedstock can therefore greatly impact growth consistency and reproducibility. A strict control over the level of oxygen in the growth atmosphere is therefore paramount in order to improve both growth speed and reproducibility, which was clearly lacking in the current literature on graphene growth by LP-CVD.

The growth model presented above considers for the first time the competitive action between growth species (methane), growth inhibitor (oxygen), and oxidation inhibitor (hydrogen) for balancing conditions entailing the final graphene surface coverage on copper. According to the

model, the graphene growth rate is essentially proportional to the methane partial pressure when the level of oxygen species tends towards zero. On the other hand, oxygen traces in methane slow down the growth reaction by allowing GIS species to desorb as CO molecules and eventually by etching graphene. Adding a flow of H_2 can counteract this last associative desorption reaction by reacting with oxygen species to form volatile H_2O. When removing oxygen impurities is difficult, additional H_2 can therefore be used to promote the growth process towards complete graphene layers, but this is at the expanse of a reduced growth speed compared to pure methane.

6.6 Conclusion

Our experimental results show that the growth rate is severely impaired by the presence of oxidizing impurities. We have shown that in the absence of oxidizing impurities continuous and uniform monolayer graphene can be formed on copper using *purified* methane within 1 min of methane exposure. Our findings highlight the necessity to control the balance between carbon supply and oxygen to hydrogen pressure ratio in order to achieve graphene full coverage on copper substrates. Based on our model in which surface reactions of CH_4, O_2 and H_2 on Cu are depicted, the lowest impurity level of O_2 with respect to H_2 should be at least below 5×10^{-6} to reach 50% of the maximum possible growth rate. Once the O_2 and H_2 pressure ratio is optimized, the growth rate is limited by the CH_4 dissociation rate constant (k_{CH_4}) and its adsorption equilibrium constant (K_{CH_4}). Finally, the growth method shown in this report is straightforward and very simple to implement in industrial manufacturing processes making graphene sheets mass production economically feasible.

Acknowledgements

The authors thank Mr. Joël Bouchard for technical support. This research was financially supported by the Natural Sciences and Engineering Research Council of Canada (NSERC), the Canada Research Chair program and the Selenium Tellurium Development Association. Sample characterization was carried out in the Thin Film Research Laboratories at Polytechnique/UdeM, which are partially supported by grants from NanoQuébec and the Fonds de Recherche du Québec.

6.7 Supporting Information

Details on the Kinetic Model

1) Surface Carbon Production Rate

The following model has been developed to simulate the effect of oxidizing impurities in the copper catalyzed graphene growth under reducing conditions. The model describes competitive reactions between the surface carbon species formed by the methane activation, inhibitor oxygen adsorbates, and anti-inhibitor hydrogen molecules. The simulation aims to determine the interplay between three main reaction channels: 1) GROWTH: methane dissociation at the copper surface to form Graphene Intermediate Species (GIS) and their reaction to grow graphene; 2) INHIBITION: adsorption and surface reaction of oxidizing impurities with GIS at the copper surface and desorption/elimination via CO gas; 3) ANTI-INHIBITION: competitive hydrogenation of the oxidizing impurities at the surface of copper and desorption of water gas.

All the reactions are assumed to occur at the Cu surface. That is, no absorption, diffusion or reaction is allowed to take place on already formed graphene layer/patches. Note that this important assumption is supported by SEM observations of monolayer and continuous graphene films.

Under these assumptions the reaction scheme - on the uncovered copper surface - can be described as follows:

$$CH_{4(g)} + * \leftrightarrow CH_4^* \; ; \quad \text{(S1)}$$

$$O_{2(g)} + * \leftrightarrow O_2^* \; ; \quad \text{(S2)}$$

$$O_2^* + * \rightarrow 2O^* \; ; \quad \text{(S3)}$$

$$CH_4^* + n^* \rightarrow CH_y^* + [nH^* \rightarrow \frac{n}{2} H_{2(g)} + n^*] \; ; \quad \text{(S4)}$$

$$CH_y^* \rightarrow C_{graphene} + [yH^* \rightarrow \frac{y}{2} H_{2(g)} + y*] \; ; \quad \text{(S5)}$$

$$CH_y^* + O^* \rightarrow CO_{(g)} + 2* + [yH^* \rightarrow \frac{y}{2} H_{2(g)} + y*] \; ; \quad \text{(S6)}$$

$$O^* + H_{2(g)} \rightarrow H_2O_{(g)} + * ; \quad \text{(S7)}$$

where CH_4 is the precursor gas, H_2 is the reducing agent, and O_2 represents oxidizing impurities. The supply of oxidizing impurities is either from impurities in CH_4 and H_2 feedstock, air leaks in the gas line, or both. The concentrations of the gas species are constant during the growth. * are unoccupied sites at the copper surface. All sites are considered equivalent.

The adsorption processes of CH_4 and O_2 on the copper surface are fast compared to graphene formation, thus pre-equilibrium approximation can be used in reactions (Equation 1S) and (Equation 2S). The rate equations:

$$r_1 = -k_1 P_{CH_4} \theta_* + k_1^{'} \theta_{CH_4} \approx 0,$$

and

$$r_2 = -k_2 P_{O_2} \theta_* + k_2^{'} \theta_{O_2} \approx 0,$$

lead with pre-equilibrium approximation to:

$$\theta_{CH_4} \approx K_1 P_{CH_4} \theta_*; \qquad \text{(S8)}$$

and

$$\theta_{O_2} \approx K_2 P_{O_2} \theta_* . \qquad \text{(S9)}$$

Here r_i is the rate of the reaction, P_X is the partial pressure of species X, θ_* is the fraction of free sites on the surface, θ_X is the fraction of sites on the surface occupied by X and finally k_i, $k_i^{'}$ and K_i are the reactions, counter reactions, and equilibrium constants of reaction (i), respectively.

Based on surface science studies, molecular hydrogen neither dissociates nor adsorbs on clean Cu surfaces, thus the adsorption of H_2 is neglected [1,2]. Reactions (S3) and (S4) are the dissociation reactions of O_2 and CH_4 on the copper surface, respectively. The decomposition of oxygen adsorbates into atomic oxygen (Equation S3) is assumed to be irreversible since copper oxide is quite stable in the range of reaction temperatures considered here [3]. The

decomposition of CH_4^* in reaction (S4) is also taken as irreversible since atomic hydrogen has a very short lifetime on copper surface [1,2].

The exact nature of the active carbon species (GIS) -produced by the decomposition of methane- adsorbed on the Cu surface leading to the formation of graphene is unknown. Consequently, the order of reaction remains unclear even if a complete successive dehydrogenation reactions of methane down to atomic carbon is considered. The reason is that copper surface sites will be quickly available due to rapid hydrogen desorption, which lowers the order of reaction. Therefore, as the exact decomposition state of the GIS is unknown, the CH_4^* decomposition reaction is kept generic and the reaction is considered as an elementary reaction that simply needs a number n of free sites. Note that since $H_{surface} + H_{surface} \rightarrow H_2(gas)$ is extremely rapid, it is not further considered in the reaction scheme. However, it is considered in the overall reaction since the level of H_2 cannot be zero and will always be a fraction of CH_4.

The GIS appear in competitive reactions: either to form graphene (Equation S5) or be oxidized/burnt by oxidizing impurities (Equation S6). Both reactions are presumed irreversible since the process temperature for Equation S5 is far below the sublimation temperature of graphite of 4000 °K [4]; thus graphene formation is stable and irreversible. Reaction (S6) is a combustion reaction and therefore carbon species can only be further oxidized.

The main effect of hydrogen addition is to provide a new reaction pathway (Equation S7) competing with the oxidizing reaction (S6). This reaction frees GIS from oxidation for subsequent graphene growth (Equation S5). As mentioned above, molecular hydrogen neither adsorbs nor dissociates on the Cu surface. We propose that hydrogen gaseous molecules react directly with atomic oxygen adsorbates to form water (Equation S7). This reaction is also considered irreversible: water molecules will rapidly desorb into the gas phase at such a high temperature regime.

The growth rate of graphene is directly proportional to the production of GIS (CH_y) as shown in reaction (S5). Thus, this system will be first solved to gives GIS coverage.

While no adsorption, diffusion or reaction are assumed to occur on the already formed graphene islands, surface species (GIS or CH_y and O^*) are considered in quasi-steady state. Therefore, we can deduce:

$$\frac{d\theta_{CH_y}}{dt} = k_4\theta_{CH_4}\theta_*^n - k_5\theta_{CH_y} - k_6\theta_{CH_y}\theta_O \approx 0,$$

which gives:

$$\theta_{CH_y} = \frac{k_4K_1P_{CH_4}}{k_5+k_6\theta_O}\theta_*^{(n+1)}. \qquad \text{(S10)}$$

and

$$\frac{d\theta_O}{dt} = 2k_3\theta_{O_2}\theta_* - k_6\theta_{CH_y}\theta_O - k_7\theta_O P_{H_2} \approx 0\ ,$$

which gives:

$$\theta_O = \frac{2k_3K_2P_{O_2}}{k_6\theta_{CH_y}+k_7P_{H_2}}\theta_*^2. \qquad \text{(S11)}$$

Equation 11S shows that hydrogen is required in order to grow graphene in the presence of oxidizing impurities. For sufficient large H_2 pressures, reaction (S7) overcomes reaction (S6). In these conditions, $k_6\theta_{CH_y}$ is much smaller than $k_7P_{H_2}$ and Equation 11S can be approximated using:

$$\theta_O \approx \frac{2k_3K_2P_{O_2}}{k_7P_{H_2}}\theta_*^2\ . \qquad \text{(S12)}$$

Substituting expression (12S) into (10S) gives:

$$\theta_{CH_y} \approx \frac{k_4K_1P_{CH_4}}{k_5+\frac{2k_3k_6K_2P_{O_2}}{k_7P_{H_2}}\theta_*^2}\theta_*^{(n+1)}. \qquad \text{(S13)}$$

2) Graphene Growth Rate

According to reaction (5S), the graphene growth rate ($\frac{d\theta_{Graphene}}{dt}$) should be simply given by $\frac{d\theta_{Graphene}}{dt} = k_5\theta_{CH_y}$. With the assumption made that no adsorption, diffusion or reaction take place on the already formed graphene islands, the steady state approximation used to solve the kinetic equations is only valid on the graphene free substrate surface. In other words, the steady state approximation is only valid if we consider the uncovered graphene area. Therefore the active area is constantly reduced with the growing graphene coverage and θ_{CH_y} is renormalized by $1 - \theta_{Graphene}$ to account for the whole surface of copper.

Considering the above statement and taking reaction (S5) into account:

$$\frac{d\theta_{Graphene}}{dt} = k_5\theta_{CH_y}\left(1 - \theta_{Graphene}\right)f(\theta_{\mathrm{Graphene}}). \quad \text{(S14)}$$

Here $f(\theta_{\mathrm{Graphene}})$ is an evolving factor that accounts for geometric and diffusion considerations related for instance to nucleation process, which is not explicitly included here. Substituting θ_{CH_y} in (S14) by (S13) a simple expression for the graphene growth rate in a reducing environment in the presence of oxidizing impurities is obtained:

$$\frac{d\theta_{Graphene}}{dt} = k_4K_1\frac{P_{CH_4}}{1+\frac{2k_3k_6K_2P_{O_2}}{k_5k_7P_{H_2}}\theta_*^2}\theta_*^{(n+1)}\left(1 - \theta_{Graphene}\right)f\left(\theta_{\mathrm{Graphene}}\right). \quad \text{(S15a)}$$

Renaming and rearranging the constants:

$$\frac{d\theta_{Graphene}}{dt} = k_{diss(CH_4^*)}K_{ads(CH_4)}\frac{P_{CH_4}}{1+k_{inhib}\frac{P_{O_2}}{P_{H_2}}\theta_*^2}\theta_*^{(n+1)}\left(1 - \theta_{Graphene}\right)f(\theta_{\mathrm{Graphene}})$$

(S15b)

3) Coverage Dependencies with Gas Pressures

Expression (S15b) indicates that graphene growth rate is influenced to a large extent by the coverage dependencies with pressures, especially if the reaction order n is high. Considering all

the species present at the surface and all sites equivalent, the available sites coverage θ_* is expressed as:

$$\theta_* = 1 - \theta_{CHy} - \theta_O - \theta_{O_2} - \theta_{CH_4} \quad \text{(S16)}$$

where θ_X is the corresponding coverage of the surface X species. $\theta_{Graphene}$ is not included in Equation (S16) since the quasi-steady state approximation limits reaction to uncovered areas. Consequently, the total number of free sites is constantly renormalizing with changing $\theta_{Graphene}$ and this is taken into account by including the factor $\left(1 - \theta_{Graphene}\right)$ in Equation (S15).

Substituting θ_X with their corresponding expressions (S8),(S9),(S10),(S12) in (S16) gives:

$$1 = \theta_* \left(1 + K_1 P_{CH_4} + K_2 P_{O_2} \left(1 + \frac{2k_3}{k_7 P_{H_2}} \theta_* \right) + \frac{k_4 K_1 P_{CH_4}}{k_5 + \frac{2k_3 k_6 K_2}{k_7} \frac{P_{O_2}}{P_{H_2}} \theta_*^2} \theta_*^n \right) . \quad \text{(S17)}$$

This expression cannot be solved explicitly for θ_* and the boundary limits will instead be evaluated. A lower limit on θ_* is found considering that $\frac{2k_3 k_6 K_2}{k_7} \frac{P_{O_2}}{P_{H_2}} \theta_*^2 \geq 0$, then

$\frac{k_4 K_1 P_{CH_4}}{k_5 + \frac{2k_3 k_6 K_2}{k_7} \frac{P_{O_2}}{P_{H_2}}} \leq \frac{k_4 K_1}{k_5} P_{CH_4}$. This results in the following expression:

$$1 \leq \theta_* \left(1 + K_1 P_{CH_4} \left(1 + \frac{k_4}{k_5} \right) + K_2 P_{O_2} \left(1 + \frac{2k_3}{k_7 P_{H_2}} \right) \right).$$

Setting a lower limit for θ_*:

$$\theta_* \geq \left(1 + K_1 P_{CH_4} \left(1 + \frac{k_4}{k_5} \right) + K_2 P_{O_2} \left(1 + \frac{2k_3}{k_7 P_{H_2}} \right) \right)^{-1} .$$

On the other hand, a higher limit for θ_* can be set using relation (S17), provided that $0 \leq \theta_* \leq 1$ and gives:

$$1 \geq \theta_* \left(1 + K_1 P_{CH_4} + K_2 P_{O_2} \right)$$

and

$$\theta_* \leq \left(1 + K_1 P_{CH_4} + K_2 P_{O_2}\right)^{-1} .$$

Boundary conditions are finally found for θ_*:

$$\frac{1}{1+K_{ads(CH_4)}P_{CH_4}\left(1+\frac{k_{diss(CH_4)}}{k_{Graphene}}\right)+K_{ads(O_2)}P_{O_2}\left(1+\frac{2k_{diss(O_2)}}{k_{H_2O}P_{H_2}}\right)} \leq \theta_* \leq \frac{1}{1+K_{ads(CH_4)}P_{CH_4}+K_{ads(O_2)}P_{O_2}} \quad \text{(S18)}$$

Based on surface science studies [5], CH_4 molecules are hard to activate and adsorb on Cu, which points towards a very small $K_{ads(CH_4)}$. In addition, P_{O_2} needs to be maintained very low -- at trace level-- to obtain growth conditions. With these considerations, we can estimate from the boundary condition of Equation (S18) that the unoccupied sites coverage θ_* will remain close to unity for graphene growth. This estimation is reinforced in a LEEM study where the equilibrium GIS coverage have been shown to be between 1-2% on metals (Ir(111) and Ru(0001)) with a maximum of 3% at nucleation [6]. This finding indicates a limited effect of the coverage parameter θ_* on the graphene growth rate expression (S15b) with varying pressures.

4) Evaluation of k_{inhib}

From the graphene growth rate ($r_{Graphene}$) Equation (S15b), the ratio between the growth rate in purified conditions $r^p_{Graphene}$ and growth rate in standard conditions $r^s_{Graphene}$ is:

$$\frac{r^p_{Graphene}}{r^s_{Graphene}} = \frac{1+k_{inhib}\frac{P^s_{O_2}}{P^s_{H_2}}\theta_*^2}{1+k_{inhib}\frac{P^p_{O_2}}{P^p_{H_2}}\theta_*^2}, \quad \text{(19S)}$$

where the subscripts *p* and *s* are for purified and standard conditions, respectively.

Because the CH_4 purifier decreases O_2 impurity level by at least a factor 1000, using $P^p_{O_2} = \frac{p^s_{O_2}}{1000}$ and $P^p_{H_2} \cong P^s_{H_2}$ in Equation (S19) can be rewritten as:

$$\frac{r^p_{Graphene}}{r^s_{Graphene}} = \frac{1+k_{inhib}\frac{P^s_{O_2}}{P^s_{H_2}}\theta_*^2}{1+k_{inhib}\frac{P^s_{O_2}}{1000P^s_{H_2}}\theta_*^2} \quad . \qquad \text{(S20)}$$

Solving Equation (S20) for k_{inhib} gives:

$$k_{inhib} = \frac{1}{\theta_*^2}\frac{P^s_{H_2}}{P^s_{O_2}}\frac{\frac{r^p_{Graphene}}{r^s_{Graphene}}-1}{1-\frac{r^p_{Graphene}}{r^s_{Graphene}}\frac{1}{1000}} . \qquad \text{(S21)}$$

k_{inhib} can be evaluated using the following estimated parameters:

- $\theta_* \approx 1$ (in growth conditions as shown earlier) ;"
- $\frac{r^p_{Graphene}}{r^s_{Graphene}} \approx 30$. This is deduced from literature where the growth duration for CVD from a methane/hydrogen mixture ranges from 5 -45 min [References in main article 1,2,5,6,12-20]. However, 30 min growth time has been consistently reported by different groups in many recipes [References in main article 1,2,3,15,16,17] and therefore, it is a safe assumption to be made.
- $r^p_{Graphene}$ < 1 min (coverage time^{-1}) in purified conditions with respect $r^s_{Graphene}$ between 20 min and 45 min in standard condition. The lower growth time limit (1 min) was dictated by limitations of our experimental set up, however , we believe that this can be even lowered than 1 min.
- $P^s_{O_2} = 7.5 \times 10^{-6}$ Torr; this is deduced using CH_4 gas feedstock with < 15 ppm O_2 and 0.5 Torr CH_4 as used in growth conditions gives $P^s_{O_2}$ of 7.5×10^{-6} Torr residual in the CVD chamber;
- $P^p_{H_2} \cong P^s_{H_2} = 0.05$ Torr.

Substituting these parameters in Equation (S21) gives:

$$k_{inhib} = \frac{0.05\ Torr}{7.5\times10^{-6}\ Torr}\frac{30-1}{1-\frac{30}{1000}} \approx \frac{0.05\ Torr}{7.5\times10^{-6}\ Torr}3 = 2 \times 10^5 .$$

Because the growth time in purified conditions could not be determined precisely and we know that it is faster than 1 min, the value $k_{inhib} = 2 \times 10^5$ is a lower bound.

References

[1] M. Balooch, M. J. Cardillo, D. R. Miller, R. E. Stickney, *Surf. Sci.* **1974**, *46*, 358−392.

[2] R. J. Madix, J. Benziger, *Annu. Rev. Phys. Chem.* **1978**, *29*, 285−306.

[3] M. T. Clavaguera-Mora, J. L. Touron, J. Rodríguez-Viejo, N. Clavaguera, *J. Alloys and Compounds*. **2004**, *377*, 8-16.

[4] F. P. Bundy, *Physica A*, **1989**,*156*, 169.

[5] C. J. Jenks, B. E. Bent, F. Zaera, *J. Phys. Chem. B.* **2000**, *104 (14)*, 3017-3027.

[6] E. Loginova, N. C. Bartelt, P. J. Feibelman, K. F. McCarty, *New J. Phys.* **2009**, *11(6)*, 063046.

6.8 References

[1] S. Bae, H. Kim, Y. Lee, X. F. Xu, J. S. Park, Y. Zheng, J. Balakrishnan, T. Lei, H. R. Kim, Y. I. Song, Y. J. Kim, K. S. Kim, B. Ozyilmaz, J. H. Ahn, B. H. Hong, and S. Iijima, *Nat. Nanotechnol.* **2010**, *5*, 574-578.

[2] X. Li, W. Cai, J. An, S. Kim, J. Nah, D. Yang, R. Piner, A. Velamakanni, I. Jung, E. Tutuc, S. K. Banerjee, L. Colombo, and R. S. Ruoff, *Science.* **2009**, *324*, 1312-4.

[3] C. Mattevi, H. Kim, and M. Chhowalla, *J. Mater. Chem.* **2011**, *21*, 3324.

[4] T. Kobayashi, M. Bando, N. Kimura, K. Shimizu, K. Kadono, N. Umezu, K. Miyahara, S. Hayazaki, S. Nagai, Y. Mizuguchi, Y. Murakami, and D. Hobara, *Appl. Phys. Lett.* **2013**, *102*, 023112.

[5] Y. Zhang, L. Zhang, and C. Zhou, *Acc. Chem. Res.* **2013**, *46*, 2329-39.

[6] L. Tao, J. Lee, H. Chou, M. Holt, R. S. Ruoff, and D. Akinwande, *ACS Nano,* **2012,** *6*, 2319-2325.

[7] A. Srivastava, C. Galande, L. Ci, L. Song, C. Rai, D. Jariwala, K. F. Kelly, and P. M. Ajayan, *Chem. Mater.* **2010**, *22*, 3457-3461.

[8] P. Zhao, A. Kumamoto, S. Kim, X. Chen, B. Hou, S. Chiashi, E. Einarsson, Y. Ikuhara, and S. Maruyama, *J. Phys. Chem. C.* **2013,** *117*, 10755-10763.

[9] Z. C. Li, P. Wu, C. X. Wang, X. D. Fan, W. H. Zhang, X. F. Zhai, C. G. Zeng, Z. Y. Li, J. L. Yang, and J. G. Hou, *ACS Nano.* **2011**, *5*, 3385-3390.

[10] B. Zhang, W. H. Lee, R. Piner, I. Kholmanov, Y. P. Wu, H. F. Li, H. X. Ji, and R. S. Ruoff, *ACS Nano.* **2012**, *6*, 2471-2476.

[11] Y. Z. Xue, B. Wu, L. Jiang, Y. L. Guo, L. P. Huang, J. Y. Chen, J. H. Tan, D. C. Geng, B. R. Luo, W. P. Hu, G. Yu, and Y. Q. Liu, *JACS.* **2012**, *134*, 11060-11063.

[12] S. S. Chen, H. X. Ji, H. Chou, Q. Y. Li, H. Y. Li, J. W. Suk, R. Piner, L. Liao, W. W. Cai, and R. S. Ruoff, *Adv. Mater.* **2013**, 25, 2062-2065.

[13] Z. Han, A. Kimouche, D. Kalita, A. Allain, H. Arjmandi-Tash, A. Reserbat-Plantey, L. Marty, S. Pairis, V. Reita, N. Bendiab, J. Coraux, and V. Bouchiat, *Adv. Funct. Mater.* **2014**, *24*, 964-970.

[14] Z. Yan, J. Lin, Z. Peng, Z. Sun, Y. Zhu, L. Li, C. Xiang, E. L. Samuel, C. Kittrell, and J. M. Tour, *ACS Nano.* **2012**, *6*, 9110-9117.

[15] X. Li, C. W. Magnuson, A. Venugopal, J. An, J. W. Suk, B. Han, M. Borysiak, W. Cai, A. Velamakanni, Y. Zhu, L. Fu, E. M. Vogel, E. Voelkl, L. Colombo, and R. S. Ruoff, *Nano Lett.* **2010**, *10*, 4328-34.

[16] S. Bhaviripudi, X. T. Jia, M. S. Dresselhaus, and J. Kong, *Nano Lett.* **2010**, *10*, 4128-4133.

[17] P. R. Kidambi, C. Ducati, B. Dlubak, D. Gardiner, R. S. Weatherup, M.-B. Martin, P. Seneor, H. Coles, and S. Hofmann, *J. Phys. Chem. C***. 2012**, *116*, 22492-22501.

[18] H. Mehdipour and K. Ostrikov, *ACS Nano.* 2012, *6*, 10276-10286.

[19] H. Kim, C. Mattevi, M. R. Calvo, J. C. Oberg, L. Artiglia, S. Agnoli, C. F. Hirjibehedin, M. Chhowalla, and E. Saiz, *ACS Nano.* **2012**, *6*, 3614-3623.

[20] R. M. Jacobberger and M. S. Arnold, *Chem. Mater.* 2013, *25*, 871-877.

[21] S. Choubak, M. Biron, P. L. Levesque, R. Martel, and P. Desjardins, *J. Phys. Chem. Lett.* **2013**, *4*, 1100-1103.

[22] S. Choubak, P. L. Levesque, E. Gaufres, M. Biron, P. Desjardins, and R. Martel, *J. Phys. Chem. C.* **2014**, *118*, 21532-21540.

[23] J. W. Suk, A. Kitt, C. W. Magnuson, Y. F. Hao, S. Ahmed, J. H. An, A. K. Swan, B. B. Goldberg, and R. S. Ruoff, *ACS Nano.***2011,** *5*, 6916-6924.

[24] P. K. Chu and L. Li, *Mater. Chem. Phys.* **2006**, *96*, 253-277.

[25] J. D. Wood, S. W. Schmucker, A. S. Lyons, E. Pop, and J. W. Lyding, *Nano Lett.* **2011**, *11*, 4547-4554.

[26] W. Zhang, P. Wu, Z. Li, and J. Yang, *J. Phys. Chem. C.* **2011**, *115*, 17782-17787.

[27] K. HoKwon, S. Eduardo, C. Manish, and M. Cecilia, *New J. Phys.* **2013**, *15*, 053012.

[28] S. Nie, W. Wu, S. Xing, Q. Yu, J. Bao, S.-s. Pei, and K. F. McCarty, *New J. Phys.* **2012**, *14*, 093028.

CHAPTER 7: FORMATION OF MULTILAYERS

7.1 Introduction

Graphene multilayer formation on copper substrate during CVD appears to be strongly influenced by synthesis conditions and is in most cases inevitable. While most groups have concentrated their effort to control bi/multilayer density during the growth, we show in the present chapter that a large fraction of bi/multilayer growth can occur during the cooling stage.

According to literature, multilayers are mainly observed at 1) higher CH_4 partial pressure [28, 45, 48-50, 76-78, 86, 87, 111-114] and 2) slow cooling rate [49, 50, 87, 112, 113]. Many studies- as detailed in chapter 2- have been conducted to control the shape and size of graphene domains and also the formation of multilayers by changing the CH_4/H_2 ratio and the total pressure of the CVD chamber [28, 45, 48-50, 76-78, 86, 87, 111-114]. Note that changing the methane concentration in the gas feed resulted in the same overall behavior in both LP-CVD and AP-CVD [49]. Since the authors of these studies considered that molecular hydrogen was an etchant during the growth and post growth processes, they postulated that graphene growth is a balance between carbon deposition and hydrogen etching. When the carbon supply is low (i.e CH_4/H_2 ratio), graphene nucleates and grows some initial structures but due to a limited carbon supply and hydrogen etching, graphene growth terminates and cannot proceed in short amount of time; however, at elevated methane partial pressures or at high CH_4/H_2 ratio, not only growth proceeds on the copper substrates and terminates, but multilayer graphene is also formed [28, 45, 48-50, 76-78, 86, 87, 111-114].

SEM images from the literature reveal that monolayer graphene is obtained following an 8 hour growth at low methane concentration (Figure 7-1a) while multilayer growth appears at high methane concentration after 30 min growth time (Figure 7-1b) [50].

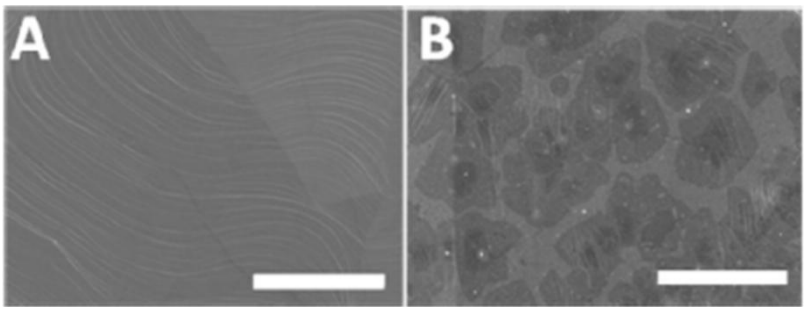

Figure 7-1. Influence of CH_4 concentration of graphene growth. A) Continuous single layer grown at low methane concentration, 30 ppm, for 8 hr, B) Multilayer growth at a higher CH_4 concentration, 150 ppm, for 30 min. Reprinted with permission from Ref. [50],© 2011, The American Chemical Society.

While elevated methane concentration was expected to result in multilayer formation during the graphene CVD, Lee et al. [112] speculated that this behavior might be related to the depletion of hydrogen and most importantly slower cooling process. They reported LP-CVD growth of bilayer graphene films on Cu at a slower cooling rate (~ 18 °C/min) compared to previous single layer graphene synthesis (40-300 °C/min). Considering copper's low carbon solubility and its catalytic role in the graphene growth process, the cooling rate had not been expected to affect the quality of graphene films in terms of thickness and uniformity [112]. However, later on, others have mentioned that the cooling process may impact the morphology of the films [49, 50, 87, 112, 113], but no data was reported and a clear understanding of this phenomenon is still lacking.

In the course of our experiments, we have observed that - in highly reduced environments - the final graphene film morphology is strongly affected by the presence or absence of purified UHP methane during the cooling down stage. Our findings are reported in this chapter but before moving forward let's recall our observations in the previous chapters in order to establish the baseline.

In chapter 5, we reported the formation of multilayers for growths carried out in highly reduced atmosphere where the level of oxidizing impurities were low. These results indicated that, in the absence of oxidizing species, graphene films cannot be etched and carbon precursors cannot be burnt at the Cu interface, leading to an excess amount of carbon species and further multilayer growth. Our results are consistent with previous published reports [28, 45, 48-50, 76-78, 86, 87, 111-114]. We found that multilayer growth formation was favored when both purified UHP

gases were present during the cooling down process. Our investigation of graphene film morphology as a function of growth time described in Chapter 6 led to a surprising result: we observed that films grown from purified gases and cooled under purified H_2 alone contained few bi- and multi-layers, independent of growth time up to 45 min. These puzzling observations motivated us to revisit our previous experiments in order to clarify the impact of the presence of methane during cooling down on the formation of multilayers in a highly reduced atmosphere. In other words, the question is: does the graphene growth continue during the cooling stage while the carbon source is still available? We thus compare film morphologies for different growth times (45, 20, and 10 min) where in one scenario the purified methane is on during cooling down and in the other one is off. We also briefly investigate the influence of the cooling rate on the formation of these multilayers.[2]

7.2 Experimental methodology

7.2.1 Copper Cleaning

The Cu foils were chemically cleaned in 1 M acetic acid (Sigma Aldrich, Reagent Plus > 99%) at 60 ºC followed by acetone and then 2-propanol (without drying) for 10 min in each step. The Cu substrates are then blown-dried with nitrogen.

7.2.2 Graphene growth

Graphene films were grown on 25-µm-thick Cu foils (Alfa Aesar, item no. 13382) at 1000 ºC in a 3.8-cm diameter (1.5 inch.) fused quartz tube inside a horizontal furnace (Lindberg/Blue M, Thermo Scientific) under low pressure conditions using purified UHP H_2/ purified UHP CH_4 gas mixture. The system is equipped with a manifold capable of ultra high vacuum (UHV) conditions. Prior to each growth, the system is evacuated to a vacuum of 5 $x10^{-6}$ Torr using a turbo molecular pump. The copper foils are then heated to 1000 ºC and annealed at this

[2] The data presented in this chapter was not specifically designed to explore this multilayer formation phenomenon. The results presented here are a collection of observations during the experimental course of this thesis and are therefore still preliminary.

temperature for 30 min under a flow of purified UHP hydrogen at 50 mTorr. Then, growth is carried out at 1000 °C for desired time with the reactor pressure maintained at 500 mTorr. Once the growth time is reached, the chamber is cooled down to room temperature in scenario number 1: under the flow of both gases, in scenario number 2: under solely purified UHP hydrogen while the UHP purified methane gas valve is closed and the chamber is immediately evacuated from it using a turbo pump. The approximate time for methane evacuation from the chamber is about 1 min.

We used purifiers that allows to decrease the residual O_2 content in UHP gases to less than 1 ppbV: (i) For H_2 (Praxair, UHP, grade 5, O_2 < 1ppm), DEOXO^{TM} (O_2 < 1ppb), and (ii) for CH_4 (Praxair, UHP, grade 3.7, O_2 < 15ppm), SAES Pure Gas Inc. MC1-950FV (H_2O and O_2 < 1ppbV) is selected.

7.3 Results

As explained above, we compare the final graphene morphologies for two different case scenarios during the cooling down process: a) both purified UHP methane and purified UHP hydrogen are present, and b) the purified UHP methane is off and evacuated from the chamber while purified UHP hydrogen in on. Figure 7-2 shows a schematic of the typical graphene LP-CVD process where the targeted growth time is set to 45 min. The only difference between Figure 7-2a and b is the presence/absence of purified UHP methane during the cooling down process. Temperature profiles as well as gas sequences are presented as a function of time for the entire growth process starting from a pre-deposition annealing stage to the graphene growth itself to the final cool-down phase.

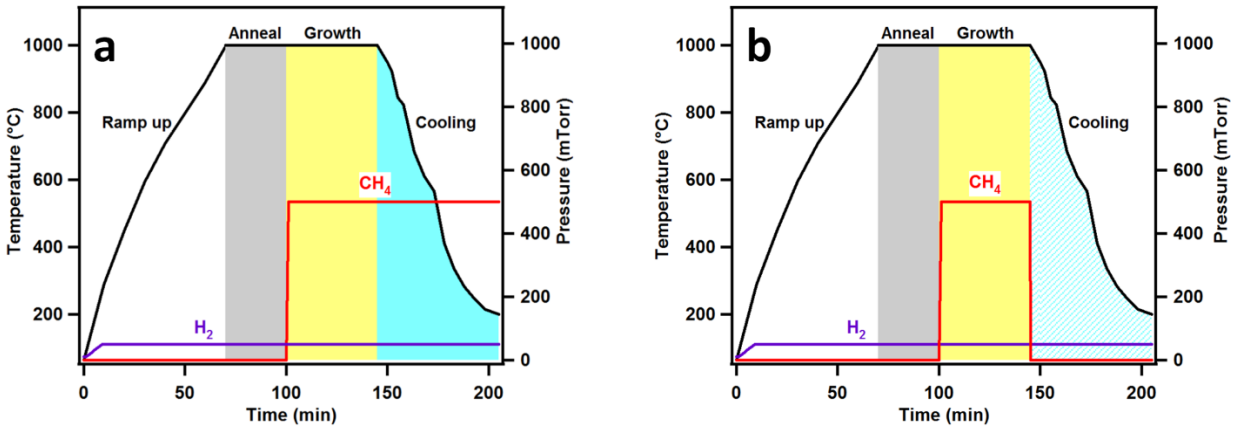

Figure 7-2. Schematic of the typical CVD growth process. Broad lines depict the temperature profile. The fine solid lines represent the partial pressure of the specific gas present during the annealing, growth, and cooling stages (i.e: H_2 purple and CH_4 red). In a) both CH_4 and H_2 are present during cooling down process while in b) the CH_4 is absent.

Figure 7-3 summarizes the complete set of experiments reported in this study. The detailed results are shown in the next section.

Batch #	Growth time	CH_4+H_2	H_2 Solely	Cooling process	Substrate/Characterization	Multilayer
25032013_Fig.7-4a	45 min	✓		Normal	Cu/SEM Hitachi	✓
25042013_Fig.7-4b						
21072014_Fig.7-4c						
28072014_Fig.7-4d	45 min		✓	Normal	Cu/SEM Hitachi	Sparse
04082014_Fig.7-4e/f					Cu/SEM Hitachi + JEOl	
14082014_Fig.7-5a	20 min	✓		Normal	Cu/ SEM Hitachi	✓
12082014_Fig.7-5b					SiO_2/SEM Hitachi	
17072014_Fig.7-5c	20 min		✓	Normal	Cu/ SEM Hitachi	Sparse
16072014_Fig.7-5d/e					Cu/ SEM Hitachi + JEOl	
20082014_Fig.7-7a	10 min	✓		Normal	Cu/ SEM Hitachi	✓
19082014_Fig.7-7b				Slow		
15012014_Fig.7-7c	10 min		✓	Normal	Cu/ SEM Hitachi	Sparse
23072014_Fig.7-7d					Cu/ SEM Hitachi	
25072014_Fig.7-7e					Cu/ SEM JEOl	

Figure 7-3. Complete sets of experiments reported in this study.

Figure 7-4 shows the SEM images of two sets of samples. The films presented in Figures 7-4 (a-c) are grown using purified UHP methane and hydrogen for 45 min in which both gases were on during the cooling down process whereas Figures 7-4(d-f) correspond to layers prepared in the same conditions except that the methane gas was shut off and evacuated during the cooling down process. The SEM images of different batches grown at different days/years (dated on the right hand corner of the image) and characterized by different SEMs (H for Hitachi and J for JEOL) show consistent and reproducible results.

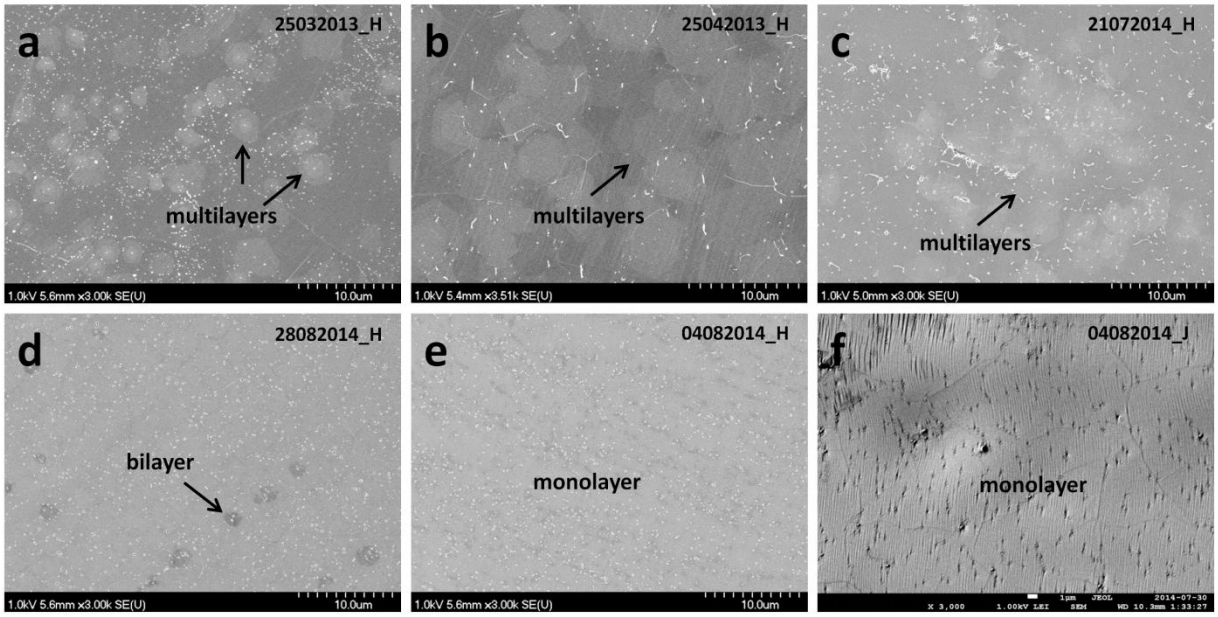

Figure 7-4. SEM images of graphene grown on Cu at 1000 °C for 45 min using purified UHP methane and hydrogen. (a-c) Purified methane was on during cool down process. (d-f) Purified methane was off and evacuated from the chamber during cool down process. The batch date as well as the SEM used for characterization was written on the right hand side of the image. Note that H and J stand for Hitachi and JEOL SEM respectively.

These SEM images reveal a clear difference in graphene film morphology in the presence (Figure 7-4(a-c)) and absence (Figure 7-4(d-f)) of purified UHP methane during the cooling down process. Multilayer growth is observed while the purified methane is on during the cool down while mostly monolayer graphene is formed once the purified methane is off. The same overall behavior has been observed in samples grown for 10 and 20 minutes. Figure 7-5 presents results for 20 min growths. Samples prepared with UHP methane present during cool down

contain a significantly larger coverage of multilayer islands compared to films for which H_2 alone was on during cooling.

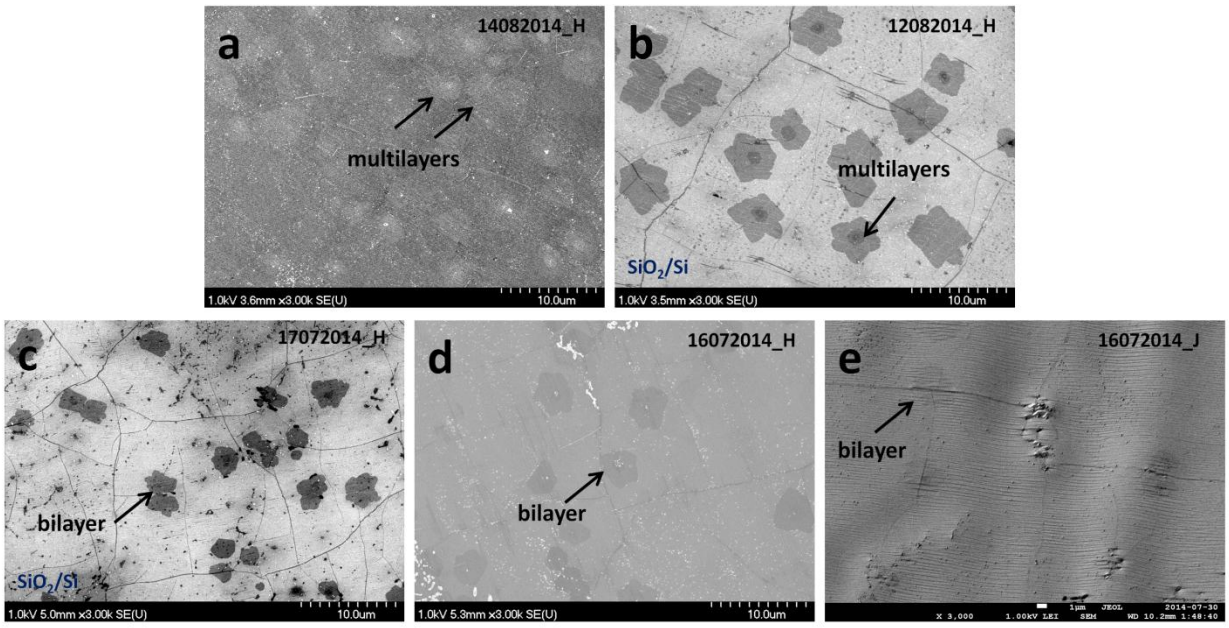

Figure 7-5. SEM images of graphene grown on Cu at 1000 °C for 20 min using purified UHP methane and hydrogen. (a-b) Purified methane was on during cool down process. (c-e) Purified methane was off and evacuated from the chamber during cool down process. The batch date as well as the SEM used for characterization was written on the right hand side of the image. Note that H and J stand for Hitachi and JEOL SEM respectively. Note that b-c are images of graphene films transferred on a SiO_2/Si substrate prior to SEM imaging.

For the 10 min growth time, we can compare not only the effect of the presence of methane during cool down but also the impact of the cooling rate. The measured temperature cool down profiles are presented in Figure 7-6 whereas SEM images from resulting films are shown in Figure 7-7.

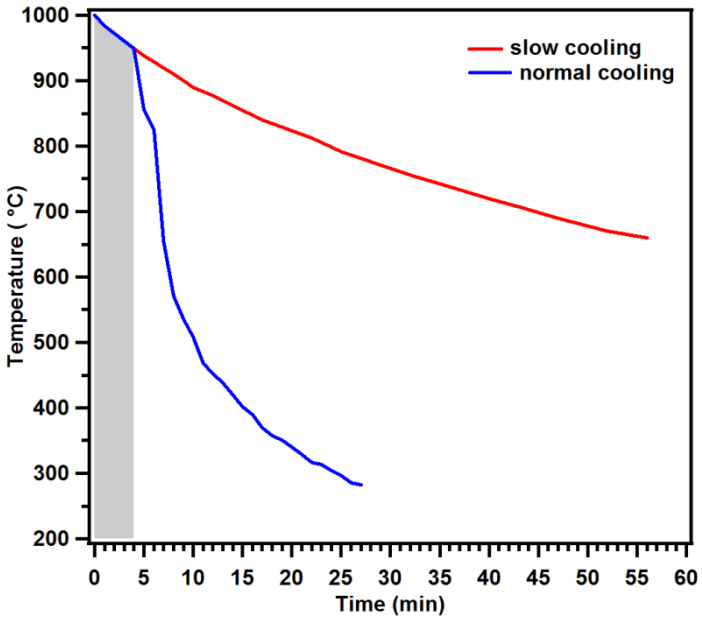

Figure 7-6. Cooling down profile of our graphene CVD growth set up.

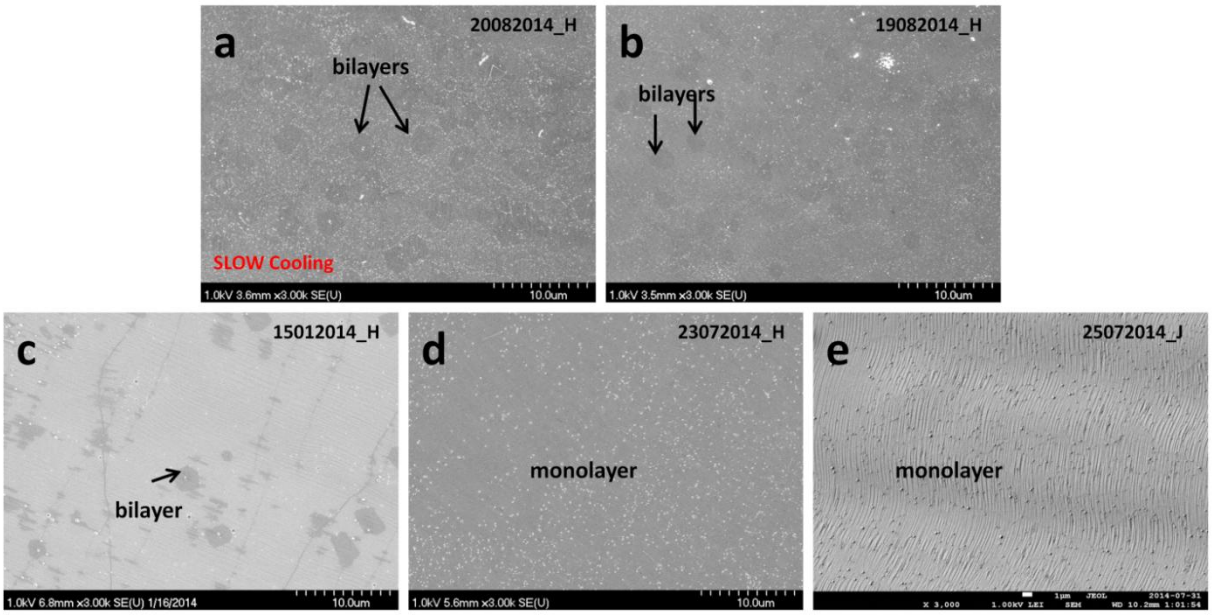

Figure 7-7. SEM images of graphene grown on Cu at 1000 °C for 10 min using purified UHP methane and hydrogen. Purified methane was on during (a) slow cool down process, and b) normal cool down. (c-e) Purified methane was off and evacuated from the chamber during cool down process. The batch date as well as the SEM used for characterization was written on the right hand side of the image. Note that H and J stand for Hitachi and JEOL SEM respectively.

The SEM images reveal no significant difference between the slow and normal cooling in the presence of purified methane in terms of graphene film morphology although the islands seem slightly larger. However, once the purified methane is off the films appear to be more homogeneous and uniform (Figure 7-7(c-e)). Although some bilayer growth is sparsely observed in one of the batches but there is clearly a difference between the films cooled down in the presence and absence of purified methane.

7.4 Discussion

Our entire set of results indicates that higher density and larger multilayers are formed while the purified methane remains ON during the cooling stage, whereas uniform and monolayer graphene films are obtained once the purified methane is off. These bilayers and multilayers are formed most likely in the early stage of the cooling process (between 1000-950 °C, shaded area in Figure 7-6) while the furnace is still at high temperature.

This observation is surprising since no further graphene growth is expected after a full layer is complete as no Cu sites are available to catalyze the CH_4 decomposition reaction. Also, we can rule out that islands present at the end of the growth stage are etched during cool down in the absence of methane based on our experiments presented in Chapter 4 and 5. We thus need to identify a mechanism that permits localized growth during cool down. We envision that the large difference in thermal expansion coefficients of graphene and Cu could lead to a local "delamination" during cool down. Indeed, as detailed below, Cu sites could become accessible for growth from CH_4 during cool down as the graphene layer is partially "lifted" from the Cu surface.

As mentioned in Chapter 2, the large negative graphene thermal expansion coefficient (TEC) ($\alpha_{graphene}=(-6\times10^{-6}$ /K)) at room temperature compared to copper ($\alpha_{copper}= 24\times10^{-6}$/K) [28, 115] leads to huge shrinkage of Cu upon cooling. It has been well established that the most common stress relaxation mechanism for graphene films on Cu involves the formation of wrinkles. As the graphene layer shrinks less rapidly than the copper substrate upon cooling, buckles, then folds develop [28, 82, 115]. In the absence of methane during the cooling stage, no further growth will occur. If methane is present in the chamber, however, such thermally-induced buckling creates

gaps at the interface. Methane can therefore reach the Cu substrate by diffusing through defect in the graphene film and decompose to form small islands underneath the complete layer.

Slow cooling rates or high methane pressures will favor larger multilayer coverage as described above and also reported in other work [82, 87, 112, 113, 115]. In our experiments, the time required to reach 950 °C is approximately 4-5 min and is the common point in all our experiments. Since the surface of Cu can be covered by graphene in approximately 1 min in highly reduced environment (see Chapter 6), we therefore expect to witness the growth of multilayers islands if the carbon source remains ON during the cooling stage. While cooling down, the growth speed will decrease exponentially until the temperature reaches a critical value where graphene is no longer formed. In a less reducing environment - due to the presence of oxygen - graphene growth is slower since oxygen can burn the C and etch graphene, thus a lower density of bilayers will be formed within the cooling time.

7.5 Conclusion

We have mainly observed the formation of multilayers in cases where both purified methane and hydrogen were ON during the cooling down process. Our results although preliminary, clearly show that multilayers can be formed during the cooling stage. This observation is in line with few studies reporting that fast cooling is key to achieve uniform and monolayer graphene films [49, 76, 112, 113]. This topic have to be investigated further to pin down the influence of cooling down process on graphene film morphology. Some of the required/potential/missing experiments are listed in Chapter 8 in the future work section.

CHAPTER 8: CONCLUSIONS, GENERAL DISCUSSION, AND PERSPECTIVES

8.1 Summary of the work and principal contributions

In conclusion, the present thesis has made significant contributions towards the advancement of the process technology and the scientific understanding of the synthesis of CVD graphene on copper. Our systematic study on the graphene CVD growth is the first report in literature claiming that molecular hydrogen does not etch graphene films on copper and that oxidizing impurities are responsible for this etching reaction. Our findings point toward the necessity to consider the influence of oxidizing species during the growth in order to achieve the essential understanding level for advancing graphene film processing in large scale and to reach the quality requirements for applications. The detailed conclusions can be summarized as follows:

Hydrogen etching reaction:

In chapter 4, despite the common belief in literature, we have established that molecular hydrogen does not etch graphene films on copper and oxidizing impurities are responsible for the graphene etching reaction through the catalytic role of copper. Furthermore, we show that different level of contaminants in the feedstock, furnace air leaks, and particularly, process gas purity are key parameters in controlling the graphene film morphology. These findings explain the presence of inconsistencies between graphene CVD growth recipes from furnace to furnace and among different groups since the role of oxygen in graphene CVD was not realized prior to our study.

Role of hydrogen and the influential role of trace amount of oxidizing impurities:

In Chapter 5, we have further investigated the role of hydrogen during LP-CVD growth of graphene films on copper and concluded *that hydrogen strongly suppresses graphene etching by removing the oxidizing species from the furnace via reduction and therefore protecting the graphene films from detrimental effect of oxygen.* Moreover, a detailed analysis and comparison of our samples grown in reducing atmosphere, where unpurified methane and purified hydrogen were used, with the samples grown in normal conditions, unpurified methane and hydrogen,

revealed that the surface coverage of bilayer domains increases by a factor of ~2 while the number of nucleation raises by a factor of ~ 2.5 when purified UHP hydrogen is used. These dissimilarities of graphene film morphologies in different growth conditions confirmed the influential role of trace amount oxygen in graphene CVD growth.

Graphene films grown using purified methane revealed even greater differences, in terms of morphology, compare to cases mentioned above. We observed a higher density of graphene bilayer domains, a higher overall bilayer coverage, and most importantly several areas of multilayers growth (bilayers, trilayers, etc.) when solely purified methane was used. *The formation of multilayers in highly reduced atmosphere indicated that in the absence of oxidizing species, graphene films cannot be etched and carbon precursors cannot be burnt at the Cu interface, leading to an excess amount of carbon species and further multilayer growth. Films grown with purified gases exhibited higher bilayer and multilayer coverage.* In some cases, these multilayers are found to be incommensurate with one another, i.e with random rotational angles between them. This suggested a different graphene growth behavior in purified and controlled conditions.

Is hydrogen necessarily required for graphene growth?

In conditions where the level of oxidizing impurities is low, we have grown uniform and continuous graphene films on copper with solely purified methane serving a double role as a copper oxide reducer and carbon supply for the growth. *This result showed that the presence of hydrogen is not necessary for graphene growth in a controlled atmosphere*. However, the formation of multilayers and different stacking order of graphene multilayers in such conditions indicated different graphene films growth behavior.

Graphene growth industrial implementation:

One of the main questions that we asked ourselves from the beginning of this thesis was: Why does it take so long (10-45 min) for one atomic layer of carbon to form on copper? At this point, the presence of oxygen could be a growth retardant because of the possible competition between carbon growth and oxygen etching during growth and cooling down of graphene films in LP-CVD reactor. This antagonistic effect was hypothesized as the main cause that makes the overall synthesis process long.

Taking an engineering approach and based on the insights we gained from our previous studies, we have minimized the level of oxidizing impurities by installing purifiers on our as-received gas bottles, and *we show that in the absence of such impurities, etching is minimized and thus copper is covered by graphene film in approximately 1 min.* This is between 5 to 45 times faster than the recipes used up to this date. The films are uniform and their quality is comparable to the best quality graphene reported in the literature. The method is compatible with industrial manufacturing processes and is shown to be an energy and cost effective way to synthesize graphene films on copper.

Formation of multilayers

During the course of our experiments, we observed multilayer growth in highly reduced atmosphere and when both gases -purified methane and purified hydrogen- were ON during the cooling down stage. *We believe that a large contribution of bi/multilayer can occur while graphene is completed in the cooling stage.* Although our results are still preliminary, they highlight the impact of the cooling stage on graphene bi/multi layer formation. A better understanding of how these bi/multilayer do form during cooling stage will be extremely beneficial in developing recipes for not only bilayer growth but also for improving the growth of single-layer graphene that is free of bilayers.

8.2 Perspectives for future work

Graphene CVD on copper turns out to be a best viable approach for production of graphene films on large scale. The scientific understanding of the graphene growth on copper is critical for the future graphene industry. While meter-scale graphene growth has been demonstrated experimentally, a good fundamental understanding of the graphene growth is crucial to the quality optimization and the cost reduction in the future graphene manufacturing industry. In particular the understanding of the growth kinetics for different pressure and flow regimes is yet to be developed. Compared to first layer growth, the secondary layer kinetics and mechanisms are even less known. Therefore, fundamental studies are becoming a popular trend among the research community. In the following, we discuss the numerous avenues and possibilities for research in this field based on the studies that we have conducted during these years.

Fundamental studies and bilayer graphene

The immediate continuation of this thesis, as mentioned in Chapter 7, is investigation of graphene film growth during cooling. It is noteworthy to mention that graphene's zero bandgap makes it unsuitable for devices with channels and incompatible in logic applications since it cannot be switched off [4, 116-118]. However, studies have shown that a controllable bandgap can be generated by applying an electric field perpendicular to bilayer graphene. Recognizing a bandgap is an avenue for utilizing bilayer graphene in digital electronics [117, 118]. Thus, understanding the growth behavior of bi/multi layer graphene during CVD will not only help us to improve the growth of single layer graphene film that is free of bi/multi layers but also open new possibilities for utilizing this material in electronics.

Although few studies have reported the CVD growth of bilayer graphene at the wafer scale [77, 112], developing conditions for uniform and reproducible synthesis continue to be challenging. According to our results in Chapter 7, we can deduce that controlling the graphene cooling rate and methane partial pressure during the cooling down stage can greatly impact the formation of bi/multi layer graphene films. Tuning these parameters can lead us to fabricate large area of bilayer graphene film using CVD. The main question is: How can one control the growth of bilayer by cooling? Some of the experiments that need to be undertaken in order to complete our study in Chapter 7 are:

1) Repeating the 20 and 10 min growth experiments with and without purified methane during cooling down stage and performing a statistical analysis of the data. Additional growth experiments for 5 and 30 min will also provide more interesting data giving a more general view of the whole spectrum of the graphene film morphology.

2) Repeating Graphene slow cooling experiments and reproducing the data will be helpful to determine the range of temperature where graphene growth still continues.

3) Increasing the methane partial pressure during the cooling down stage will also give us insight about the formation of multilayers. We expect larger bi/ multilayers and therefore higher coverage across the copper foil since a higher amount of carbon precursor will be available with increasing the methane partial pressure.

Finally, compiling the results of experiments mentioned above and a careful analysis of the data will clarify the influence of the cooling stage on the formation of multilayers. The information will ultimately pave the way towards developing recipes for the formation of bi and multilayer graphene in a controllable manner and subsequently using the films in practical applications.

I strongly believe that going deeper into the subject and running more experiments designed to explore this particular phenomena will open up avenues to control and manipulate the growth of these bi/multi layers.

Scaling-up Schemes

The next fairly simple project is to design an automated set up and devise a method of making the material in large volume without degrading its quality. Based on our results, graphene can be grown in highly reduced atmosphere- purified methane and purified hydrogen- where the cooling rate is extremely fast or the sample can be taken out from the chamber once the growth is complete. With this method/set up, we can improve graphene production process by reducing the entire process time and hence save energy. This method will be a test-bed for graphene growth for its scale up from lab scale manufacturing to roll to roll production units.

How to grow graphene single crystal?

One of the most exciting and challenging subject will be to add impurities intentionally -with control- during graphene CVD growth in order to etch the defects and let the carbon to nucleate at desired locations. This will ultimately create graphene single crystal. We have done some preliminary investigations in this area. We used carbon dioxide as the impurity to etch graphene films. According to Boudouard reaction [119], $2CO_{(g)} \rightarrow C_{(s)} + CO_{2(g)} + Heat$, graphene can be etched using carbon dioxide at high temperature through an endothermic reaction. Some preliminary results of this investigation is listed in the appendix. I believe this is another avenue to grow graphene films in a controllable manner and ultimately make continuous single crystal graphene film.

REFERENCES

[1] A. K. Geim and K. S. Novoselov, "The Rise of Graphene," *Nat. Mater.,* 6, 183-191, 2007.

[2] P. Avouris, Z. Chen, and V. Perebeinos, "Carbon-Based Electronics," *Nat. Nano.,* 2, 605-615, 2007.

[3] F. Xia, D. B. Farmer, Y-M. Lin, and P. Avouris, "Graphene Field-Effect Transistors with High On/Off Current Ratio and Large Transport Band Gap at Room Temperature," *Nano Lett.,* 10, 715-718, 2010.

[4] P. Avouris and C. Dimitrakopoulos, "Graphene: Synthesis and Applications," *Mater. Today,* 15, 86-97, 2012.

[5] R. H. Baughman, A. A. Zakhidov, and W. A. de Heer, "Carbon Nanotubes-the Route Toward Applications," *Science,* 297, 787-792, 2002.

[6] P. Avouris and R. Martel, "Progress in Carbon Nanotube Electronics and Photonics," *MRS Bulletin,* 35, 306-313, 2010.

[7] A. K. Geim, "Graphene: Status and Prospects," *Science,* 324, 1530-1534, 2009.

[8] K. I. Bolotin, K. J. Sikes, Z. Jiang, M. Klima, G. Fudenberg, J. Hone, P. Kim, and H. L. Stormer, "Ultrahigh Electron Mobility in Suspended Graphene," *Solid State Comm.,* 146, 351-355, 2008.

[9] X. Du, I. Skachko, A. Barker, and E. Y. Andrei, "Approaching Ballistic Transport in Suspended Graphene," *Nat. Nano.,* 3, 491-495, 2008.

[10] F. Bonaccorso, Z. Sun, T. Hasan, and A. C. Ferrari, "Graphene Photonics and Optoelectronics," *Nat. Photon.,* 4, 611-622, 2010.

[11] J. S. Bunch, A. M. van der Zande, S. S. Verbridge, I. W. Frank, D. M. Tanenbaum, J. M. Parpia, H. G. Craighead, and P. L. McEuen, "Electromechanical Resonators from Graphene Sheets," *Science,* 315, 490-493, 2007.

[12] X. Huang, X. Qi, F. Boey, and H. Zhang, "Graphene-Based Composites," *Chem.Soc. Rev.,* 41, 666-686, 2012.

[13] S. Kataria, S. Wagner, J. Ruhkopf, A. Gahoi, H. Pandey, R. Bornemann, S. Vaziri, A. D. Smith, M. Ostling, and M. C. Lemme, "Chemical Vapor Deposited Graphene: From Synthesis to Applications," *phys. status solidi (A)* 211, 11,2439-2449, 2014.

[14] K. S. Novoselov, A. K. Geim, S. V. Morozov, D. Jiang, Y. Zhang, S. V. Dubonos, I. V. Grigorieva, and A. A. Firsov, "Electric Field Effect in Atomically Thin Carbon Films," *Science,* 306, 666-669, 2004.

[15] K. S. Novoselov, V. I. Falko, L. Colombo, P. R. Gellert, M. G. Schwab, and K. Kim, "A Roadmap for Graphene," *Nature,* 490, 192-200, 2012.

[16] H. A. Becerril, J. Mao, Z. Liu, R. M. Stoltenberg, Z. Bao, and Y. Chen, "Evaluation of Solution-Processed Reduced Graphene Oxide Films as Transparent Conductors," *ACS Nano,* 2, 463-470, 2008.

[17] J. K. Wassei and R. B. Kaner, "Graphene, A Promising Transparent Conductor," *Materials Today,*13, 52-59, 2010.

[18] Y-M Lin, K. A. Jenkins, D. B Farmer, H-Y Chiu, A. Grill, P. Avouris, "100-GHz Transistors From Wafer-Scale Epitaxial Graphene," *Science,* 327, 1, 2010.

[19] Y. M. Lin, K. A. Jenkins, A. Valdes-Garcia, J. P. Small, D. B. Farmer, and P. Avouris, "Operation of Graphene Transistors at Gigahertz Frequencies," *Nano Lett.,* 9 (1), 422-426, 2009.

[20] M. D. Stoller, S. Park, Y. Zhu, J. An, and R. S. Ruoff, "Graphene-Based Ultracapacitors," *Nano Lett.,* 8, 3498-3502, 2008.

[21] C. Wang, D. Li, C. O. Too, and G. G. Wallace, "Electrochemical Properties of Graphene Paper Electrodes Used in Lithium Batteries," *Chem. Mater.,* 21, 2604-2606, 2009.

[22] J. Xiao, D. Mei, X. Li, W. Xu, D. Wang, G. L. Graff, W. D. Bennett, Z. Nie, L. V. Saraf, I. A. Aksay, J. Liu, and J.G. Zhang, "Hierarchically Porous Graphene as a Lithium–Air Battery Electrode," *Nano Lett.,*11, 5071-5078, 2011.

[23] S. Stankovich, D. A. Dikin, G. H. B. Dommett, K. M. Kohlhaas, E. J. Zimney, E. A. Stach, R. D. Piner, S. T. Nguyen, and R. S. Ruoff, "Graphene-Based Composite Materials," *Nature,* 442, 282-286, 2006.

[24] Y. Hernandez, V. Nicolosi, M. Lotya, F. M. Blighe, Z. Sun, S. De, I. T. McGovern, B. Holland, M. Byrne, Y. K. Gunko, J. J. Boland, P. Niraj, G. Duesberg, S. Krishnamurthy, R. Goodhue, J. Hutchison, V. Scardaci, A. C. Ferrari, and J. N. Coleman, "High-Yield Production of Graphene by Liquid-Phase Exfoliation of Graphite," *Nat. Nano.,* 3, 563-568, 2008.

[25] X. Huang, Z. Yin, S. Wu, X. Qi, Q. He, Q. Zhang, Q. Yan, F. Boey, and H. Zhang, "Graphene-Based Materials: Synthesis, Characterization, Properties, and Applications," *Small,* 7, 1876-1902, 2011.

[26] W. A. de Heer, C. Berger, X. Wu, P. N. First, E. H. Conrad, X. Li, T. Li, M. Sprinkle, J. Hass, M. L. Sadowski, M. Potemski, and G. Martinez, "Epitaxial Graphene," *Solid State Comm.*,143, 92-100, 2007.

[27] Y.M. Lin, A. Valdes-Garcia, S.J. Han, D. B. Farmer, I. Meric, Y. Sun, Y. Wu, C. Dimitrakopoulos, A. Grill, P. Avouris, and K. A. Jenkins, "Wafer-Scale Graphene Integrated Circuit," *Science*, 332, 1294-1297, 2011.

[28] C. Mattevi, H. Kim, and M. Chhowalla, "A Review of Chemical Vapour Deposition of Graphene on Copper," *J.Mater.Chem.*, 21, 3324-3334, 2011.

[29] J. Wintterlin and M. L. Bocquet, "Graphene on Metal Surfaces," *Surf. Sci.*, 603, 1841-1852, 2009.

[30] X. S. Li, W. W. Cai, J. H. An, S. Kim, J. Nah, D. X. Yang, R. Piner, A. Velamakanni, I. Jung, E. Tutuc, S. K. Banerjee, L. Colombo, and R. S. Ruoff, "Large-Area Synthesis of High-Quality and Uniform Graphene Films on Copper Foils," *Science*, 324, 1312-1314, 2009.

[31] N. A. Vinogradov, A. A. Zakharov, V. Kocevski, J. Rusz, K. A. Simonov, O. Eriksson, A. Mikkelsen, E. Lundgren, A. S. Vinogradov, N. Mårtensson, and A. B. Preobrajenski, "Formation and Structure of Graphene Waves on Fe(110)," *Phys. Rev. Lett.*, 109, 026101, 2012.

[32] T. Oznuluer, E. Pince, E. O. Polat, O. Balci, O. Salihoglu, and C. Kocabas, "Synthesis of Graphene on Gold," *Appl. Phys. Lett.*, 98, 183101, 2011.

[33] X. Li, W. Cai, L. Colombo, and R. S. Ruoff, "Evolution of Graphene Growth on Ni and Cu by Carbon Isotope Labeling," *Nano Lett.*, 9, 4268-4272, 2009.

[34] J. M. Wofford, S. Nie, K. F. McCarty, N. C. Bartelt, and O. D. Dubon, "Graphene Islands on Cu Foils: The Interplay between Shape, Orientation, and Defects," *Nano Lett.*, 10, 4890-4896, 2010.

[35] E. Loginova, N. C. Bartelt, P. J. Feibelman, and K. F. McCarty, "Evidence for graphene growth by C cluster attachment," *New J. Phys.*, 10, 2008.

[36] C. Johann, T. N. D. Alpha, E. Martin, B. Carsten, W. Dirk, B. Niemma, J. H. Frank, G. Raoul van, P. Bene, and M. Thomas, "Growth of Graphene on Ir(111)," *New J. Phys.*, 11, 023006, 2009.

[37] T. Fujita, W. Kobayashi, and C. Oshima, "Novel Structures of Carbon Layers on a Pt(111) surface," *Surf. Interface.Anal.*, 37, 120-123, 2005.

[38] S.Y. Kwon, C. V. Ciobanu, V. Petrova, V. B. Shenoy, J. Bareño, V. Gambin, I. Petrov, and S. Kodambaka, "Growth of Semiconducting Graphene on Palladium," *Nano Lett.*, 9, 3985-3990, 2009.

[39] S. Nie, J. M. Wofford, N. C. Bartelt, O. D. Dubon, and K. F. McCarty, "Origin of the Mosaicity in Graphene Grown on Cu(111)," *Phys. Rev. B*, 84, 2011.

[40] Y. Zhang, L. Zhang, and C. Zhou, "Review of Chemical Vapor Deposition of Graphene and Related Applications," *Acc. Chem. Res.*, 46, 2329-39, 2013.

[41] H. Kim, C. Mattevi, M. R. Calvo, J. C. Oberg, L. Artiglia, S. Agnoli, C. F. Hirjibehedin, M. Chhowalla, and E. Saiz, "Activation Energy Paths for Graphene Nucleation and Growth on Cu," *ACS Nano*, 6, 3614-3623, 2012.

[42] T. Kobayashi, M. Bando, N. Kimura, K. Shimizu, K. Kadono, N. Umezu, K. Miyahara, S. Hayazaki, S. Nagai, Y. Mizuguchi, Y. Murakami, and D. Hobara, "Production of a 100-m-Long High-Quality Graphene Transparent Conductive Film by Roll-to-Roll Chemical Vapor Deposition and Transfer Process," *Appl. Phys. Lett.*,102, 2013.

[43] S. Bae, H. Kim, Y. Lee, X. F. Xu, J. S. Park, Y. Zheng, J. Balakrishnan, T. Lei, H. R. Kim, Y. I. Song, Y. J. Kim, K. S. Kim, B. Ozyilmaz, J. H. Ahn, B. H. Hong, and S. Iijima, "Roll-to-Roll Production of 30-inch Graphene Films for Transparent Electrodes," *Nat. Nanotechnol.*, 5, 574-578, 2010.

[44] L. B. Gao, W. C. Ren, J. P. Zhao, L. P. Ma, Z. P. Chen, and H. M. Cheng, "Efficient Growth of High-Quality Graphene Films on Cu Foils by Ambient Pressure Chemical Vapor Deposition," *Appl. Phys. Lett.*, 97, 2010.

[45] S. Bhaviripudi, X. T. Jia, M. S. Dresselhaus, and J. Kong, "Role of Kinetic Factors in Chemical Vapor Deposition Synthesis of Uniform Large Area Graphene Using Copper Catalyst," *Nano Lett.*, 10, 4128-4133, 2010.

[46] X. S. Li, C. W. Magnuson, A. Venugopal, J. H. An, J. W. Suk, B. Y. Han, M. Borysiak, W. W. Cai, A. Velamakanni, Y. W. Zhu, L. F. Fu, E. M. Vogel, E. Voelkl, L. Colombo, and R. S. Ruoff, "Graphene Films with Large Domain Size by a Two-Step Chemical Vapor Deposition Process," *Nano Lett.*,10, 4328-4334, 2010.

[47] X. Li, C. W. Magnuson, A. Venugopal, R. M. Tromp, J. B. Hannon, E. M. Vogel, L. Colombo, and R. S. Ruoff, "Large-Area Graphene Single Crystals Grown by Low-Pressure Chemical Vapor Deposition of Methane on Copper," *J.Amer.Chem. Soc.*, 133, 2816-9, 2011.

[48] Y. Zhang, L. Zhang, P. Kim, M. Ge, Z. Li, and C. Zhou, "Vapor Trapping Growth of Single-Crystalline Graphene Flowers: Synthesis, Morphology, and Electronic Properties," *Nano Lett.*,12, 2810-6, 2012.

[49] P. R. Kidambi, C. Ducati, B. Dlubak, D. Gardiner, R. S. Weatherup, M.-B. Martin, P. Seneor, H. Coles, and S. Hofmann, "The Parameter Space of Graphene Chemical Vapor Deposition on Polycrystalline Cu," *J.Phys.Chem. C,*116, 22492-22501, 2012.

[50] I. Vlassiouk, M. Regmi, P. F. Fulvio, S. Dai, P. Datskos, G. Eres, and S. Smirnov, "Role of Hydrogen in Chemical Vapor Deposition Growth of Large Single-Crystal Graphene," *ACS Nano,* 5, 6069-6076, 2011.

[51] M. Losurdo, M. M. Giangregorio, P. Capezzuto, and G. Bruno, "Graphene CVD growth on copper and nickel: role of hydrogen in kinetics and structure," *Phys Chem Chem Phys,* vol. 13, pp. 20836-43, Dec 14 2011.

[52] Y. C. Shin and J. Kong, "Hydrogen-Excluded Graphene Synthesis via Atmospheric Pressure Chemical Vapor Deposition," *Carbon,* 59, 439-447, 2013.

[53] Y. Zhang, Z. Li, P. Kim, L. Y. Zhang, and C. W. Zhou, "Anisotropic Hydrogen Etching of Chemical Vapor Deposited Graphene " *ACS Nano,* 6, 6526-6526, 2012.

[54] Y. Hao, M. S. Bharathi, L. Wang, Y. Liu, H. Chen, S. Nie, X. Wang, H. Chou, C. Tan, B. Fallahazad, H. Ramanarayan, C. W. Magnuson, E. Tutuc, B. I. Yakobson, K. F. McCarty, Y. W. Zhang, P. Kim, J. Hone, L. Colombo, and R. S. Ruoff, "The Role of Surface Oxygen in the Growth of Large Single-Crystal Graphene on Copper," *Science,* 342, 720-3, 2013.

[55] L. Tao, J. Lee, H. Chou, M. Holt, R. S. Ruoff, and D. Akinwande, "Synthesis of High Quality Monolayer Graphene at Reduced Temperature on Hydrogen-Enriched Evaporated Copper (111) Films," *ACS Nano,* 6, 2319-2325, 2012.

[56] A. Srivastava, C. Galande, L. Ci, L. Song, C. Rai, D. Jariwala, K. F. Kelly, and P. M. Ajayan, "Novel Liquid Precursor-Based Facile Synthesis of Large-Area Continuous, Single, and Few-Layer Graphene Films," *Chem.Mater.*, 22, 3457-3461, 2010.

[57] P. Zhao, A. Kumamoto, S. Kim, X. Chen, B. Hou, S. Chiashi, E. Einarsson, Y. Ikuhara, and S. Maruyama, "Self-Limiting Chemical Vapor Deposition Growth of Monolayer Graphene from Ethanol," *J. Phys.Chem. C,*117,10755-10763, 2013.

[58] Z. C. Li, P. Wu, C. X. Wang, X. D. Fan, W. H. Zhang, X. F. Zhai, C. G. Zeng, Z. Y. Li, J. L. Yang, and J. G. Hou, "Low-Temperature Growth of Graphene by Chemical Vapor Deposition Using Solid and Liquid Carbon Sources," *ACS Nano,* 5, 3385-3390, 2011.

[59] B. Zhang, W. H. Lee, R. Piner, I. Kholmanov, Y. P. Wu, H. F. Li, H. X. Ji, and R. S. Ruoff, "Low-Temperature Chemical Vapor Deposition Growth of Graphene from Toluene on Electropolished Copper Foils," *ACS Nano,* 6, 2471-2476, 2012.

[60] F. Schwierz, "Graphene Transistors," *Nat. Nano.,* 5, 487-496, 2010.

[61] J. Basu, J. K. Basu, and T. K. Bhattacharyya, "The Evolution of Graphene-Based Electronic Devices," *Int. J. Smart Nano Mater.*,1, 201-223, 2010.

[62] A. C. Ferrari, J. C. Meyer, V. Scardaci, C. Casiraghi, M. Lazzeri, F. Mauri, S. Piscanec, D. Jiang, K. S. Novoselov, S. Roth, and A. K. Geim, "Raman Spectrum of Graphene and Graphene Layers," *Phys. Rev. Lett.,* 97, 2006.

[63] M. S. Dresselhaus, A. Jorio, M. Hofmann, G. Dresselhaus, and R. Saito, "Perspectives on Carbon Nanotubes and Graphene Raman Spectroscopy," *Nano Lett.*,10, 751-8, 2010.

[64] A. C. Ferrari and D. M. Basko, "Raman Spectroscopy as a Versatile Tool for Studying the Properties of Graphene," *Nat. Nano.,* 8, 235-246, 2013.

[65] R. W. Havener, H. L. Zhuang, L. Brown, R. G. Hennig, and J. Park, "Angle-Resolved Raman Imaging of Inter layer Rotations and Interactions in Twisted Bilayer Graphene," *Nano Lett.*,12, 3162-3167, 2012.

[66] V. Carozo, C. M. Almeida, E. H. Ferreira, L. G. Cancado, C. A. Achete, and A. Jorio, "Raman Signature of Graphene Superlattices," *Nano Lett.*,11, 4527-34, 2011.

[67] J. Campos-Delgado, L. G. Cançado, C. A. Achete, A. Jorio, and J.-P. Raskin, "Raman Scattering Study of the Phonon Dispersion in Twisted Bilayer Graphene," *Nano Res.*,6, 269-274, 2013.

[68] R. He, T. F. Chung, C. Delaney, C. Keiser, L. A. Jauregui, P. M. Shand, C. C. Chancey, Y. N. Wang, J. M. Bao, and Y. P. Chen, "Observation of Low Energy Raman Modes in Twisted Bilayer Graphene," *Nano Lett.*,13, 3594-3601, 2013.

[69] A. C. Ferrari, "Raman Spectroscopy of Graphene and Graphite: Disorder, Electron–Phonon Coupling, Doping and Nonadiabatic Effects," *Solid State Comm.*,143, 47-57, 2007.

[70] L. M. Malard, M. A. Pimenta, G. Dresselhaus, and M. S. Dresselhaus, "Raman Spectroscopy in Graphene," *Phys. Rep.*,473, 51-87, 2009.

[71] J. W. Suk, A. Kitt, C. W. Magnuson, Y. F. Hao, S. Ahmed, J. H. An, A. K. Swan, B. B. Goldberg, and R. S. Ruoff, "Transfer of CVD-Grown Monolayer Graphene onto Arbitrary Substrates," *ACS Nano,* 5, 6916-6924, 2011.

[72] T.-o. Terasawa and K. Saiki, "Growth of Graphene on Cu by Plasma Enhanced Chemical Vapor Deposition," *Carbon,* 50, 869-874, 2012.

[73] H. I. Rasool, E. B. Song, M. J. Allen, J. K. Wassei, R. B. Kaner, K. L. Wang, B. H. Weiller, and J. K. Gimzewski, "Continuity of Graphene on Polycrystalline Copper," *Nano Lett.*,11, 251-6, 2011.

[74] W. Liu, H. Li, C. Xu, Y. Khatami, and K. Banerjee, "Synthesis of High-Quality Monolayer and Bilayer Graphene on Copper using Chemical Vapor Deposition," *Carbon*, 49, 4122-4130, 2011.

[75] I. V. Markov, *Crystal growth for beginners*: World Scientific, 1995.

[76] A. W. Robertson and J. H. Warner, "Hexagonal Single Crystal Domains of Few-Layer Graphene on Copper Foils," *Nano Lett.*,11,1182-9, 2011.

[77] K. Yan, H. Peng, Y. Zhou, H. Li, and Z. Liu, "Formation of Bilayer Bernal Graphene: Layer-by-Layer Epitaxy via Chemical Vapor Deposition," *Nano Lett.*,11,1106-10, 2011.

[78] S. Nie, W. Wu, S. Xing, Q. Yu, J. Bao, S.-s. Pei, and K. F. McCarty, "Growth from Below: Bilayer Graphene on Copper by Chemical Vapor Deposition," *New J.Phy.*,14, 093028, 2012.

[79] Q. Y. Li, H. Chou, J. H. Zhong, J. Y. Liu, A. Dolocan, J. Y. Zhang, Y. H. Zhou, R. S. Ruoff, S. S. Chen, and W. W. Cai, "Growth of Adlayer Graphene on Cu Studied by Carbon Isotope Labeling," *Nano Lett.*,13, 486-490, 2013.

[80] W. Fang, A. L. Hsu, R. Caudillo, Y. Song, A. G. Birdwell, E. Zakar, M. Kalbac, M. Dubey, T. Palacios, and M. S. Dresselhaus, "Rapid Identification of Stacking Orientation in Isotopically Labeled Chemical-Vapor Grown Bilayer Graphene by Raman Spectroscopy," *Nano Lett.*,13, 1541-1548, 2013.

[81] X. Zhang, L. Wang, J. Xin, B. I. Yakobson, and F. Ding, "Role of Hydrogen in Graphene Chemical Vapor Deposition Growth on a Copper Surface," *J.Amer.Chem. Soc.*,136, 3040-3047, 2014.

[82] M. Kalbac, O. Frank, and L. Kavan, "The Control of Graphene Double-Layer Formation in Copper-Catalyzed Chemical Vapor Deposition," *Carbon*, 50, 3682-3687, 2012.

[83] D. Geng, B. Wu, Y. Guo, L. Huang, Y. Xue, J. Chen, G. Yu, L. Jiang, W. Hu, and Y. Liu, "Uniform Hexagonal Graphene Flakes and Films Grown on Liquid Copper Surface," *Proc. National Academy Sci.*, 109, 7992-7996, 2012.

[84] B. Wu, D. Geng, Z. Xu, Y. Guo, L. Huang, Y. Xue, J. Chen, G. Yu, and Y. Liu, "Self-Organized Graphene Crystal Patterns," *NPG Asia Mater.*, 5, p. e36, 2013.

[85] Y. Yao and C.P. Wong, "Monolayer Graphene Growth using Additional Etching Process in Atmospheric Pressure Chemical Vapor Deposition," *Carbon*, 50, 5203-5209, 2012.

[86] Y. G. Yao, Z. Li, Z. Y. Lin, K. S. Moon, J. Agar, and C. P. Wong, "Controlled Growth of Multilayer, Few-Layer, and Single-Layer Graphene on Metal Substrates," *J. Phys.Chem. C*, 115, 5232-5238, 2011.

[87] Z. Han, A. Kimouche, D. Kalita, A. Allain, H. Arjmandi-Tash, A. Reserbat-Plantey, L. Marty, S. Pairis, V. Reita, N. Bendiab, J. Coraux, and V. Bouchiat, "Homogeneous Optical and Electronic Properties of Graphene Due to the Suppression of Multilayer Patches During CVD on Copper Foils," *Adv. Func. Mater.,* 24, 964-970, 2014.

[88] L. X. Liu, H. L. Zhou, R. Cheng, Y. Chen, Y. C. Lin, Y. Q. Qu, J. W. Bai, I. A. Ivanov, G. Liu, Y. Huang, and X. F. Duan, "A Systematic Study of Atmospheric Pressure Chemical Vapor Deposition Growth of Large-Area Monolayer Graphene," *J. Mater. Chem.,* 22, 1498-1503, 2012.

[89] H. Ago, Y. Ogawa, M. Tsuji, S. Mizuno, and H. Hibino, "Catalytic Growth of Graphene: Toward Large-Area Single-Crystalline Graphene," *J. Phys. Chem. Lett.,*3, 2228-2236, 2012.

[90] I. Vlassiouk, P. Fulvio, H. Meyer, N. Lavrik, S. Dai, P. Datskos, and S. Smirnov, "Large Scale Atmospheric Pressure Chemical Vapor Deposition of Graphene," *Carbon,* 54, 58-67, 2013.

[91] R. J. Madix and J. Benziger, "Kinetic Processes on Metal Single-Crystal Surfaces," *Annu. Rev. Phys. Chem.,* 29, 285-306, 1978.

[92] M. Balooch, M. J. Cardillo, D. R. Miller, and R. E. Stickney, "Molecular Beam Study of the Apparent Activation Barrier Associated with Adsorption and Desorption of Hydrogen on Copper," *Surf. Sci.,* 46, 358-392, 1974.

[93] Y. Z. Xue, B. Wu, L. Jiang, Y. L. Guo, L. P. Huang, J. Y. Chen, J. H. Tan, D. C. Geng, B. R. Luo, W. P. Hu, G. Yu, and Y. Q. Liu, "Low Temperature Growth of Highly Nitrogen-Doped Single Crystal Graphene Arrays by Chemical Vapor Deposition," *J. Am. Chem. Soc.,*134, 11060-11063, 2012.

[94] N. Lisi, F. Buonocore, T. Dikonimos, E. Leoni, G. Faggio, G. Messina, V. Morandi, L. Ortolani, and A. Capasso, "Rapid and Highly Efficient Growth of Graphene on Copper by Chemical Vapor deposition of Ethanol," *Thin Solid Films,* 571, 1, 139-144, 2014.

[95] C. Z. Congqin Miao, Owen Liang and Ya-Hong Xie, "Chemical Vapor Deposition of Graphene, Physics and Application of Graphene," *Intech*, 52, 5, 2011.

[96] E. F. Rosenblatt, "Method of Removing Free Oxygen or Free Hydrogen from a Gaseous Medium," Google Patents, 1952.

[97] A. Guermoune, T. Chari, F. Popescu, S. S. Sabri, J. Guillemette, H. S. Skulason, T. Szkopek, and M. Siaj, "Chemical Vapor Deposition Synthesis of Graphene on Copper with Methanol, Ethanol, and Propanol Precursors," *Carbon,* 49, 4204-4210, 2011.

[98] J. P. S. Jining Xie. Imaging Graphene via Low Voltage Field Emission Scanning Electron Microscope. Available: http://www.toyo.co.jp/file/pdf/spm/files/agi/5991-0781EN.pdf

[99] J.P. Spallas and J. Xie, "Different Contrast Mechanisms on SEM Imaging of Graphene."Available: http://www.toyo.co.jp/file/pdf/spm/files/agi/5991-0782EN.pdf

[100] A. Asahina, T. Togashi, O. Terasaki, S. Takani, T. Adschiri, M. Shibata, N. Erdman,"High Resolution Low Voltage Scanning Electron Microscope Study of NanostructuresDetails,"Available:http://www.jeolusa.com/DesktopModules/Bring2mind/DMX/Download.aspx?EntryId=926&Command=Core_Download&PortalId=2&TabId=320

[101] Y. Fan, L. Yangqiao, W. Wei, C. Wei, G. Lian, and S. Jing, "A Facile Method to Observe Graphene Growth on Copper Foil," *Nanotechnology,* 23, 475705, 2012.

[102] J. C. Riviere, "Auger and X-Ray Photoelectron Spectroscopy," *Practical Surface Analysis*". Briggs ed. Chapter 2, J. Wiley and Sons Ltd, New York, 1990.

[103] L. W. Drummond, "XPS: Instrumention and Performance," *Surface Analysis by Auger and X-Ray Photpelectron Spectroscopy".* Briggs ed: IM Publicationand Surface Spectra Limited, 2003.

[104] T.A. Delchar and D.P. Woodruff, "*Modern Techniques of Surface Science*". Chapter 3, Cambridge University Press, 1994.

[105] W. Telieps, "Surface Imaging with LEEM," *Appl. Phys. A*, 44, 55-61, 1987.

[106] E. Bauer, "LEEM Basics," *Surf. Rev. Lett.*,5, 6, 1275-1286, 1998.

[107] R. M. Tromp, "Low-energy Electron Microscopy," *IBM J. Res. Develop.*, 44, 4, 503-516, 2000.

[108] E. Bauer, "Low Energy Electron Microscopy," *Rep. Prog. Phys.,* 57, 895-938, 1994.

[109] L. G. Cancado, A. Jorio, E. H. Ferreira, F. Stavale, C. A. Achete, R. B. Capaz, M. V. Moutinho, A. Lombardo, T. S. Kulmala, and A. C. Ferrari, "Quantifying Defects in Graphene via Raman spectroscopy at Different Excitation Energies," *Nano Lett.,* 11, 3190-6, 2011.

[110] S. Marcet, M. Verhaegen, S. Blais-Ouellette, and R. Martel, "Raman Spectroscopy Hyperspectral Imager based on Bragg Tunable Filters," *Proc. SPIE, Photonics North*, 8412, 84121J-7,2012.

[111] X. Li, C. W. Magnuson, A. Venugopal, J. An, J. W. Suk, B. Han, M. Borysiak, W. Cai, A. Velamakanni, Y. Zhu, L. Fu, E. M. Vogel, E. Voelkl, L. Colombo, and R. S. Ruoff, "Graphene Films with Large Domain Size by a Two-Step Chemical Vapor Deposition Process," *Nano Lett.*,10, 4328-34, 2010.

[112] S. Lee, K. Lee, and Z. Zhong, "Wafer Scale Homogeneous Bilayer Graphene Films by Chemical Vapor Deposition," *Nano Lett.*,10, 4702-7,2010.

[113] W. Wu, Q. K. Yu, P. Peng, Z. H. Liu, J. M. Bao, and S. S. Pei, "Control of Thickness Uniformity and Grain Size in Graphene Films for Transparent Conductive Electrodes," *Nanotechnology*, 23, 2012.

[114] N. Van Tu, L. Huu Doan, N. Van Chuc, Tam N. Thi Thanh, L. Dinh Quang, N. Xuan Nghia, and P. Ngoc Minh, "Synthesis of Multi-Layer Graphene Films on Copper Tape by Atmospheric Pressure Chemical Vapor Deposition Method," *Adv. Nat. Sci.: Nanosci. Nanotechnol.*,4, 035012, 2013.

[115] G. H. Han, F. Gunes, J. J. Bae, E. S. Kim, S. J. Chae, H. J. Shin, J. Y. Choi, D. Pribat, and Y. H. Lee, "Influence of Copper Morphology in Forming Nucleation Seeds for Graphene Growth," *Nano Lett.*,11, 4144-8, 2011.

[116] P. Avouris and F. Xia, "Graphene Applications in Electronics and Photonics," *MRS Bulletin*, 37, 1225-1234, 2012.

[117] T. Ohta, A. Bostwick, T. Seyller, K. Horn, and E. Rotenberg, "Controlling the Electronic Structure of Bilayer Graphene," *Science*, 313, 951-954, 2006.

[118] Y. Zhang, T. T. Tang, C. Girit, Z. Hao, M. C. Martin, A. Zettl, M. F. Crommie, Y. R. Shen, and F. Wang, "Direct Observation of a Widely Tunable Bandgap in Bilayer Graphene," *Nature*, 459, 820-3, 2009.

[119] J. Hunt, A. Ferrari, A. Lita, M. Crosswhite, B. Ashley, and A. E. Stiegman, "Microwave-Specific Enhancement of the Carbon–Carbon Dioxide (Boudouard) Reaction,"*J. Phys.Chem. C*,117, 26871-26880, 2013.

ANNEX

Here we show the preliminary results of the graphene etching reaction on copper using carbon dioxide. According to Boudouard reaction, $2CO_{(g)} \rightarrow C_{(s)} + CO_{2(g)} + Heat$, graphene can be etched using carbon dioxide at high temperature through an endothermic reaction.

Methodology

Graphene growth

Graphene films were grown on 25 μm thick Cu foils (Alfa Aesar, item no. 13382) at 1000 °C in a 1.5 inch. fused quartz tube at low pressure. The system consists of a manifold capable of UHV conditions where the gases are introduced into the chamber. The system's base pressure prior to gas insertion is below $5x10^{-6}$ Torr. The Cu foils were heated to 1000 °C and annealed at this temperature for 30 min under the flow of H_2 at 50 mTorr. In order to grow graphene, CH_4 was introduced into the chamber and the total pressure reached 500 mTorr. After 45 min (growth time), the chamber was cooled down to room temperature under the flow of H_2 and CH_4. Graphene samples were examined under SEM (Hitachi S-4700) prior to any treatment.

CO_2 purifier

We used a SAES Pure Gas Inc. MC1- 804FV (H_2O and $O_2 < 1$ppbV) for CO_2 (Praxair, Anaerobic, grade 4, 99.99% purity).

Annealing experiments:

All the annealing experiments were conducted in the same CVD system. We used a three zone furnace where we could target different temperature at different zones. We calibrated the furnace in order to have a precise idea of the temperature at each position. Once we characterized the as-grown graphene samples with SEM, we placed them into the designated position in the furnace. Next we vacuum the chamber below $5x10^{-6}$ Torr. Once the desired temperature was reached, we exposed the sample to a flow of *purified* CO_2 for 25 min at 40 mTorr . Then, we evacuated the chamber from the CO_2 using a turbo pump. We cooled down the samples to room temperature in vacuum.

Furnace position

The temperature at which each sample is held at different positions of the furnace is shown in Figure A-1 and A-2 for the three different runs. The arrows show the direction of the flow into the furnace and S is the abbreviation for the samples.

Run #1:

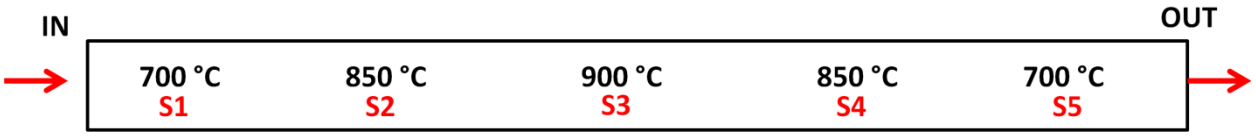

Figure A-0-1. The temperature of different part of the furnace. S is the abbreviation for sample and the arrows show the CO_2 flow direction.

Run #2 and # 3:

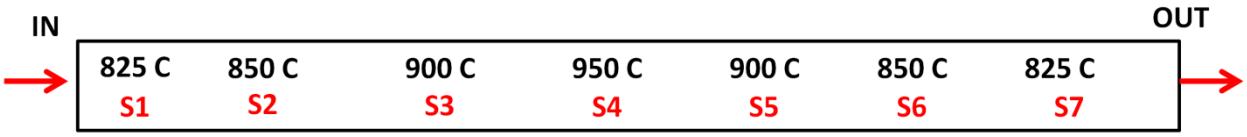

Figure A-0-2. The temperature of different part of the furnace. S is the abbreviation for sample and the arrows show the CO_2 flow direction.

Results

Run#1:

We have selected five samples and we have placed them at five different positions in our CVD furnace. The samples S1 and S5 were heated to 700 °C, while S2 and S4 were at 850 °C and S5 at 900 °C (Figure A-1). Based on Boudouard inverse reaction [119], the reaction temperature at which CO_2 starts etching graphene is above 800 °C, however, at temperature higher than 400 °C [90], oxygen can etch graphene films. In order to verify that oxygen play no role in this experiment- no air leaks into the furnace and the CO_2 purifier is working - and CO_2 is the sole reactant, we have placed two samples S1 and S5 at 700 °C. These samples should remain intact after CO_2 exposure. Note that prior to any treatment, we have characterized the as-grown film

with SEM. As shown in Figure A-3 top row, the film is continuous with many bilayers. The bottom row of Figure 3 shows the SEM pictures of the samples after CO_2 exposure. As expected, S1 and S5 remained intact after being exposed to CO_2. This means that the level of oxygen in the chamber is very low and thus oxygen is not responsible for graphene etching reaction. Samples S2 and S4 which were held at 850 °C are etched in some areas whereas the sample held at 900 °C is mostly etched and mainly the bilayers remained on the copper surface.

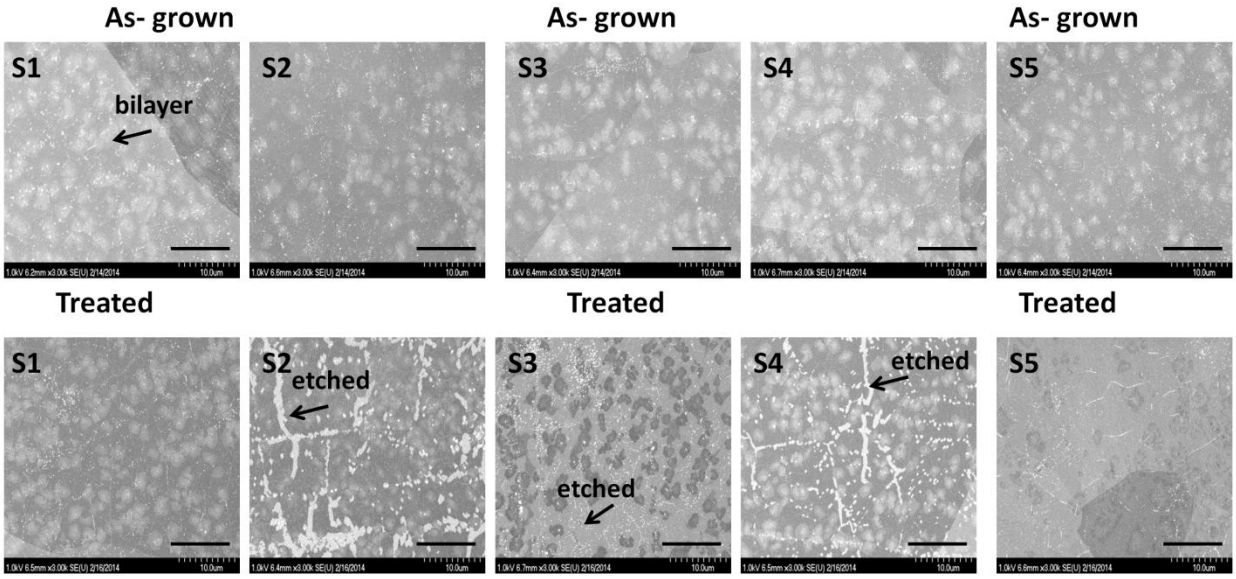

Figure A-0-3. Top row: SEM images of as-grown graphene film on copper prior to any treatment. Bottom row: SEM images of the samples exposed to a flow of purified CO_2 at 40 mTorr while being held at different temperature at different position in the furnace (refer to figure 1). S1 and S5 were at 700 °C, while S2 and S4 at 850 °C , and S3 at 900 °C. The scale bar is 10um.

Run#2 and #3:

In order to investigate further the CO_2 graphene etching reaction, more samples were placed in the furnace at higher temperature at once. The goal of these experiments was to explore the behavior and etching mechanism of graphene films. For instance, what is the ultimate temperature at which graphene can be etched in a controllable manner? or where does the etching start?

In these experiments, we used 7 samples which were placed at different positions in the furnace holding different temperatures (refer to Figure A-2). S1 and S7 were held at 825 °C, S2 and S6 at 850 °C, S3 and S5 at 900 °C, while S4 was at 950 °C.

Figure A-4 and Figure A-6 show the SEM images of graphene films used in Run #2 and Run #3 respectively. The top row shows the images of as-grown graphene samples prior to any CO_2 annealing treatment. The films are continuous with bilayers. The bottom row is the results' images after the CO_2 exposure.

Run# 2:

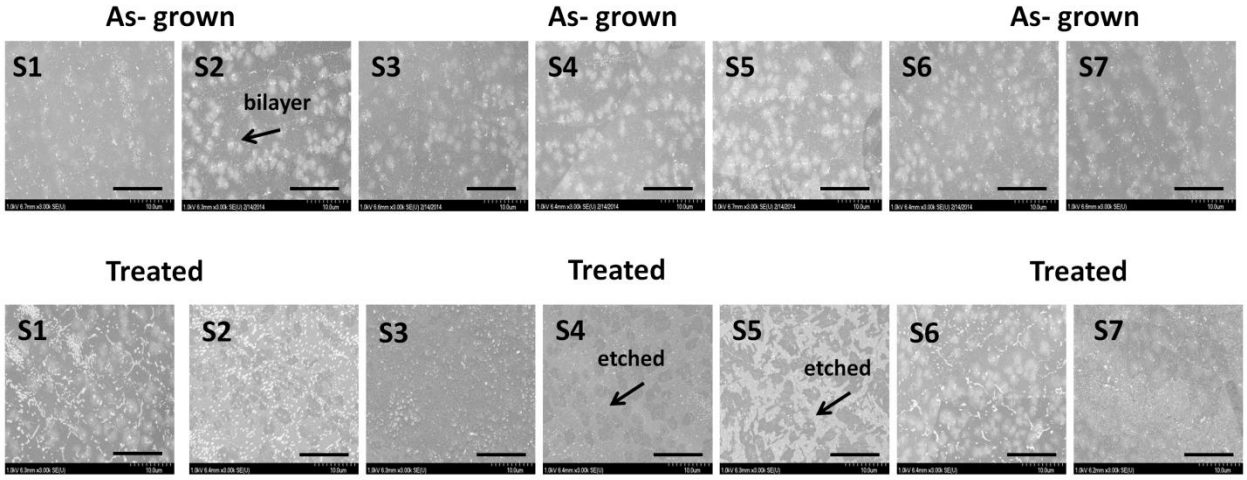

Figure A-0-4. Run #2: top row: SEM images of as-grown graphene film on copper prior to any treatment. Bottom row: SEM images of the samples exposed to a flow of purified CO_2 at 40 mTorr while being held at different temperature at different position in the furnace (refer to Figure A-2). S1 and S7 were at 825 °C, S2 and S6 at 850 °C , S3 and S5 at 900 °C, and S4 at 950 °C. The scale bar is 10um.

As seen in the images of the bottom row of Figure A-4 and Figure A-5, graphene samples (S2,S3,S4, and S5) are mostly etched with the bilayers remaining on the copper surface. Whereas, in S1 and S6 etching is just started and S7 stayed intact. Note that Figure A-5 is a zoom in image of SEM pictures shown in the bottom row of Figure A- 4.

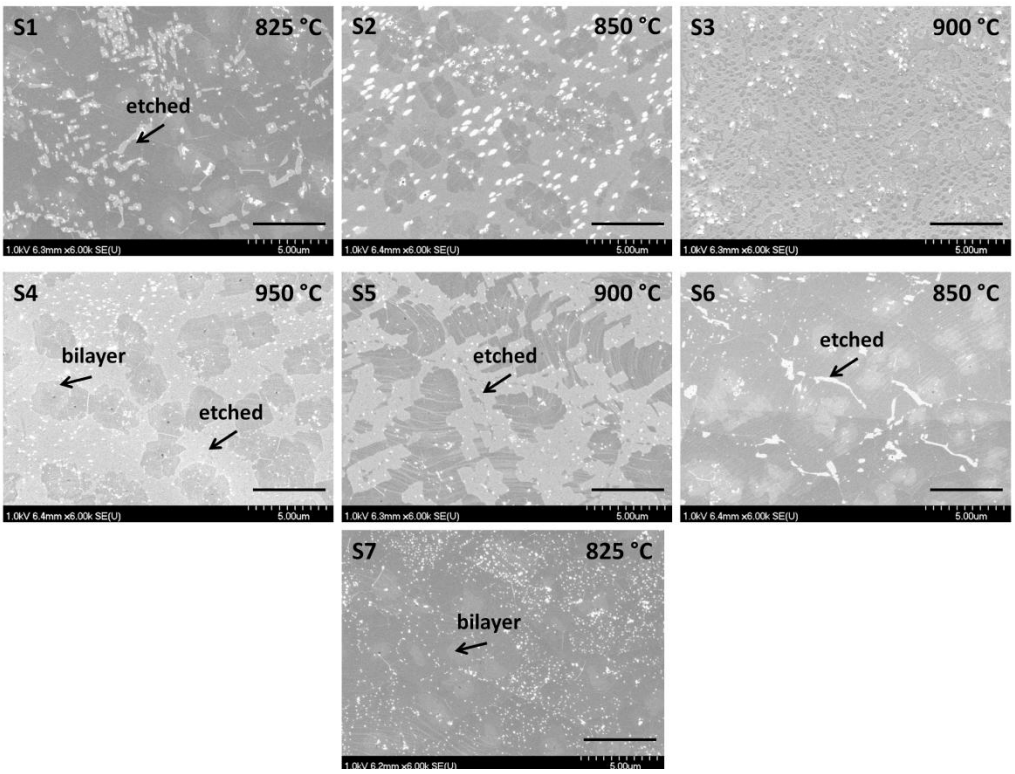

Figure A-0-5. Run #2 : zoom in SEM images of the samples exposed to a flow of purified CO_2 at 40 mTorr shown in the bottom row of Figure A- 4. The scale bar is 5um.

Run #3:

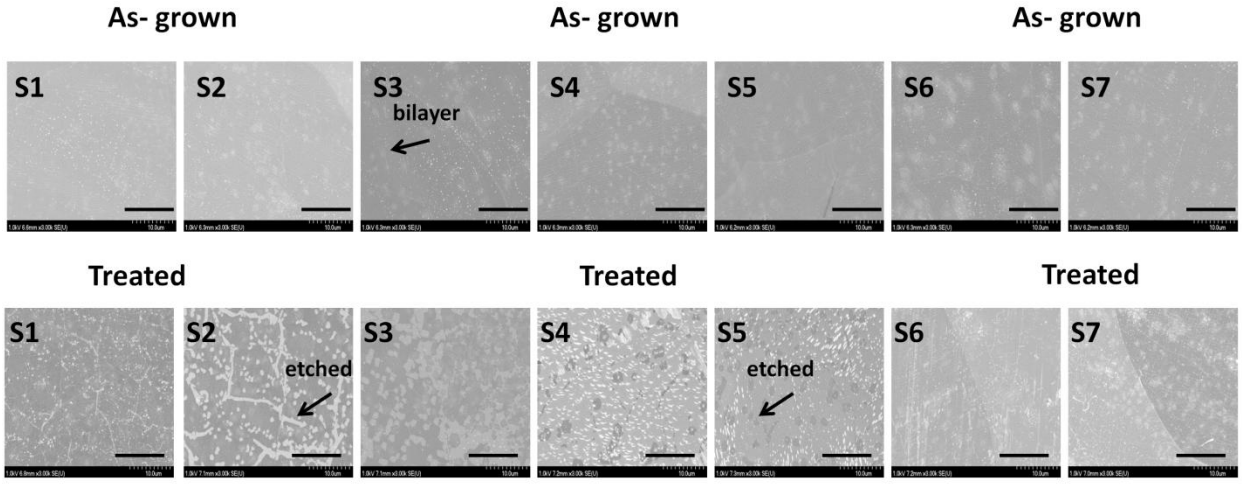

Figure A-0-6. Run #3: top row: SEM images of as-grown graphene film on copper prior to any treatment. Bottom row: SEM images of the samples exposed to a flow of purified CO_2 at 40 mTorr while being held at different temperature at different position in the furnace (refer to Figure A-2). S1 and S7 were at 825 °C, S2 and S6 at 850 °C, S3 and S5 at 900 °C, and S4 at 950 °C. The scale bar is 10um.

As seen in the images of the bottom row of Figure A-6 and Figure A-7, graphene samples (S4, and S5) are mostly etched with the bilayers remaining on the copper surface. Whereas, in S1, S2, and S6 etching is just started, S3 is partially etched and S7 stayed intact. Note that Figure A-7 is a duplicate image of SEM pictures shown in the bottom row of Figure A-6.

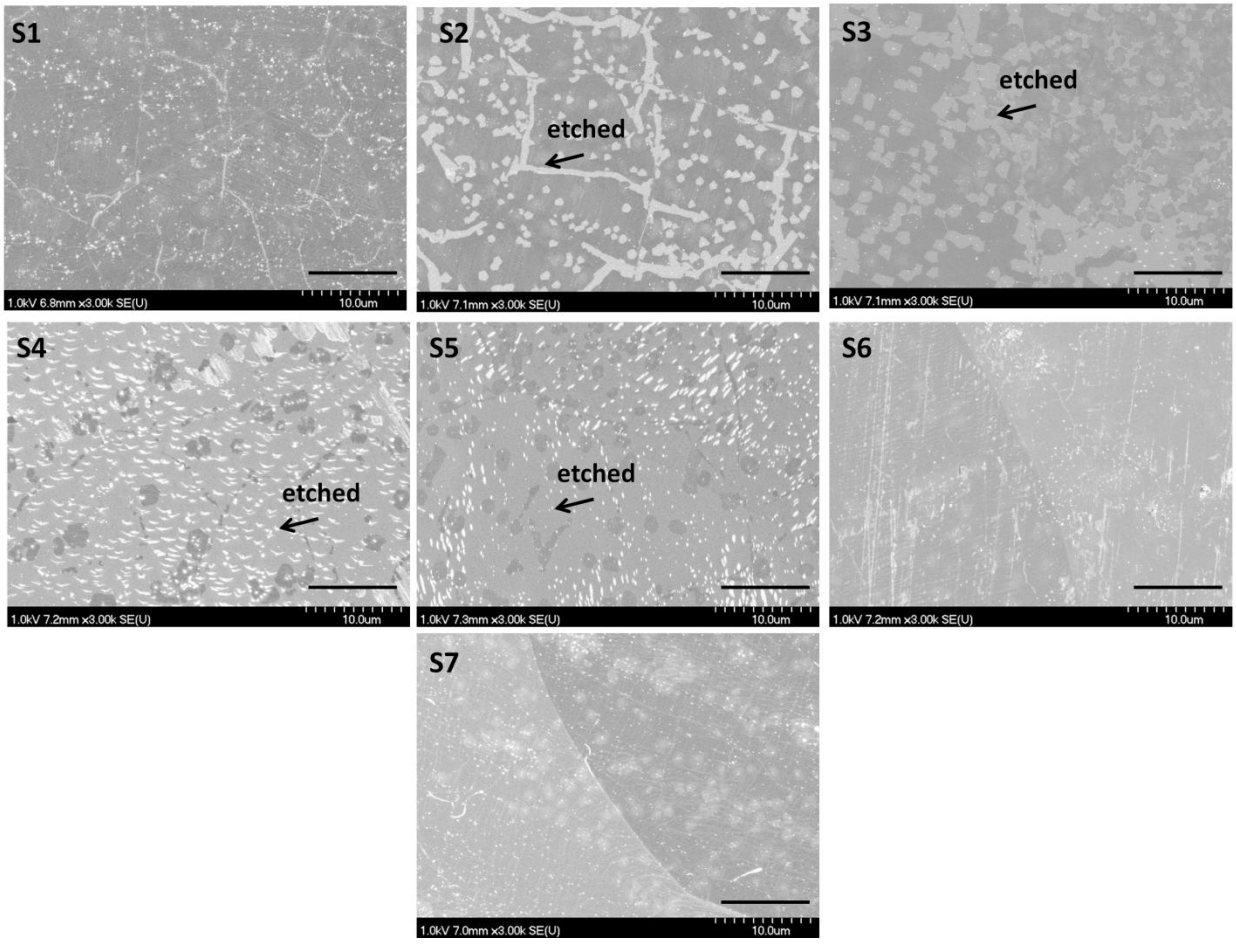

Figure A-0-7. Run #3 : duplicate SEM images of the samples exposed to a flow of purified CO_2 at 40 mTorr shown in the bottom row of Figure A-6. The scale bar is 10um.

We have further characterized our samples with scanning auger microscopy (SAM), mainly to investigate the composition of the "white beads" or "white spots" on the samples exposed to purified CO_2 and also confirm the contrast where bright areas in the SEM images indicate the absence of graphene while dark areas affirm its presence.

We have chosen S2 and S5 from run#2 and S4 from run #4 for Auger characterization. Figure A-8, 9, and 10 shows SEM images and chemical composition table of the sample 2, 5, and 4 respectively.

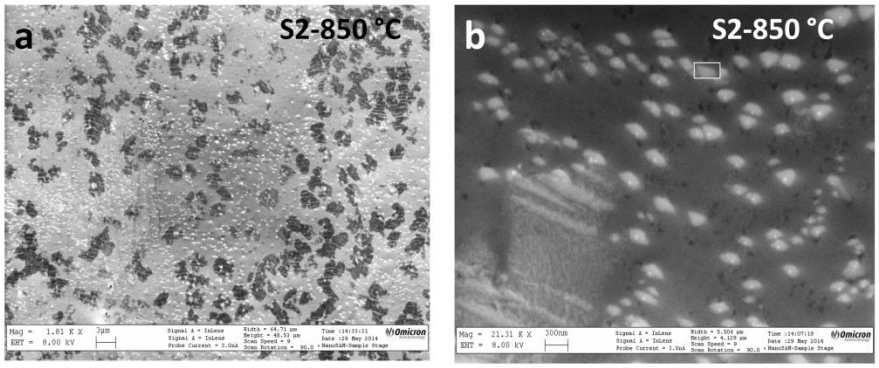

Sample	Location of measurement	Peak to peak height (counts)						
		C	O	Cu	Si	C/Cu	O/Cu	C/O
S2_RUN #2	Dark region	192	76	244	---	0.79	0.31	2.53
	Light region	107	186	486	---	0.22	0.38	0.58

Figure A-0-8. SEM images of the sample (S2, Run #2) exposed to a flow of purified CO_2 at 40 mTorr at 850 °C. a) a broad view of the sample morphology, and b) zoom in image of (a). Table shows the chemical composition of the region of interest (i.e dark regions and bright regions).

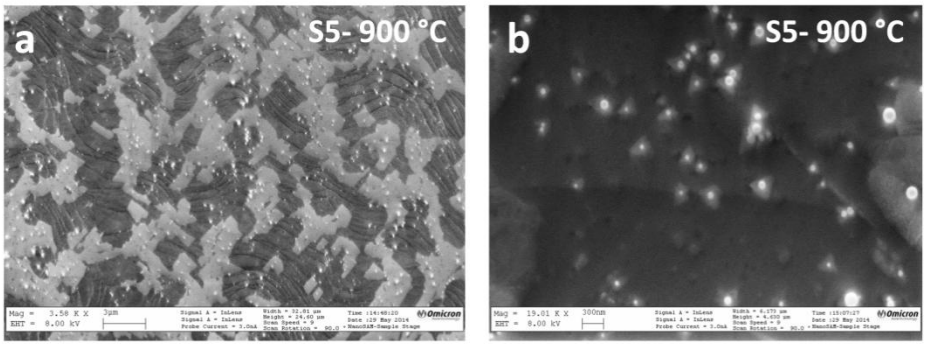

Sample	Location of measurement	Peak to peak height (counts)						
		C	O	Cu	Si	C/Cu	O/Cu	C/O
S5_Run #2	"White bead"	27	84	233	---	0.12	0.36	0.32
	Dark region	77	74	157	---	0.49	0.47	1.04
	Light region	41	87	217	---	0.19	0.40	0.47

Figure A-0-9. SEM images of the sample (S5, Run #2) exposed to a flow of purified CO_2 at 40 mTorr at 900 °C. a) a broad view of the sample morphology, and b) zoom in image of (a). Table shows the chemical composition of the region of interest (i.e dark regions, bright regions, and white spots).

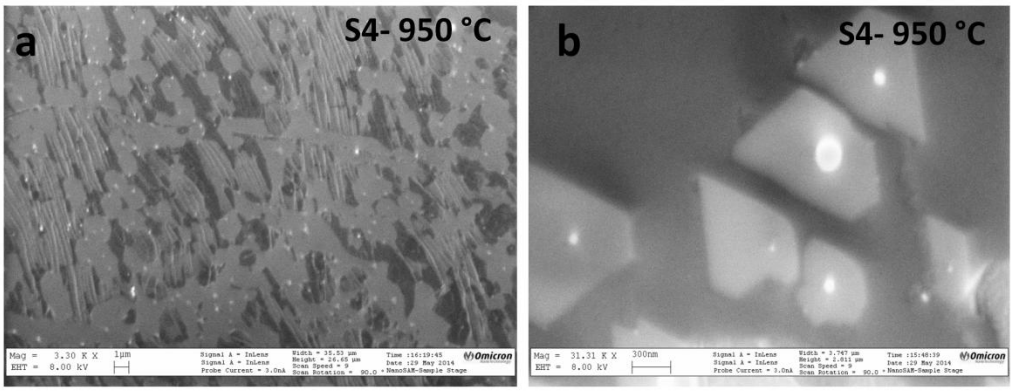

Sample	Location of measurement	Peak to peak height (counts)						
		C	O	Cu	Si	C/Cu	O/Cu	C/O
S4_Run # 3	"White bead"	---	23	102	---	---	0.23	---
	Dark region	23	15	85	---	0.27	0.18	1.53
	Light region	8	27	108	---	0.07	0.25	0.30

Figure A-0-10. SEM images of the sample (S4, Run #3) exposed to a flow of purified CO_2 at 40 mTorr at 950 °C. a) a broad view of the sample morphology, and b) zoom in image of (a). Table shows the chemical composition of the region of interest (i.e dark regions, bright regions, and white spots).

Based on the Auger measurements, we can deduce that 1) the white beads are mainly composed on copper and oxygen (copper oxide), 2) the white regions in the SEM images are copper and and copper oxide and no graphene remained in those areas, and 3) the dark regions contain carbon, copper and oxygen which is indicative of the presence of graphene in these regions.

Conclusion and Perspective

We have shown that purified CO_2 can etch graphene films in a fairly controllable manner. Thus it can be used during the graphene CVD growth in order to etch defective graphene and compete with methane as the growth agent. The ultimate goal is to tune these growth and etching reactions in a way that single crystal graphene can be grown. Due to our set up limitation, precise control of temperature at different positions in the furnace and CO_2 flow rate from one run to the other was not possible. We believe these are the reasons for inconsistencies in our results in Run #2 and #3. Furthermore, in order to approach this etching reaction mechanism piece by piece, design of a systematic experimental plan is necessarily required.